N 71 11361

NASA CR-72768

ANALYTIC STUDY OF A DEPRESSED COLLECTOR FOR LINEAR BEAM MICROWAVE AMPLIFIERS

CASE FILE COPY

by

Dr. T. G. Mihran and W. Neugebauer

GENERAL ELECTRIC COMPANY

prepared for

NATIONAL AERONAUTICS AND SPACE ADMINISTRATION

NASA Lewis Research Center
Contract NAS3-11530
P. Ramins, Project Manager

NOTICE

This report was prepared as an account of Government-sponsored work. Neither the United States, nor the National Aeronautics and Space Administration (NASA), nor any person acting on behalf of NASA:

A.) Makes any warranty or representation, expressed or implied, with respect to the accuracy, completeness, or usefulness of the information contained in this report, or that the use of any information, apparatus, method, or process disclosed in this report may not infringe privately-owned rights; or

B.) Assumes any liabilities with respect to the use of, or for damages resulting from the use of, any information, apparatus, method or process disclosed in this report.

As used above, "person acting on behalf of NASA" includes any employee or contractor of NASA, or employee of such contractor, to the extent that such employee or contractor of NASA or employee of such contractor prepares, disseminates, or provides access to any information pursuant to his employment or contract with NASA, or his employment with such contractor.

Requests for copies of this report should be referred to

National Aeronautics and Space Administration
Scientific and Technical Information Facility
P.O. Box 33
College Park, Md. 20740

NASA CR-72768

FINAL REPORT

ANALYTIC STUDY OF A DEPRESSED COLLECTOR for LINEAR BEAM MICROWAVE AMPLIFIERS

by

Dr. T. G. Mihran and W. Neugebauer

GENERAL ELECTRIC COMPANY
Tube Department
Microwave Tube Operation
Schenectady, New York

prepared for

NATIONAL AERONAUTICS AND SPACE ADMINISTRATION

July 8, 1970

CONTRACT NAS3-11530

NASA Lewis Research Center
Cleveland, Ohio
P. Ramins, Project Manager
Spacecraft Technology Division

FOREWORD

The work reported herein was conducted at the General Electric Company, Schenectady, New York, under NASA Contract NAS3-11530. The study was performed jointly by Dr. T. G. Mihran of the Research and Development Center and Mr. W. Neugebauer of the Microwave Tube Operation. Mr. Peter Ramins, Spacecraft Technology Division, NASA-Lewis Research Center, was Project Manager assisted by Dr. Henry Kosmahl.

TABLE OF CONTENTS

	Page
SUMMARY	1
INTRODUCTION	3
ANALYTIC COLLECTOR STUDY	5
Literature Survey	5
Collector Classification Chart	8
Basic Concepts and Definitions	10
Computer Programs	13
Preliminary Evaluation of Collectors	20
Intermediate Evaluation of TEF Collectors	23
Theoretical Analysis of Collectors	29
Approximate Collector Analysis Using Flat Spent Beam Power Distribution	33
Effect of Number of Electrodes	47
Final Collector Design and Evaluation	68
DISCUSSION OF RESULTS	81
RECOMMENDATIONS FOR FUTURE WORK	83
CONCLUSIONS	85
Appendix A - SPENT BEAM ENERGY DISTRIBUTIONS IN TWT's AND KLYSTRONS	87
Appendix B - LIST OF SYMBOLS	91
REFERENCES	93

ABSTRACT

An analytic study has been made of a wide variety of depressed collectors, utilizing magnetic fields, for use with klystrons and traveling-wave tubes. Final calculations were implemented by use of a pair of analog computers which permitted space charge to be considered in approximate form.

An optimized collector, employing a tilted electric field and an axial magnetic field, was designed for use on a 12-GHz klystron. The calculated collector efficiency ranges from 65 to 80 percent depending upon electrode number. This collector should increase the power conversion efficiency of a tube from 50 to approximately 80 percent.

SUMMARY

An extensive survey of depressed collector types for klystrons and traveling-wave tubes (TWT's) is presented. A general collector classification chart has been devised which gives an integrated perspective of past work and suggests promising new collector types employing magnetic fields. A general analog computer program has been developed to analyze electron trajectories, including an approximate treatment of space charge. Preliminary and intermediate evaluations, omitting space charge, show the most promising collector to have a tilted electric field and an axial magnetic field. This collector was chosen for final evaluation using the approximate space charge model.

Several choices of electrode potential arrangements were investigated analytically, namely: (1) collectors which treat all energy classes equally, (2) collectors in which the most negative electrode is at cathode potential, and (3) collectors in which the electrode arrangement is weighted according to the spent beam current density and energy distributions. Design curves were established for the collector efficiency of klystrons and TWT's as a function of electrode number and undepressed tube efficiency. The importance of an "intrinsic" margin, which limits the usefulness of an increase in electrode number in a given collector, was established. Efficiency improvement by collector depression is more effective with TWT's than with klystrons.

A design was established for a 12 GHz, 4-kW klystron using a ten-stage collector with its most negative electrode at cathode potential. The computed collector efficiency of 67 percent can be increased to 78 percent by the use of twenty-stage collector in which the most negative electrode is below that of cathode potential. A collector efficiency of 78 percent will increase the net power conversion efficiency of a tube from 50 to over 80 percent.

INTRODUCTION

High power conversion efficiency from dc to rf is a prime requirement for space broadcasting applications because of the high cost of the prime power source and the heat rejection system. The power conversion efficiency of most commercial klystrons and traveling-wave tubes (TWT's) currently available ranges from 30 to 60 percent; thus roughly one-half of the dc power supplied to these tubes is wasted as heat dissipation in the collector. It is generally recognized that a collecting structure utilizing one or more electrodes operated at potentials lower than the beam voltage can reduce the heat dissipation in the collector and thus increase the overall operating efficiency of the tube-collector system.

Depressed collectors have been built in the past, but in general their performance has been disappointing. Work in this field has been characterized by a lack of progressive improvement -- a general inability of one investigator to extend and to improve upon the work of his predecessors. The reason for this appears to be that most collector work has been "hardware-oriented". Collectors were built and tested; in general, they did not perform as well as expected; consequently, the matter was dropped without probing the reasons for the failure. It would appear that this lack of persistence in the past has occurred because high efficiency was generally not a prime concern in most ground-based applications.

The possibility of high power broadcasting from space has stimulated a new interest in the development of a successful depressed collector. A number of years have elapsed since the bulk of past work on depressed collectors was done. The rapid development of new analytical techniques, such as analog and digital computation, may provide the design ability needed to unify and advance knowledge in this field.

A specific example of such an advance was the reflex collector invented in 1968 by T. G. Mihran and W. Neugebauer as a result of analog computer studies of electron trajectories.[1] The unexpected refocussing of reflected electrons in this electrostatic collector became evident from numerous analog computer runs, and this observation suggested that electron collection be done after electrons had passed through their minimum energy point, not before. The reduction of this idea to practice is currently underway on a parallel NASA Contract NAS3-11532.

The primary purpose of the present study was to ascertain whether or not the addition of a magnetic field could increase collector efficiency to a value higher than that achieveable in a purely electrostatic collector. On the basis of new analytic work presented herein, we find the answer to this question to be in the affirmative. Current electrostatic collector designs are producing calculated average collection efficiencies of approximately 62 percent. Using the same method of analysis, this report gives the specific design of a new type of collector, utilizing a longitudinal magnetic field and a tilted electric field with calculated efficiency ranging from 67 to 78 percent for 10- and 20-electrode systems, respectively. This improvement in efficiency has not been optimized in detail, since the new collector has many more parameters to investigate and optimize than the reflex collector. Based on the results of our study it appears that the addition of a magnetic field to a collector system definitely can increase collector efficiency over that of an electrostatic system.

In subsequent sections of this report the following subjects are discussed, respectively; the literature survey demonstrating that, to date, collector depression has usually added only ten points to the efficiency of well designed high efficiency tubes. The collector classification chart which was used as a basis for the systematic evaluation of sixty-four collector types, most of which utilize a magnetic field; the basic concepts and definitions that are required for preliminary and intermediate evaluation of collector types; the analog computer program used for collector evaluation, including an approximate treatment of space charge in asymmetric collectors; the preliminary and intermediate evaluations leading to the selection of the most promising collector type; the establishment of an accurate basis for final collector evaluation; the justification for the approximate evaluation of collector performance on an area basis; the effect of electrode number on collector efficiency; the final evaluation of the most promising collector type as applied to a 12-GHz klystron.

ANALYTIC COLLECTOR STUDY

LITERATURE SURVEY

The concept of depressing collector potential to increase the efficiency of linear beam-type microwave tubes had its origin in the early 1940's. Haeff and Nergaard[2] (1940) and C. V. Litton[3] (1943) have been credited with the earliest suggestions of this principle. However, not until a decade later were serious attempts made to devise and operate depressed collectors on klystrons and traveling-wave tubes. A summary of the work on depressed collectors which was reported prior to the inception of the present work is listed chronologically and referenced in Table I. Each collector is identified as to whether it is electrostatic (ES) or employs both electric and magnetic fields (E-B). Also, the symmetrical or asymmetrical nature of the collector as well as the number of stages of collector depression is indicated. In addition, the application to either klystrons or TWT's is listed, and the tube efficiency without and with collector depression, η_o and η, respectively, is given. The approximate chart classification listed in Table I is discussed in the following section.

The efficiency data shown in Table I are plotted in Figure 1. In this figure, efficiency with depression is plotted as a function of efficiency without depression. The hollow circles indicate TWT data reported from 1953 to 1963, and the solid points indicate klystron data for the same period. More recent data are indicated as follows: Walder (klystrons, 1965) - solid triangles, Okoski, et al (TWT, 1968) - hollow squares, and Sauseng (TWT, 1968) - hollow triangles. Thus, in Figure 1 all solid points represent klystron data and all hollow points represent TWT data.

The historical data in Table I and Figure 1 can be summarized as follows: For tubes (mostly TWT's) with base efficiency in the 10-30 percent range, collector depression has added approximately 20 points to tube efficiency; for tubes with base efficiency in the 35-55 percent range, collector depression has added approximately 10 points to tube efficiency.

In general, the efficiency enhancement achieved in practice seldom approaches the performance predicted by theory. One exception is the outstanding efficiency reported by Sterzer for a two-stage collector. The general impression gained from the literature survey is that many depressed collector types have been tried, but on the basis of the performance achieved, no single type stands out as the most promising. Furthermore, there has

TABLE I - SUMMARY OF LITERATURE SURVEY OF DEPRESSED COLLECTORS

Date	Ref.	Author's Name	Collector Description			Approx. Chart Class	Tube		
			ES or E-B	Sym. or Asym.	No. of Stages		TWT or Klys.	Efficiency η_o	Efficiency η
1953	(4)	Cutler, et al	E-B	Asym.	1	2.4	TWT	11	20
1954	(5)	Winkler	ES	Sym.	1	2.1	Klys.	21	28
		Winkler	ES	Sym.	2	2.1	Klys.	~21	~28
		Winkler	ES	Sym.	3	2.1	Klys.	~21	~28
1956	(6)	Laico, et al	ES	Sym.	1	2.1	TWT	14	28
1958	(7)	Wolkstein	E-B	Sym.	1	2.4	TWT	10	35
1958	(8)	Sterzer	E-B	Sym.	1	2.2	TWT	24.5	46
		Sterzer	E-B	Sym.	2	2.2	TWT	24.5	57
1959	(9)	Dunn, et al	E-B	Asym.	2	~5.3	-	-	-
1960	(10)	Dunn, et al	E-B	Asym.	8	~5.56	-	-	-
1960	(11)	Murata, et al	E-B	Sym.	2	2.2	Klys.	42	49
1960	(12)	Hansen, et al	E-B	Asym.	2	2.4	TWT	20	37
1961	(13)	McCune	ES	Sym.	1	2.1	Klys.	41	48
		McCune	ES	Sym.	1	2.1	Klys.	35	42
1961	(14)	Met	ES	Sym.	2	2.1	Klys.	40	52
1963	(15)	Chen	E-B	Asym.	8	5.3	TWT	16	38
1965	(16)	Walder	ES	Sym.	1	2.1	Klys.	48	58
		Walder	ES	Sym.	1	2.1	Klys.	54.5	62.5
		Walder	ES	Sym.	1	2.1	Klys.	56.5	63.5
		Walder	ES	Sym.	1	2.1	Klys.	58	62.5
1968	(17)	Okoshi, et al	E-B	Asym.	2	4.3	TWT	10	22
		Okoshi, et al	E-B	Asym.	2	4.3	TWT	20	35
		Okoshi, et al	E-B	Asym.	2	4.3	TWT	30	42.5
		Okoshi, et al	E-B	Asym.	2	4.3	TWT	40	53
1968	(18)	Sauseng*	ES	Sym.	2	2:1	TWT	38	50
		Sauseng	ES	Sym.	2	2:1	TWT	40	57
		Sauseng	ES	Sym.	2	2:1	TWT	45	51
		Sauseng	ES	Sym.	2	2:1	TWT	46	57
		Sauseng	ES	Sym.	2	2:1	TWT	50	58
		Sauseng	ES	Sym.	2	2:1	TWT	53	62

* Most of these TWT tubes use voltage jumps with the output section at an elevated potential but with the collector grounded. Hence the η_o is not a true measure of the undepressed tube efficiency.

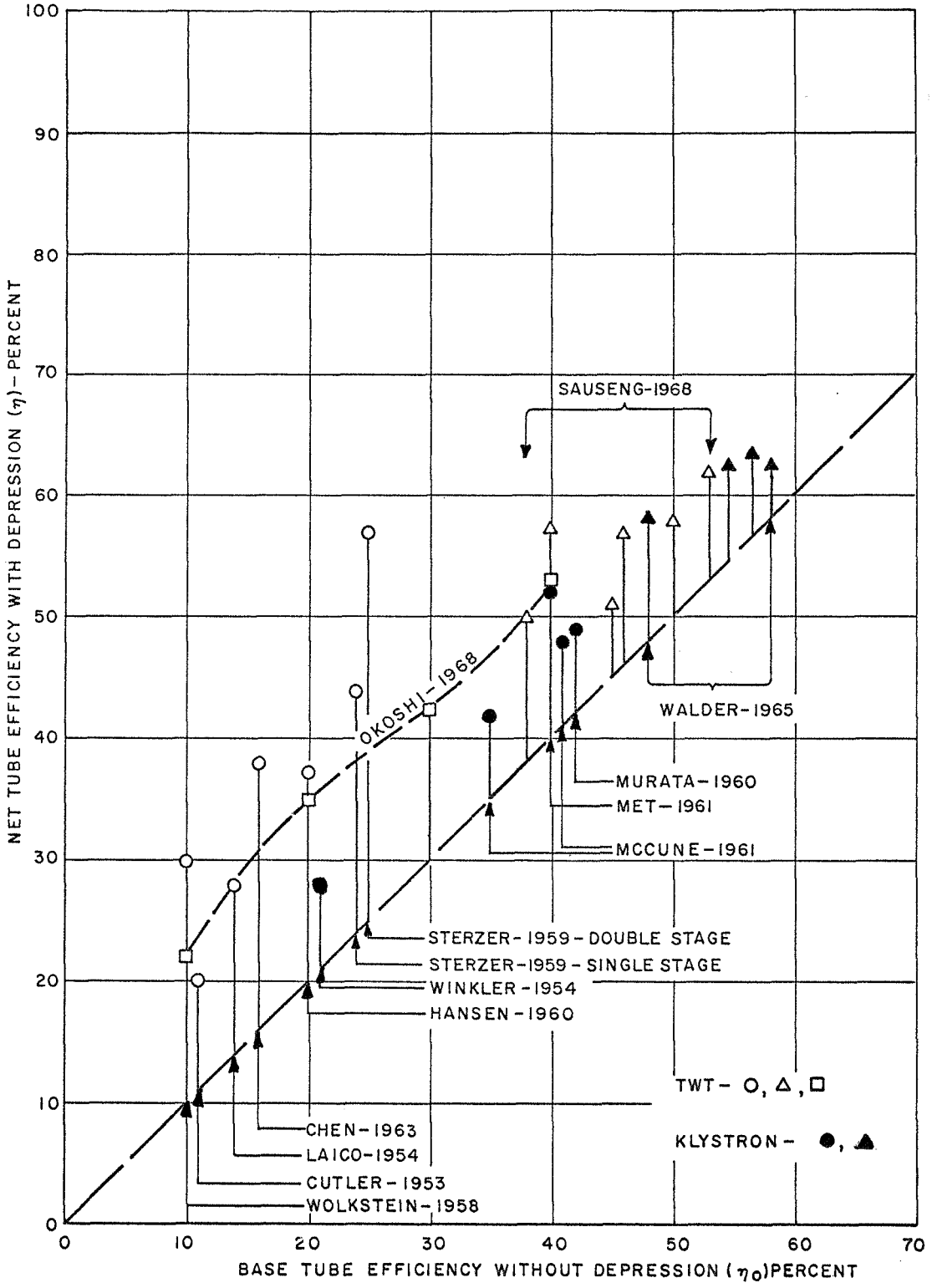

Figure 1 - Survey of Measured Improvement in Klystron and TWT Power Conversion Efficiency by Use of Depressed Collectors

been a distinct lack of effort to identify and probe the discrepancies between theoretical predictions and experimental performance. Therefore, it seems desirable to initiate a broad program for the consideration and re-evaluation of as many different collector types as possible. In the following section a general method of classifying a large variety of collectors is described.

COLLECTOR CLASSIFICATION CHART

In order to investigate various collector geometries systematically, it was desirable to devise a method of classification which covered not only all collectors which have been built in the past, but which would suggest new geometries of potential interest. Such a classification chart has been devised to guide the present investigation. According to this method all collectors were classified according to the nature and direction of the electric and magnetic fields employed in the collector. For both the E and the B field, five geometric orientations were considered, of which three were axially symmetric and two were antisymmetric. These orientations are listed in the headings of each of the five columns shown in Figure 2. The symmetric field orientations are: (1) zero, (2) spreading (radial plus axial) and (3) axial; the antisymmetric field orientations are (4) tilted (transverse plus axial), and (5) transverse. These five field orientations can be applied to either E or B fields, or both, and their application leads to the twenty-five field combinations shown in Figure 2. In this figure the solid lines indicate magnetic field and the dashed lines indicate electric field. The circles, solid and dashed, refer to zero field.

This matrix of twenty-five field combinations can be conveniently classified as to row and column, thus a Type 4.3 collector employs a tilted electric field and an axial B field. Note that a Type 2.1 collector is purely electrostatic in operation, employing a spreading E field and zero magnetic field.

It is clear that not all of the field configurations shown in Figure 2 will yield useful collectors. For instance, collectors shown in the entire first row of the illustration can be discarded immediately as no electric field is present to decelerate electrons. A complication arises concerning the four antisymmetric E and antisymmetric B cases in the lower right hand corner of the Figure. For example, a Type 5.5 collector, which employs transverse E and B fields, must further be defined as to the relative directions of the two transverse fields. Still another complication is introduced when the polarities of the two fields are allowed to assume independent values.

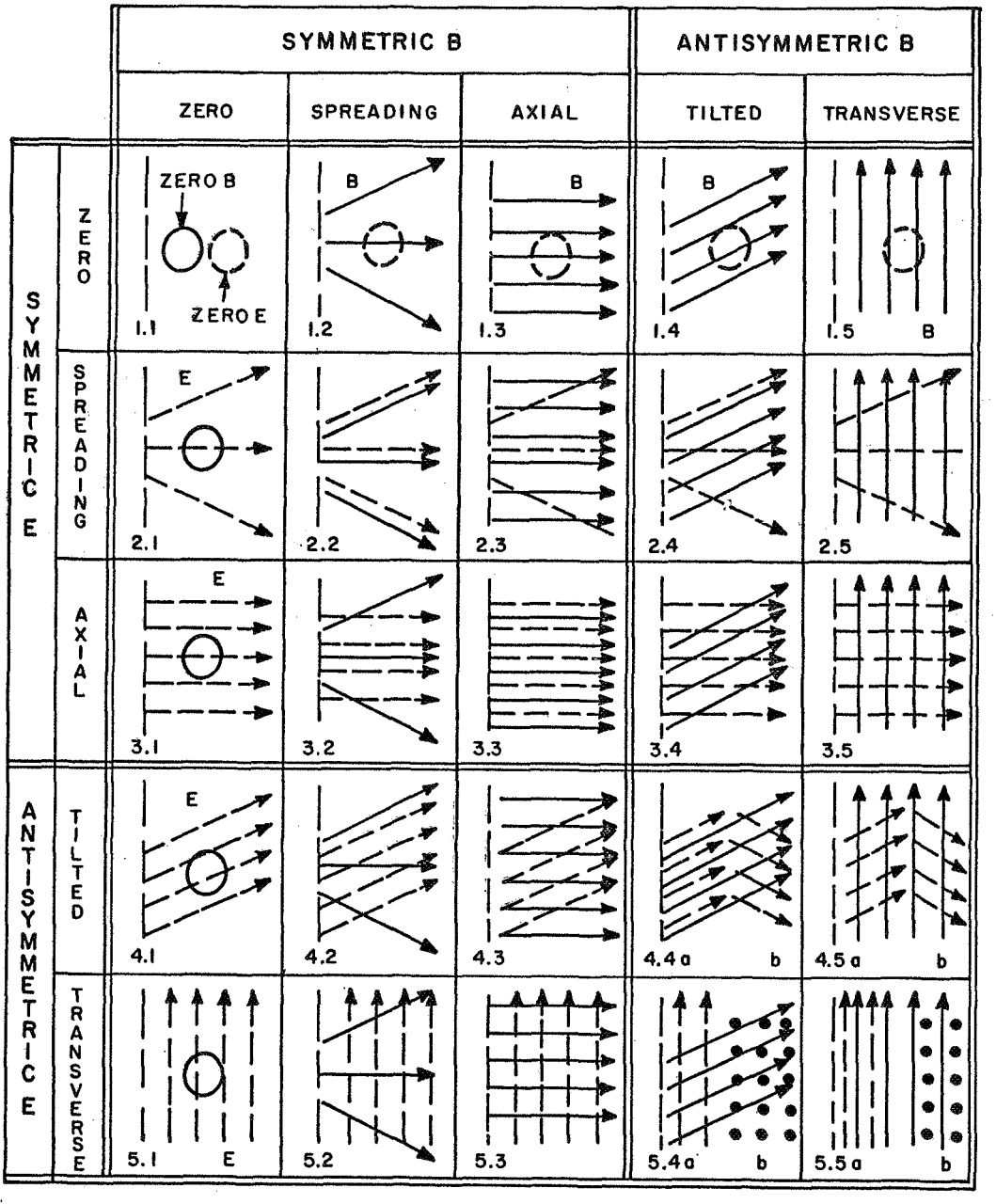

Figure 2 - Classification Chart of Possible Orientations of Electric (Dashed Lines) and Magnetic (Solid Lines) Fields in Collectors

The complications listed above increase the number of collector types that need to be investigated, to sixty four, as discussed in the section titled, "Preliminary Evaluation of Collectors"; however, the classification chart presented in this section does not include all possible collector types. It would be possible, for example, to cascade two collector regions, each using a different pair of field orientations. Investigation of such multiple-region collectors is not within the scope of the present work. In the following section, basic concepts and definitions that are needed for the approximate evaluation of collectors are established.

BASIC CONCEPTS AND DEFINITIONS

The most practical measure of the quality of a collector is its ability to increase the efficiency of a tube from η_o, the tube efficiency without depression, to a higher efficiency, η. Although this characterization is very useful, it inextricably mixes the tube performance with the collector performance. For collector evaluation it is desirable to define a collector efficiency under actual operating rf conditions, η_{c-rf}. This parameter describes the ability of the collector to remove power from the spent beam impinging upon it. If the beam emerges from the output gap of a tube with an undepressed efficiency η_o, the fraction of the original beam power I_oV_o entering the collector is $(1-\eta_o)I_oV_o$. Of this power, a fraction $(1-\eta_{c-rf})$ is not recovered; therefore, overall tube efficiency may be written as

$$\eta = \frac{\text{rf out}}{\text{dc in}} = \frac{\eta_o}{\eta_o + (1-\eta_o)(1-\eta_{c-rf})} = \frac{\eta_o}{1-(1-\eta_o)\eta_{c-rf}} \tag{1}$$

It is important to note that rf collector efficiency is defined on the basis of spent beam energy entering the collector and not on the basis of total dc beam power prior to rf interaction.

Equation (1) may be used to generate a set of curves as a function of η_o, with η_{c-rf} as a parameter, as shown in Figure 3. This set of curves may be used to obtain the collector efficiency for any data pair η, η_o. Alternately, Equation (1) may be solved for η_{c-rf}.

$$\eta_{c-rf} = \frac{1-\eta_o/\eta}{1-\eta_o} \tag{2}$$

Collector efficiency as defined in Equation (2) still has the disadvantage that it depends upon rf tube performance. In order to evaluate a wide variety

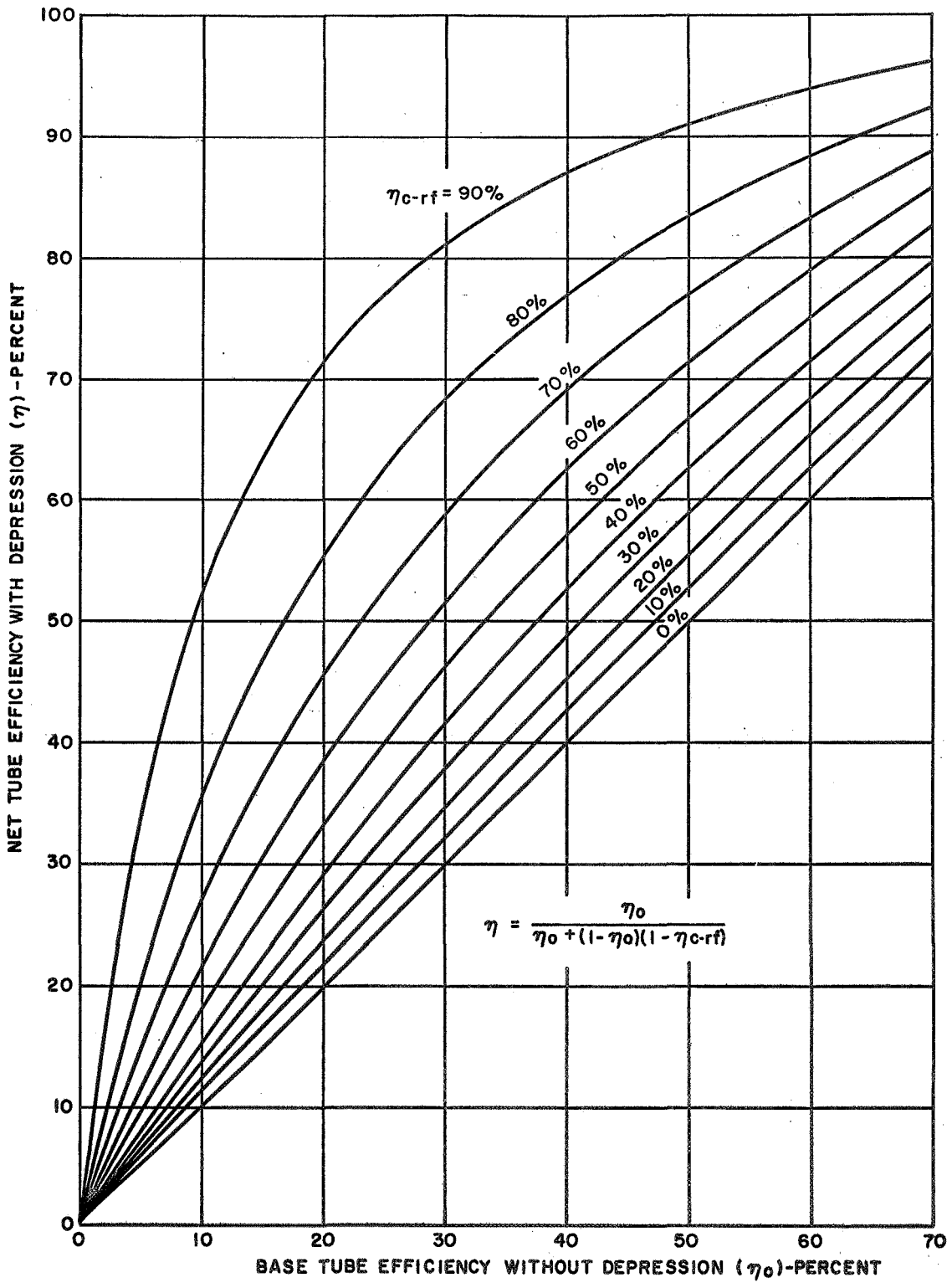

Figure 3 - Improvement in Power Conversion Efficiency with Collector Depression, with RF Collector Efficiency as a Parameter

of collector types on the analog computer, it is desirable to define a measure of collector quality that is related to dc, not rf, quantities. The simplest dc quantities that can be identified in a given collector are the currents I_i that flow to the various electrodes placed at potentials $-V_i$ with respect to the drift tube. Referring to the schematic shown in Figure 4, a monoenergetic beam leaves a cathode at potential $-V_o$ and travels down a drift tube at ground potential. The current flowing to the "i"th electrode causes a power dissipation of $I_i(V_o - V_i)$ in the form of heat at the electrode surface. Thus, the recovered power is $I_i V_i$, and the collection efficiency for a collector with N electrodes is given by the summation:

$$\eta_c = \frac{1}{I_o V_o} \sum_{i=1}^{N} I_i V_i \qquad \text{(dc case only)} \qquad (3)$$

This equation assumes that current interception on the drift tube is zero, a viewpoint that will be consistently taken in the present work.

Equation (3) gives the collection efficiency η_c at a given monoenergetic beam voltage, V_o. If this evaluation is repeated at M values of beam voltage equally spaced between zero and the maximum particle potential in a spent beam, and if the collector electrode potentials are held constant, a plot can be made of the collection efficiency as a function of beam voltage. For the preliminary and intermediate collector evaluations, the average height $\overline{\eta}_c$

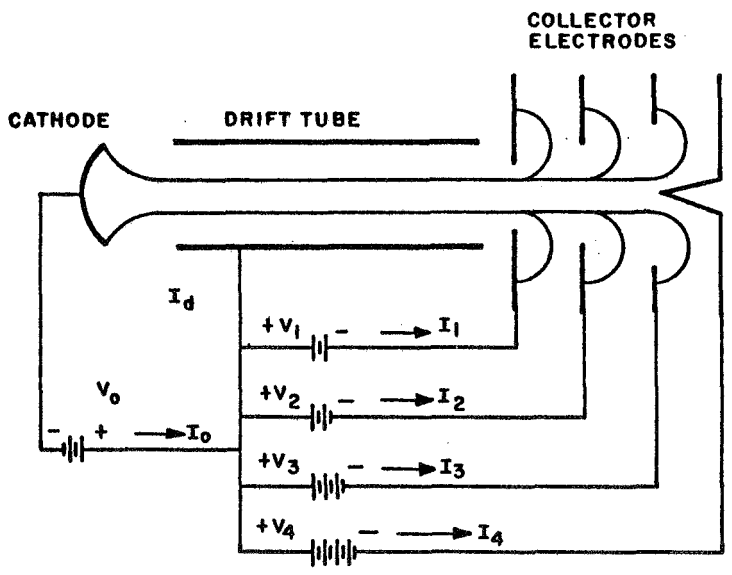

Figure 4 - Schematic of Electrode Potentials and Current Flow in a Depressed Collector

of this curve

$$\bar{\eta}_c = \frac{1}{M} \sum_{j=1}^{M} \eta_c (V_{oj}) \tag{4}$$

has been taken as a measure of collector quality. It will be shown in this report that $\bar{\eta}_c$ is a reasonably accurate measure of collector efficiency even under rf conditions, provided that the power distribution spectrum of the spent beam is reasonably flat and that the basic tube efficiency η_o is greater than 40 percent.

In subsequent sections the analog computer program used for this work, and the preliminary and intermediate evaluations of various collector types will be described.

COMPUTER PROGRAMS

To analyze the performance of a wide variety of symmetric and asymmetric collectors, a versatile program having good accuracy is required. While both digital and analog programs were available for analyzing symmetric depressed collectors, there was no program capable of handling asymmetric collectors with sufficient accuracy. Since analog computer programs are much more easily modified and checked, it was decided to base the entire analytic collector study on various extensions of an existing basic gun analysis program. In addition, two analog computers were available 100 percent of the time for this project, thereby eliminating the delays customary with digital computers. The greater precision possible with digital computers was deemed unnecessary for this study program.

Analog Computer Program

The basic equation of electron motion is the Lorentz force equation which, in Cartesian coordinates, becomes

$$\begin{aligned} \ddot{x} &= -\frac{e}{m} (E_x + \dot{y}B_z - \dot{z}B_y) \\ \ddot{y} &= -\frac{e}{m} (E_y + \dot{z}B_x - \dot{x}B_z) \\ \ddot{z} &= -\frac{e}{m} (E_z + \dot{x}B_y - \dot{y}B_x) \end{aligned} \tag{5}$$

where the dots refer to time differentiation, e/m is the electronic charge to mass ratio, and E and B represent the electric and magnetic field components. If the field components are constant in space and time, these equations are easily programmed on an analog computer for analysis. The diagram for the program is shown in Figure 5 and the above equations are mechanized with the integrators numbered 30, 31, 00, 01, 05, and 06. Three multipliers, SM0, SM1, and SM3 are used to compute the instantaneous kinetic energy of the electron by squaring and adding the velocity components. This part of the program was used for all the early studies made under this contract. The spent electron beam was launched in various configurations of constant magnetic and electric fields and was tested for energy recovery and backstreaming. No space charge effects were included at that time.

Space Charge Effects

In high frequency, high power tubes, the effects of space charge in spreading the spent beam become quite large and cannot be neglected. Also, for reasons given below a true space charge analysis in a three-dimensional asymmetric collector is extremely difficult to perform and was considered beyond the scope of this study. For these reasons an approximate space charge model based on two electrons was developed. The model requires that both the central and an off-axis trajectory be computed simultaneously. By Gauss's law, the beam current lying between these two trajectories gives rise to forces which in Cartesian coordinates can be expressed as

$$
\begin{aligned}
m\ddot{x} &= \frac{e}{2\pi\epsilon_o}\,\frac{(x-x_o)\,I}{d^2\,|v|} \\
m\ddot{y} &= \frac{e}{2\pi\epsilon_o}\,\frac{(y-y_o)\,I}{d^2\,|v|} \\
m\ddot{z} &= \frac{e}{2\pi\epsilon_o}\,\frac{(z-z_o)\,I}{d^2\,|v|}
\end{aligned}
\tag{6}
$$

where e and m are the electronic charge and mass, d is the distance between the two particles, I is the beam current, ϵ_o is the permittivity of free space, $|v|$ is the average particle velocity, and the subscript o refers to the central trajectory. To mechanize this set of equations, another "main program" was patched on a second analog computer to calculate the central trajectory.

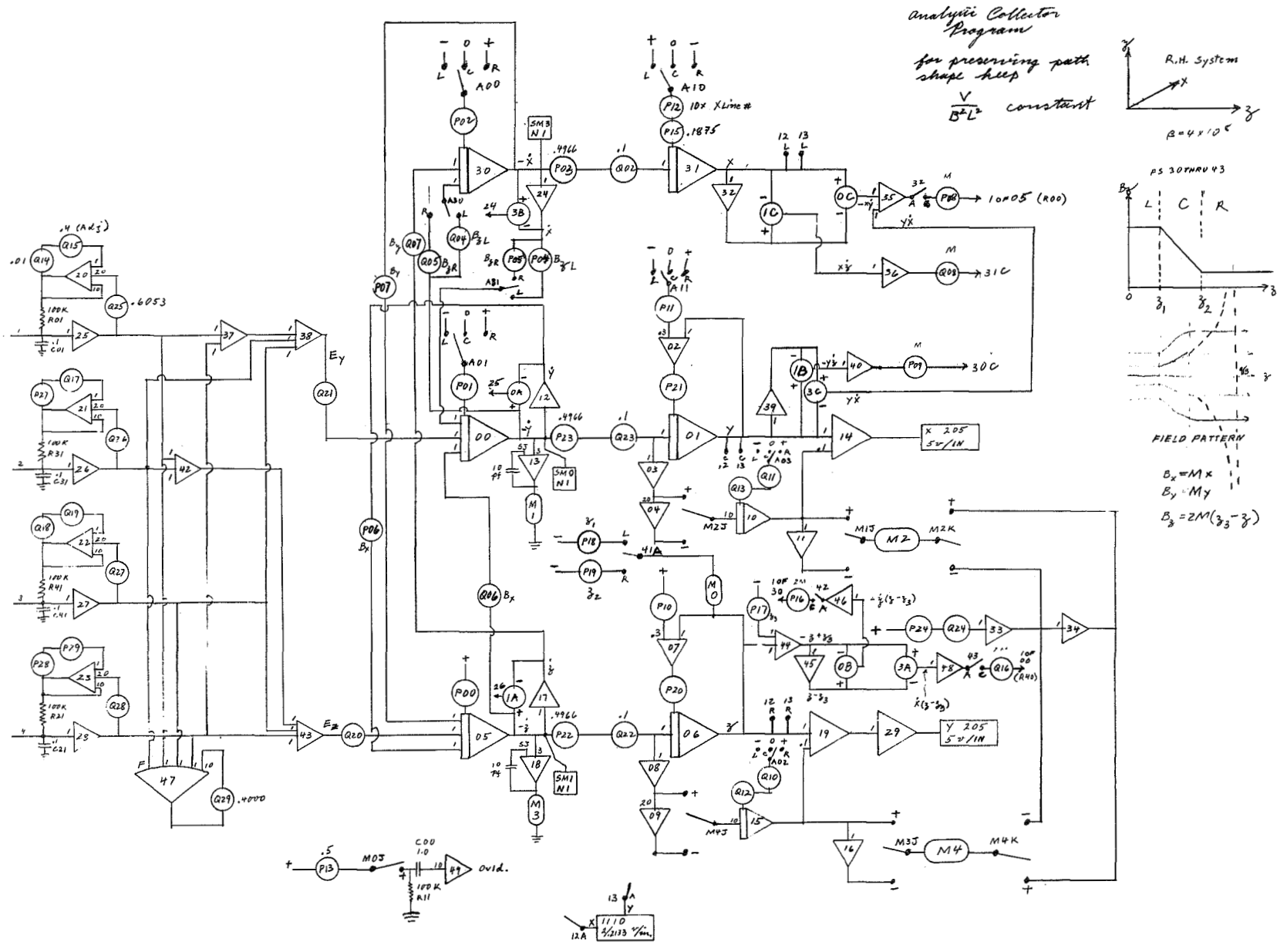

Figure 5 - Block Diagram of the Main Analog Computer Program

The difference in the coordinate positions is then analyzed according to the above equations and is fed back to the integrators calculating the off-axis trajectory, as shown in Figures 6a and 6b.

The two-electron model for calculating space charge effects has been used extensively on the analog computer for the study of electron beams having axial symmetry. Thermal power density distributions in standard, undepressed collectors are routinely calculated with this model and are found to be sufficiently accurate for tube design purposes. Agreement with the results of a many-electron digital computer program is also very good in cases with axial symmetry. The extension of the more accurate digital computer treatment of space charge to include asymmetric geometries is a formidable problem. It would require a three-dimensional relaxation technique operating on a vastly greater number of mesh points. It is estimated that a program of this nature would require a memory and running time which are two orders of magnitude greater than the present 30K, 10-minute, two-dimensional axially symmetric program. Such a program would require larger and faster digital computers than are presently available, hence it could not be considered for this work, nor for work to be done in the near future.

Another method of improving the space charge calculation is the use of more than two electrons in the present model. This can be done either by the addition of more analog computers or it can be done digitally, depending on the equipment available. The electron beam would be broken into pieces each specified by a radial, angular, and axial location. The space charge calculation would consist of applying the coulomb law between all particle pairs as their trajectories are simultaneously computed. The associated Laplace field would still be an approximation based on two-dimensional models.

Magnetic Field Profile

In order to allow for a reduction in magnetic field from tube to collector, the final analog computer program established a three-region magnetic field profile, as follows: (1) an initial, constant high field region, associated with the main focussing field in the tube, (2) a spreading field characterized by the equations

$$\begin{aligned} B_x &= Mx \\ B_y &= My \\ B_z &= 2M(z_3 - z) \end{aligned} \qquad (7)$$

and (3) a final, constant low field region in the main body of the collector. M is a magnitude and z_3 is the location along the axis where the axial field component would reverse sign if the taper were continued. This field pattern satisfies the divergence equation and is used in the analog computation as a transition region from the high field in the tube to a lower field in the collector. The angular spin that is imparted to the electrons as they leave the main magnetic field is, therefore, included in the calculation. Both Brillouin and immersed beams can be analyzed by the program.

Initial Conditions

The analog computer program allows arbitrary initial positions x, y, and z of a trajectory and arbitrary initial velocity components. In the trajectory calculations the initial conditions were set to correspond to the approximate conditions present in a spent beam. The angular velocity is given by the law of momentum conservation and the axial velocities are a function of the energy distribution of the beam. Radial velocities can be included in the program. Most calculations, however, were started at a point along the spent beam where radial velocities are still very low, and the computer calculated the correct radial velocities as the electron moved through the magnetic field transition region. The effects of space charge and angular velocity in the magnetic transition region are thereby included in the calculation.

Lens Effects

As an electron beam emerges from its cylindrical drift tube into a possibly asymmetric collector structure, it will be subject to certain lens effects associated with the transition from the drift tube to the collector. The analog computer program was expanded so that an available resistor network could be used to simulate this transition region at least in two dimensions. A full three dimensional treatment of this problem is very difficult, much like the space charge problem. The program as shown in Figure 5 is capable of analyzing the lens effect in the y-z plane. For the coordinate x different from zero, this analysis is no longer accurate. It was observed, however, that the defocusing effect of this transition region is quite weak when compared with the space charge and magnetic field defocusing actions. A two-dimensional treatment of this problem was therefore deemed sufficient at this time.

Amplifiers 20 through 28 in Figure 5 form the unloading networks used with the resistor network probe. This probe has a very high input impedance

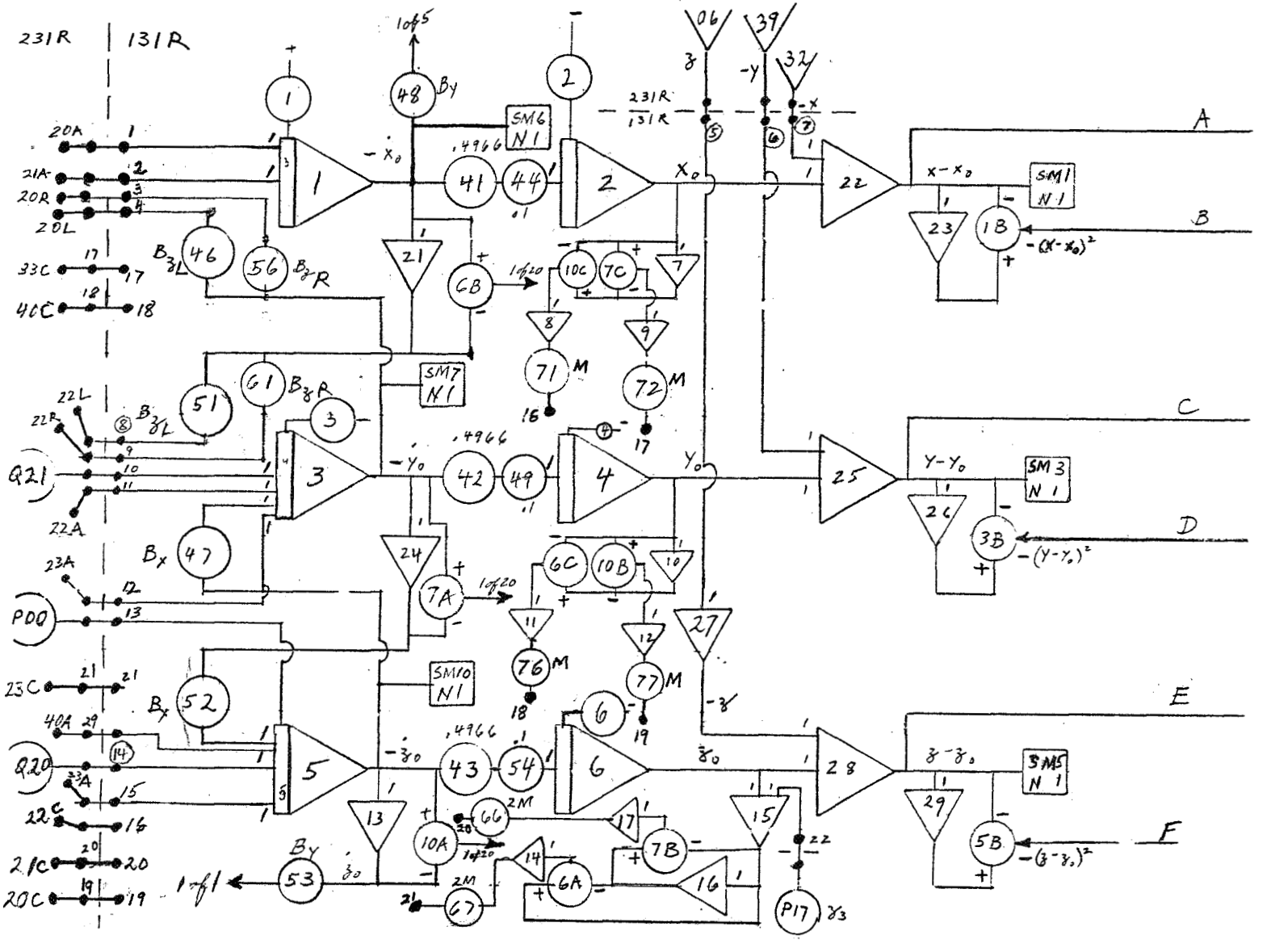

Figure 6a - Block Diagram for Program Extension for the Inclusion Space Charge

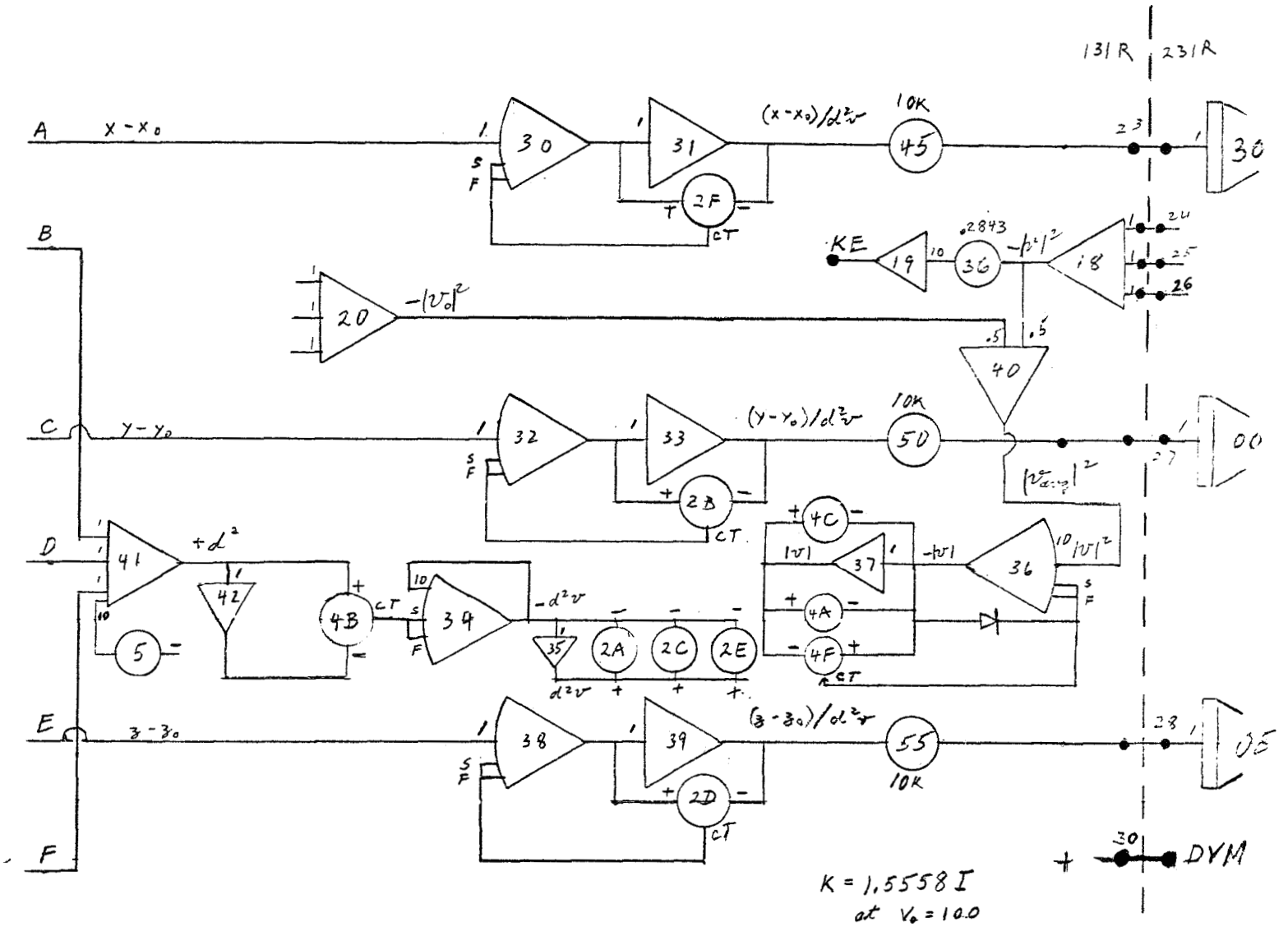

Figure 6b - Block Diagram for Program Extension for the Inclusion Space Charge

so that it will not disturb the local potentials on the network. Integrators 10 and 15, together with amplifiers 03, 04, 08, 09, 11, 16, 33, and 34 form the quantizing network which steps the probe from mesh-to-mesh as the trajectory is being computed.

In the preliminary and intermediate collector evaluations, space charge was ignored, but for the final evaluation trajectories were calculated both with and without space charge.

PRELIMINARY EVALUATION OF COLLECTORS

The conceptual discussion included in "The Collector Classification Chart" section and the analog computer program outlined in "Computer Programs" section provide a simple framework on which a preliminary evaluation of collector types may be performed. The basic structure of the collector classification chart is shown in Figure 2, but the addition of polarities and relative directions of E and B fields greatly increases the number of collector types to be investigated, as shown in Table II. In this table, the twenty-five cases shown in Figure 2 have been increased to sixty-four by allowing the polarity of the E and B field components to be positive or negative. This means that the angle between the E and B fields in the lower right hand four cases in Figure 2 takes on eight values, spaced 45 degrees apart. To identify the cases in Table II, an additional digit has been added to the original Type designation. In Table II, the axial direction is designated by the z component, the x is one of the transverse directions, and the r direction is radial. Only $+E_z$ fields are allowed since $-E_z$ fields would generally accelerate rather than retard electrons.

The sixty-four cases in Table II were given two preliminary screening tests on the analog computer omitting space charge. The first test was simply to determine whether a significant amount of retardation results when an on-axis, z-directed electron is injected into a specific field configuration. The notation "F" following the field polarity structure of a given collector in Table II indicates that the structure failed to remove at least half of the initial energy of the test electron. A letter "P" indicates that the collector met the requirements of the retardation test. The adjacent column marked "Test B" indicates the passage or failure of a simple backstreaming test. For instance, a Type 3.1 collector would satisfactorily retard electrons to zero energy, but these electrons would be reaccelerated directly back down the drift tube. Thus, a Type 3.1 collector fails the backstreaming test, as indicated by the "F" in the appropriate column in Table II.

TABLE II - COLLECTOR CLASSIFICATION LISTING, INCLUDING FIELD POLARITIES, SHOWING RESULTS OF PRELIMINARY RETARDING AND BACKSTREAMING TESTS

Name	Case	$B_{x,r}$	B_z	E_x	E_y	E_z	Tests	
							R	B
	1.11	0	0	0	0	0	F	F
	1.21	+	+	0	0	0	F	
	2	-	+	0	0	0	F	
	1.31	0	+	0	0	0	F	F
	1.41	+	+	0	0	0	F	
	1.51	+	0	0	0	0	F	
Reflex	2.11*	0	0	-	+		P	P
	2	0	0	+	+		P	F
	2.21	+	+	-	+		P	F
	2	+	+	+	+		P	F
	3	-	+	-	+		P	F
	4	-	+	+	+		P	F
	2.31	0	+	-	+		P	F
	2	0	+	+	+		P	F
	2.41	+	+	-	+			
	2	+	+	+	+			
	2.51	+	0	-	+			
	2	+	0	+	+			
	3.11	0	0	0	0	+	P	F
	3.21	+	+	0	0	+	P	F
	2	-	+	0	0	+	P	F
	3.31	0	+	0	0	+	P	F
TMF	3.41*	+	+	0	0	+	P	P
	3.51*	+	0	0	0	+	P	P
	4.11*	0	0	+	0	+	P	P
	4.21	+	+	+	0	+		
	2	-	+	+	0	+		
TEF	4.31*	0	+	+	0	+	P	P
	4.41*	+	+	0	-	+	P	P
	2	+	+	0	+	+	F	P

Continued on following page

TABLE II - (Continued)

Name	Case	$B_{x,r}$	B_z	E_x	E_y	E_z	Tests	
							R	B
	4.43	+	+	-	0	+	F	P
	4	+	+	+	0	+	F	P
	5	+	+	-	-	+	F	P
	6	+	+	-	+	+	F	P
	7*	+	+	+	-	+	P	P
	8	+	+	+	+	+	F	P
	4.51*	+	0	0	-	+	P	P
	2	+	0	0	+	+	F	P
	3	+	0	-	0	+	F	P
	4	+	0	+	0	+	F	P
	5*	+	0	-	-	+	P	P
	6	+	0	-	+	+	F	P
	7*	+	0	+	-	+	P	P
	8	+	0	+	+	+	F	P
	5.11	0	0	+	0	0	F	P
	5.21	+	+	+	0	0		
	2	-	+	+	0	0		
	5.31	0	+	+	0	0	F	P
	5.41	+	+	0	-	0	F	P
	2	+	+	0	+	0	F	P
	3	+	+	-	0	0	F	P
	4*	+	+	+	0	0	P	P
	5	+	+	-	-	0	F	P
	6	+	+	-	+	0	F	P
	7*	+	+	+	-	0	P	P
	8	+	+	+	+	0	F	P
Dunn	5.51*	+	0	0	-	0	P	P
	2	+	0	0	+	0	F	P
	3	+	0	-	0	0	F	P
	4	+	0	+	0	0	F	P
	5	+	0	-	-	0	F	P
	6	+	0	-	+	0	F	P
	7	+	0	+	-	0	F	P
	8	+	0	+	+	0	F	P

*Denotes collectors which pass both the retardation and the backstreaming test

Of the sixty-four cases shown in Table II, only thirteen cases passed both preliminary screening tests on the analog computer. The locations of these examples on the collector classification matrix are indicated in Table III. Although investigations of the "spreading-field" cases have not been as detailed as in other cases, the three cases, indicated in parenthesis, have also been considered as potential types to meet the requirements of both tests.

A more detailed evaluation of the sixteen collector types listed in Table III is given in Table IV. In this table, the degree of energy removal is indicated in the first column with the relative radial displacement at the minimum energy location shown in the second column. The latter is an indication of freedom from backstreaming. Collector performance has been rated "poor", "fair", or "good" according to energy removal percentages of <75, 70-90, and >90 percent, respectively. These ratings should be regarded only as approximations of potential collector performance until more detailed optimization studies are made. It should be emphasized that space charge was omitted in the preliminary evaluation.

Four collector Types (4.3, 4.41, 5.47 and 5.51) listed in Table IV appeared to show a good potential for further study. The latter type utilized a transverse magnetic field to deflect electrons; however, since it was similar to a collector being studied under another contract, no further investigation was made. Hence, only the first three collectors were considered for further study. Types 4.41 and 5.47 required a tilted magnetic field, whereas Type 4.3 utilized an axial magnetic field. The tilted magnetic field posed some practical shielding problems, which were not present with an axial field only. Thus, the Type 4.3 collector proved to be the most promising of the sixty-four cases considered originally. This collector type is identical with the TEF collector of Okoshi, et al.[16] The designation "Type 4.3 (TEF)" collector will be used to distinguish this collector from a Type 4.1 (TEF) collector, which also employs a tilted electric field but no magnetic field.

INTERMEDIATE EVALUATION OF TEF COLLECTORS

Preliminary screening of collector types was implemented on the basis of a full energy on-axis particle with no transverse velocity at the input plane, and without space charge. The most promising collector to emerge from this screening is the Type 4.3 (TEF) collector. Two fundamental parameters of this collector are: (1) the tilt angle θ_E of the electric field with respect to the z-axis, and (2) the strength of the magnetic field. The effect of these

TABLE III - COLLECTOR TYPES WHICH MEET PRELIMINARY RETARDATION AND BACKSTREAMING REQUIREMENTS

E FIELD \ B FIELD	zero N = .1	spread .2	axial .3	tilt .4	trans. .5
M = 1. zero					
2. spread	2.11			(2.4)	(2.5)
3. axial				3.4	3.5
4. tilt	4.1	(4.2)	4.3	4.41 4.47	4.51 4.55 4.57
5. trans.				5.44 5.47	5.51

TABLE IV - PRELIMINARY EVALUATION OF PROMISING COLLECTOR TYPES BASED ON ENERGY REMOVAL AND LACK OF BACKSTREAMING

Collector Type	Degree of Energy Removal	Relative Radius at V_{min}	Performance		
			Poor	Fair	Good
1. 2.11	-	-	-	-	-
2. (2.4)	-	-	-	-	-
3. (2.5)	-	-	-	-	-
4. 3.4	83%	1.25		x	
5. 3.5	83%	1.25		x	
6. 4.1	50%	.6	x		
7. (4.2)	-	-	-	-	-
8. 4.3	100%	.33			x
9. 4.41	96%	.4			x
10. 4.47	89%	1.22		x	
11. 4.51	0	0.6			
12. 4.55	63%	1.15	x		
13. 4.57	63%	1.05	x		
14. 5.44	68%	3.0	x		
15. 5.47	97%	2.9			x
16. 5.51	100%	2.88			x

parameters are evaluated in this section. The results of these evaluations show that the presence of a magnetic field significantly improves the efficiency of a TEF collector, and that a tilt angle of 45 degrees is a reasonably optimum choice for this parameter.

Effect of Tilt Angle of Electric Field

From Figure 2 note that starting with a Type 4.3 (TEF) collector, as the tilt angle of the electric field with respect to the z-axis is varied from 0 to 90 degrees, the resulting triad of cases constitute the sequence of collector Types 3.3, 4.3 and 5.3. An even simpler sequence of TEF collectors is the triad of Types 3.1, 4.1 and 5.1, in which case the magnetic field strength is zero. In the latter case the visualization of trajectories is much simpler than in the case with finite magnetic field, since the trajectories lie in the plane of the E field. Furthermore, the sequence of Types 3.1, 4.1 and 5.1 represents a limiting case for the sequence of Types 3.3, 4.3 and 5.3 as magnetic field is reduced to zero. Hence, the performance of collectors utilizing no magnetic field is a convenient focal point for planning and discussing techniques for intermediate collector evaluation.

A very significant difference between the two sequences of collectors mentioned above was disclosed by a simple test and the results are shown in Figure 7. As the tilt angle is increased in the zero magnetic field TEF sequence of Types 3.1, 4.1 and 5.1, the ability of the collector to remove energy is reduced. For instance, from Figure 7 it is evident that for a tilt angle of 45 degrees, the collector is able to remove only one-half of the initial energy before the particle begins to be re-accelerated. The energy removal efficiency of this sequence of collectors is unity for an angle of zero degrees, in which case the collector is a Type 3.1 collector. However, a Type 3.1 collector fails the backstreaming test, according to Table II, therefore, this collector cannot be considered for final use.

As the upper curves in Figure 7 show, the addition of a magnetic field greatly improves the performance of a TEF collector. Not evident from Figure 7 is the fact that the plane of the trajectory rotates 90 degrees such that the main motion is in a direction at right angles to the transverse E component. This motion is discussed more thoroughly in the section entitled, "Final Collector and Evaluation". Of significance here is the great improvement in collector efficiency for all angles of electric field tilt by the addition of a magnetic field. For the highest magnetic field strength, the efficiency of energy removal is virtually 100 percent, regardless of electric field tilt.

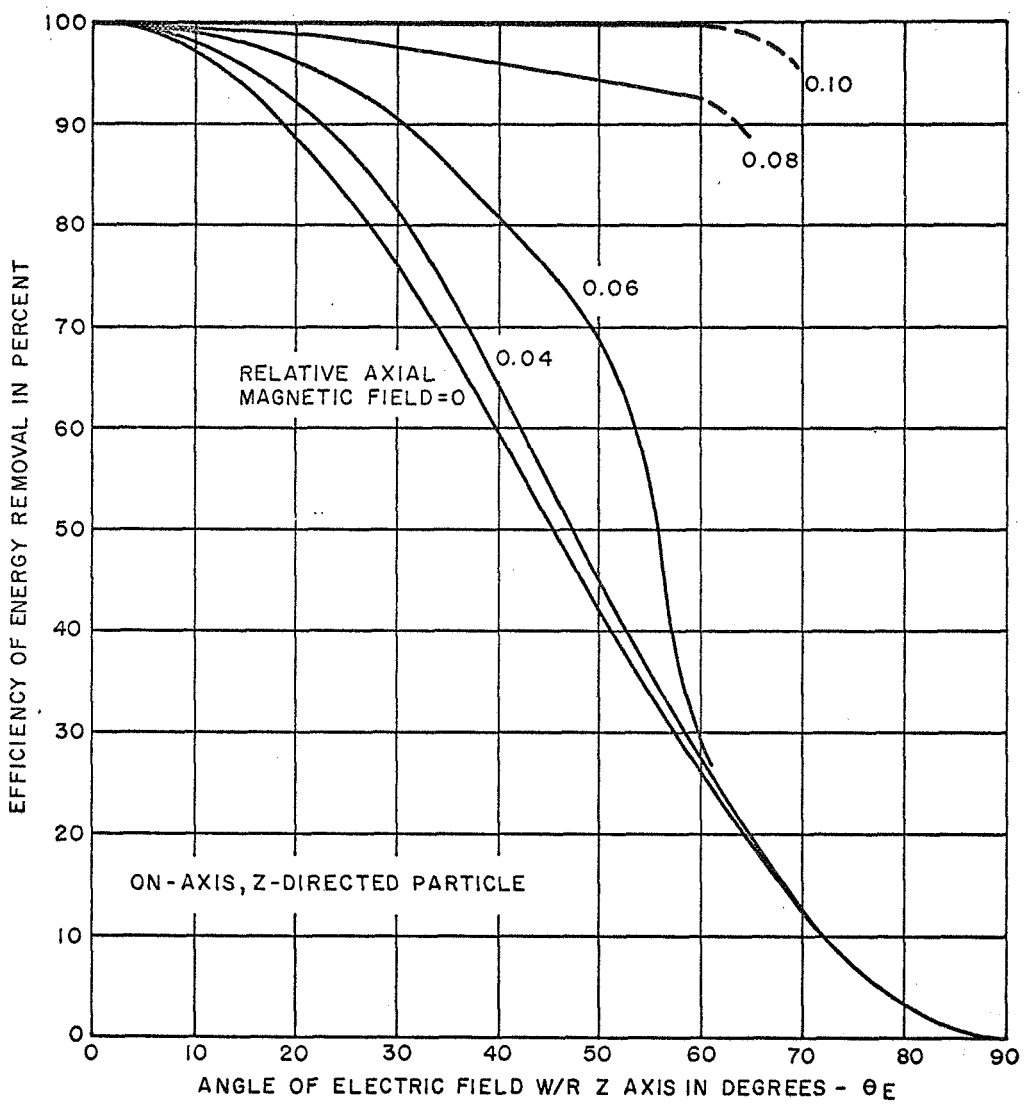

Figure 7 - Efficiency of Energy Removal in TEF Collectors as a Function of Tilt Angle of Electric Field, with Axial Magnetic Field Strength as a Parameter

Effect of Transverse Velocities and Energy Spread

The energy removal efficiency of nearly 100 percent for the TEF collector with a magnetic field (see Figure 7) was very encouraging, but three important considerations were disregarded in this primary examination: (1) input energy spread, (2) transverse velocities at the input plane, and (3) finite beam diameter. In the second step of the intermediate evaluation described below, constraints (1) and (2) were removed; the third constraint was removed in the final evaluation.

At the intermediate stage of the evaluation it was necessary to determine the locus of an electrode edge. In this section it has been assumed that a large number of electrodes was used, so that there was no deterioration of efficiency due to electrode number. This constraint, which is discussed in detail later, was removed in the final evaluation.

To determine the electrode edge locus for a given collector, the trajectories of ten z-directed electrons were plotted as a function of input energy for electrons with energies ranging from 0.1 V_o to 1.0 V_o in steps of 0.1 V_o. The minimum energy points on these trajectories were noted, and these points were connected with a line which was taken to be the electrode edge locus. Once this locus was established, transverse velocities were introduced. To keep the investigation within bounds at this stage the number of energy classes under consideration was now reduced to four, namely, 0.25 V_o, 0.50 V_o, 0.75 V_o and 1.0 V_o. For each of these energy classes, in addition to the z-directed electron trajectory, four additional trajectories were plotted. Beginning from the same point on the z-axis, input transverse velocities of appropriate magnitudes (see next paragraph) were applied in both transverse directions: $\pm \dot{x}_o$ and $\pm \dot{y}_o$. The energies with which these four particles crossed the previously established electrode edge locus line were noted. Thus, five energy numbers were obtained for each of four input energy classes. The five numbers were averaged to give an average energy removal efficiency for each of the four energy classes. These four numbers were then averaged with equal weighting to give collector efficiency in the presence of an energy spread and transverse velocities. This "picket fence" approach gave a number that was approximately indicative of collector efficiency under typical rf conditions, when the energy of the spent beam was more or less uniformly spread across the energy sprectrum.

The transverse velocities associated with each energy class were chosen to give entry angles of 20, 15, 10 and 5 degrees for initial energies of 0.25 V_o, 0.5 V_o, 0.75 V_o, and 1.0 V_o, respectively. These numbers

were based on the results of some early analog computer beam trajectory work done at General Electric Company, and are consistent with some early unpublished work by H. Kosmahl. This point was not pursued in greater detail here because in the final evaluation these angles were determined by the calculation and were not arbitrarily imposed as done here.

The final results of the intermediate evaluation of collection efficiency are shown in Figure 8. The average collection efficiency is plotted as a function of tilt angle with normalized field strength $eB_z/10m\beta$ as a parameter, where β is the computer time scale factor. With zero magnetic field the optimum tilt angle for the chosen input conditions is about 20 degrees, at which point the collection efficiency is 70 percent. The addition of a small magnetic field increases both the optimum tilt angle and the collector efficiency. At the highest value that was tried for the magnetic field parameter ($eB/10m\beta = 0.5$), the optimum tilt angle is slightly larger than 45 degrees, and the collection efficiency approaches 90 percent.

On the basis of these data, the angle of the electric field was fixed at 45 degrees for the final evaluation of the Type 4.3 (TEF) collector. In the following section, the exact basis for collector analysis is established, and following this, several illustrative examples are explained.

THEORETICAL ANALYSIS OF COLLECTORS

The exact analysis of collector performance requires knowledge of both the collector efficiency characteristic and the spent beam power distribution characteristic. In this section exact expressions are derived which can be used to calculate collector efficiency if both of these characteristics are known in detail for a specific tube.

Efficiency as a Function of Energy

An easily measured or computed characteristic of any depressed collector is the curve relating dc collector efficiency and electron energy. Experimentally this curve can be established approximately by measuring collector efficiency for a dc beam for various values of cathode voltage, while keeping the collector electrode voltages and the magnetic field constant. This method neglects the transverse velocity effects in the spent beam which are due to the rf interaction process. It does include the transverse velocity effects caused by magnetic field spreading and possible beam scalloping. Computationally, this characteristic is established by injecting electrons of

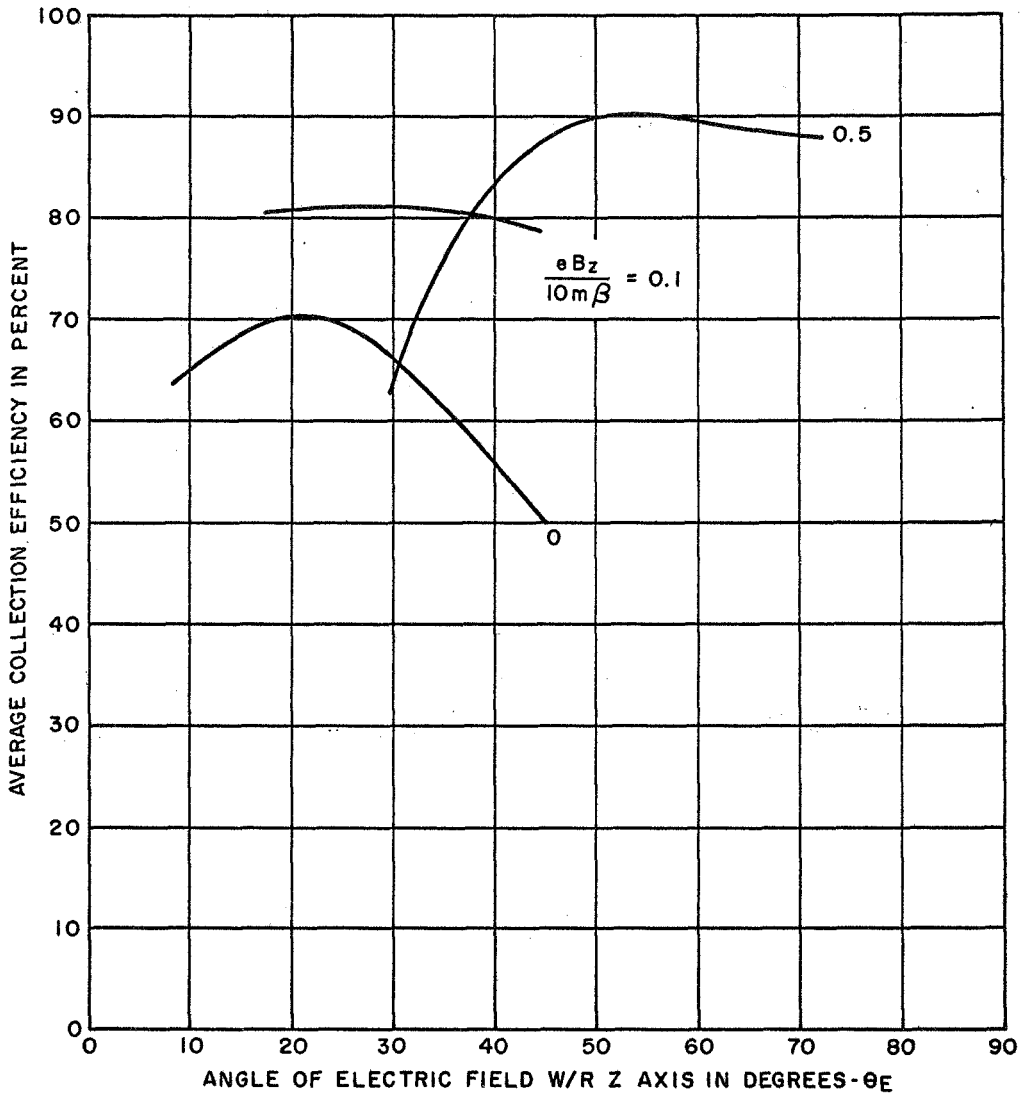

Figure 8 - Average Collection Efficiency in TEF Collectors as a Function of Tilt Angle of Electric Field, with Axial Field Strength as a Parameter

various energies with their associated transverse velocities into the collector and calculating collection efficiency as a function of energy. In general, this characteristic is a curve similar to the one shown in Figure 9a, where η_c is the ratio of recovered to incident energy for any given energy class. The parameter V_o is the cathode voltage. Very low energy electrons are unable to reach any depressed electrodes and, therefore, show zero collection efficiency. Faster electrons, in general, allow considerable energy recovery as shown. Once this characteristic of a collector is established, and the spent beam energy distribution is known, it is possible to predict the performance under rf conditions.

Spent Beam Energy Distribution

Before a depressed collector can be successfully matched to a klystron or traveling wave tube, something must be known about the electron beam after it has passed through the rf interaction region. Again, this characteristic may be established either experimentally or computationally. The most useful form of this characteristic, from the standpoint of collector analysis, is a curve of power density as a function of electron energy. Typical curves of this nature are shown in Figure 9b for both klystrons and traveling wave tubes. In general, very few electrons have energies approaching twice the dc beam voltage, but a considerable number have energies below it. A given power density can be established by either many electrons per second traveling slowly or a few electrons per second traveling very fast. The current density distribution of the spent beam is proportional to p(V)/V.

Two important constraints must be satisfied by the distributions in Figure 9b. First, energy must be conserved. If η_o is the base efficiency of the tube and P_o is the dc beam power, energy conservation requires that

$$(1 - \eta_o)P_o = \int_o^{2V_o} p(V)dV \tag{8}$$

In words, the power in the spent beam must be equal to the dc beam power less the rf power, assuming perfect beam transmission. The second constraint is implied by the law of charge conservation. In the absence of beam interception, the total cathode current I_o must reach the collector. Therefore, the relation

$$I_o = \int_o^{2V_o} \frac{p(V)}{V} dV \tag{9}$$

must also be satisfied by the distribution of Figure 9b.

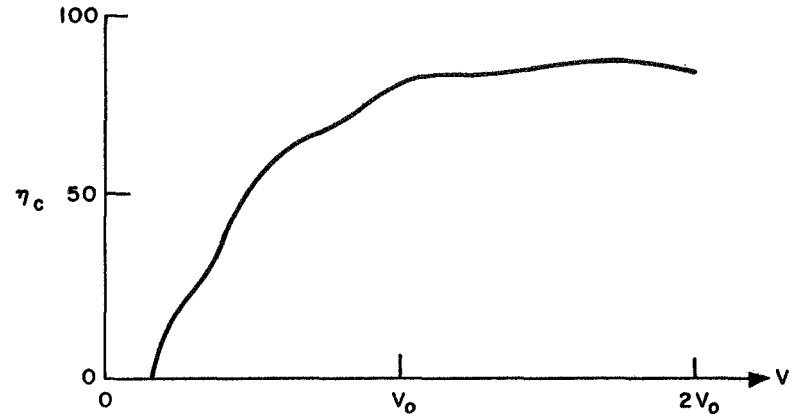

Figure 9a - Collection Efficiency as a Function of Beam Energy in a Typical Collector

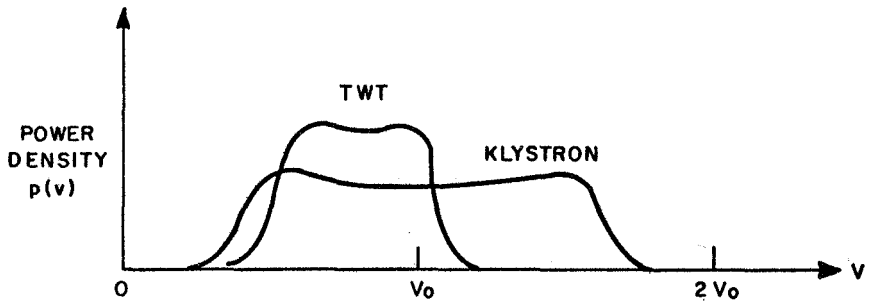

Figure 9b - Spent Beam Power Distributions as a Function of Beam Energy in a Typical Klystron and TWT

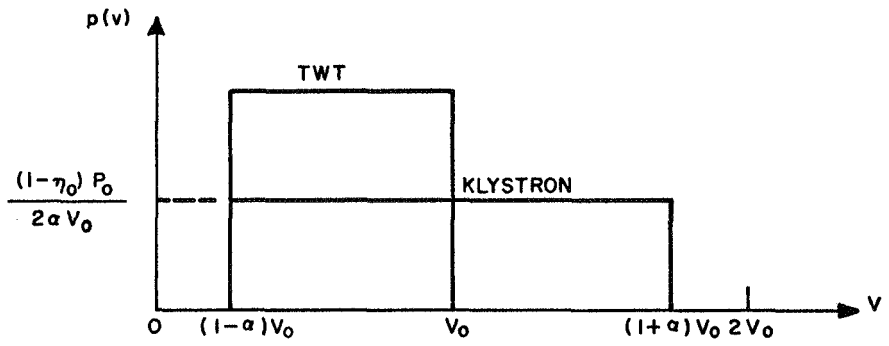

Figure 9c - Idealized Flat Symmetrical and One-Sided Power Density Distributions as a Function of Beam Energy

Prediction of Collector Performance

The power, P_{rec}, recovered from the spent beam by a depressed collector is a summation of the increments of power recovered from each energy class, or, in the limit

$$P_{rec} = \int_{o}^{2V_o} \eta_c(V)p(V)dV \tag{10}$$

where p(V) is subject to the constraints mentioned earlier. The collector efficiency η_{c-rf} associated with a p(V) power distribution is the ratio of the recovered power to the total spent beam power as given in Equation (8).

$$\eta_{c-rf} = \frac{P_{rec}}{P_o(1-\eta_o)} = \frac{1}{P_o(1-\eta_o)} \int_{o}^{2V_o} \eta_c(V)p(V)dV \tag{11}$$

Once the collector efficiency is known, the net tube efficiency η can be written in terms of the base efficiency η_o and η_{c-rf}, as shown under "Basic Concepts and Definitions".

$$\eta = \frac{\eta_o}{1 + (1-\eta_o)(1-\eta_{c-rf})} \tag{12}$$

In summary, therefore, if the collector characteristic $\eta_c(V)$ and the spent beam power distribution p(V) are known, the tube and collector performance can be predicted using the equations developed in this section. In order to achieve a broader view of collector performance on klystrons and TWTs, it is necessary to resort to some simplifying assumptions regarding spent beam power distribution. This is done in the following section.

APPROXIMATE COLLECTOR ANALYSIS USING FLAT SPENT BEAM POWER DISTRIBUTIONS

The exact expressions developed in the preceding section may be used to predict collector performance for a specific tube. However, it is desirable to make a more general evaluation of collectors, without restriction to a specific spent beam power distribution. In this section the simplifying assumption of an idealized flat spent beam power spectrum will be used to develop some useful approximate expressions for rf collector efficiency.

Approximate expressions for rf collector efficiency will be developed for two cases: (1) a symmetrical flat power distribution extending from $(1-\alpha)V_o$ to $(1+\alpha)V_o$, and (2) a one-sided flat power distribution extending from $(1-\alpha)V_o$ to V_o. The parameter α is termed the "spectrum width" parameter. In Appendix A it is shown that the symmetrical case corresponds roughly to the spent beam power distribution found in a klystron. In a TWT, the bulk of the spent beam electrons arrive at the collector with energies less than eV_o, hence, a one-sided power spectrum can be taken as a first approximation to the spent beam spectrum. The two idealized power spectra are illustrated in Figure 9c.

Based on the simplifying assumption of a flat spectrum, the characteristics of two distinct collector types were studied: (1) a "constant-margin collector", so called because the energy loss due to heating of the collector is the same for all velocity classes, and (2) a collector with its most negative electrode at cathode potential. In general, the constant margin collector has a higher efficiency than the latter. However, a collector having no electrodes more negative than the cathode has the advantage of requiring less complex power conditioning circuitry.

Relationship Between Base Tube Efficiency and Power Distribution Width for Symmetric and One-Sided Spectra

The constraining Equations (8) and (9) will now be applied to the symmetric and asymmetric flat spent beam power spectra, respectively, to arrive at the relationship between the spectrum width parameter α and the undepressed tube efficiency η_o. The energy conservation constraint Equation (8) when applied to the symmetrical distribution requires that its amplitude be $(1-\eta_o)P_o/2\alpha V_o$. The charge conservation constraint (9) requires that the relation

$$1 = \frac{1-\eta_o}{2\alpha} \ln\left(\frac{1+\alpha}{1-\alpha}\right) \tag{13}$$

be satisfied. When this equation is solved for η_o it yields

$$\eta_o = 1 - 2\alpha / \ln\left(\frac{1+\alpha}{1-\alpha}\right) \quad \text{(symmetric spectrum)} \tag{14}$$

which is one of the curves plotted in Figure 10. The assumption of a flat power distribution and a symmetrical voltage spectrum has led to a specific relation between η_o and the width of the spectrum. For example, a tube having a base efficiency η_o equal to 39 percent must have a spent beam spectrum extending between the limits of $(1 \pm .9)V_o$ if the symmetrical flat power distribution assumption is to be valid. This is a very reasonable

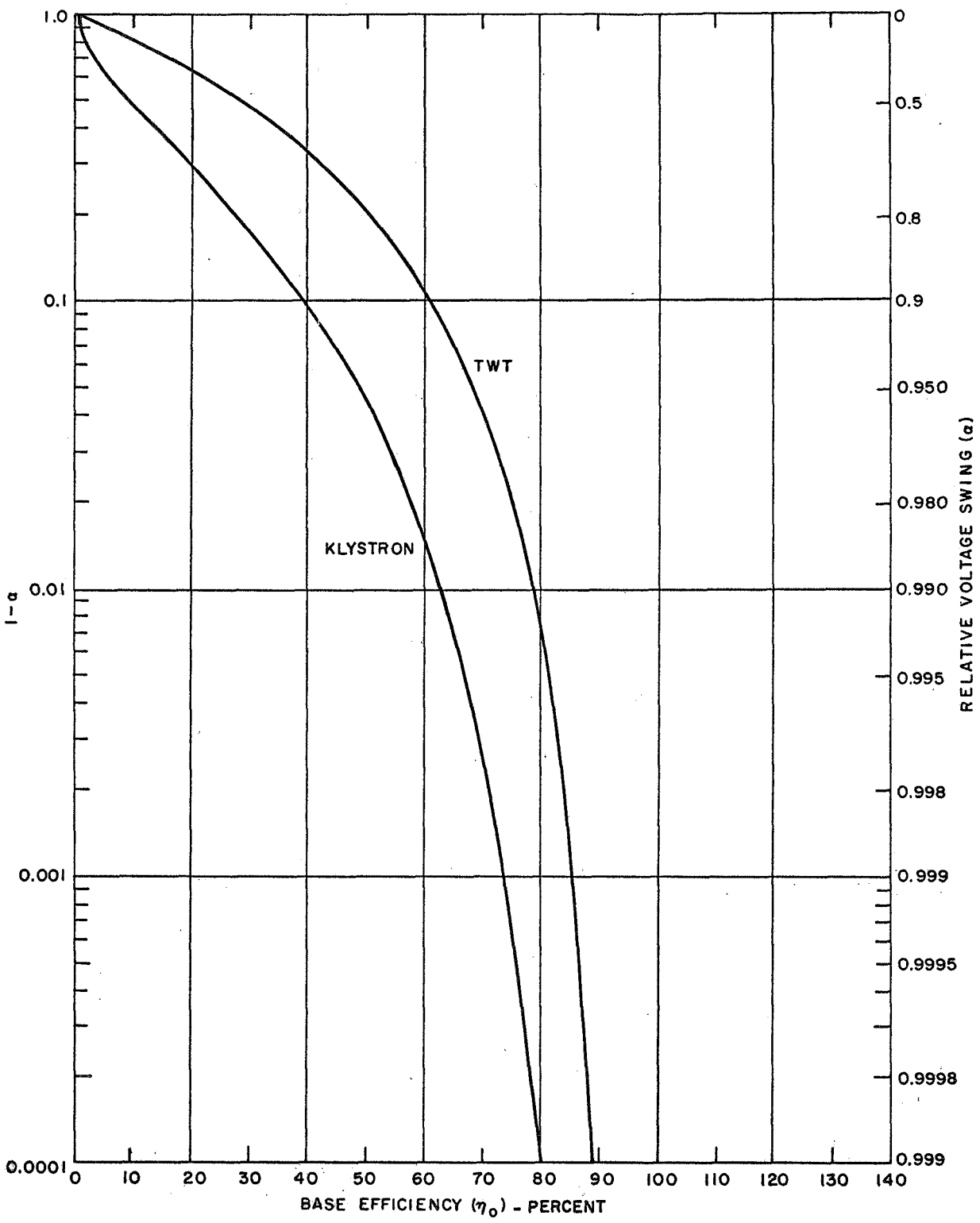

Figure 10 - Spectrum Width Parameter as a Function of Base Tube Efficiency for Symmetric and One-Sided Flat Power Density Distribution

relationship, and it is close to that existing in a practical klystron, adding credibility to the approximate applicability of a symmetrical flat spent beam power spectrum to klystrons.

When constraining Equations (8) and (9) are applied to the one-sided flat power distribution shown in Figure 9c the relation between tube efficiency and voltage swing becomes

$$\eta_o = 1 + \frac{\alpha}{\ell n\,(1 - \alpha)} \qquad \text{(one-sided spectrum)} \qquad (15)$$

which is also shown in Figure 10. It is evident from Figure 10 that for a given base efficiency η_o the voltage swing with a symmetric spent beam power distribution must be larger than with a one-sided distribution. The use of a one-sided spectrum is shown in the section entitled, "Effect of Number of Electrodes", to give a result reasonably close to that obtained using an accurate spent beam power distribution for a TWT.

Constant-Margin Collectors

There is a unique form of collector which leads to an unusually simple conceptual and mathematical result. It is called a "constant-margin" collector. The margin, m, is defined as the normalized residual energy with which the electrons impinge on the collector electrodes, and is expressed as a fraction of the dc beam voltage:

$$\text{Energy lost per electron} = mV_o \text{ electron volts} \qquad (16)$$

A perfect collector would have a margin equal to zero, but since some energy is lost by the sorting, secondary suppression, and transverse velocity effects, the margin can never be zero. Typical collectors exhibit a margin between 0.1 and 0.2 while an excellent collector may exhibit a margin near 0.05.

The feature that makes "margin" a useful concept is that experience has shown that collectors often exhibit the unusual property of having a margin which is practically independent of the energy class of the entering electrons.

In the case of a constant-margin collector, the collector efficiency η_c as shown in Figure 9a can be written as a simple analytic expression. If mV_o is lost as heat by each electron then $V - mV_o$ is the recovered energy and the efficiency is given by

$$\eta_c = \frac{V - mV_o}{V} = 1 - m\,\frac{V_o}{V} \qquad \frac{V}{V_o} > m$$

$$= 0 \qquad \frac{V}{V_o} < m \tag{17}$$

Using Equation (17) the rf collector efficiency η_{c-rf} for a constant-margin collector can now be computed using both forms of flat power density distribution.

Use of a symmetrical voltage swing power density distribution in a constant-margin collector yields the expression

$$\eta_{c-rf} = \begin{cases} \dfrac{1}{2\alpha V_o} \displaystyle\int_{(1-\alpha)V_o}^{(1+\alpha)V_o} \left(1 - \frac{mV_o}{V}\right) dV & m < 1-\alpha \\[2ex] \dfrac{1}{2\alpha V_o} \displaystyle\int_{mV_o}^{(1+\alpha)V_o} \left(1 - \frac{mV_o}{V}\right) dV & m > 1-\alpha \end{cases} \tag{18}$$

The indicated integrations are easy to perform with the result

$$\eta_{c-rf} = \begin{cases} 1 - \dfrac{m}{(1-\eta_o)} & m < 1-\alpha \\[2ex] 0.5 + \dfrac{1-m}{2\alpha} - \dfrac{m}{2\alpha}\,\ell n\left(\dfrac{1+\alpha}{m}\right) & m > 1-\alpha \end{cases} \tag{19}$$

where the constraint Equation (13) must be applied to the second part of Equation (19). In the first part of Equation (19) it was possible to eliminate α by direct substitution. The rf collector efficiency is shown as a function of the base efficiency η_o in Figure 11 for various values of the margin. At zero base efficiency the collector is subjected to the monoenergetic dc beam and the collector efficiency clearly is 1 - m. At high base efficiencies the rf collector efficiency approaches the average value of the collector efficiency

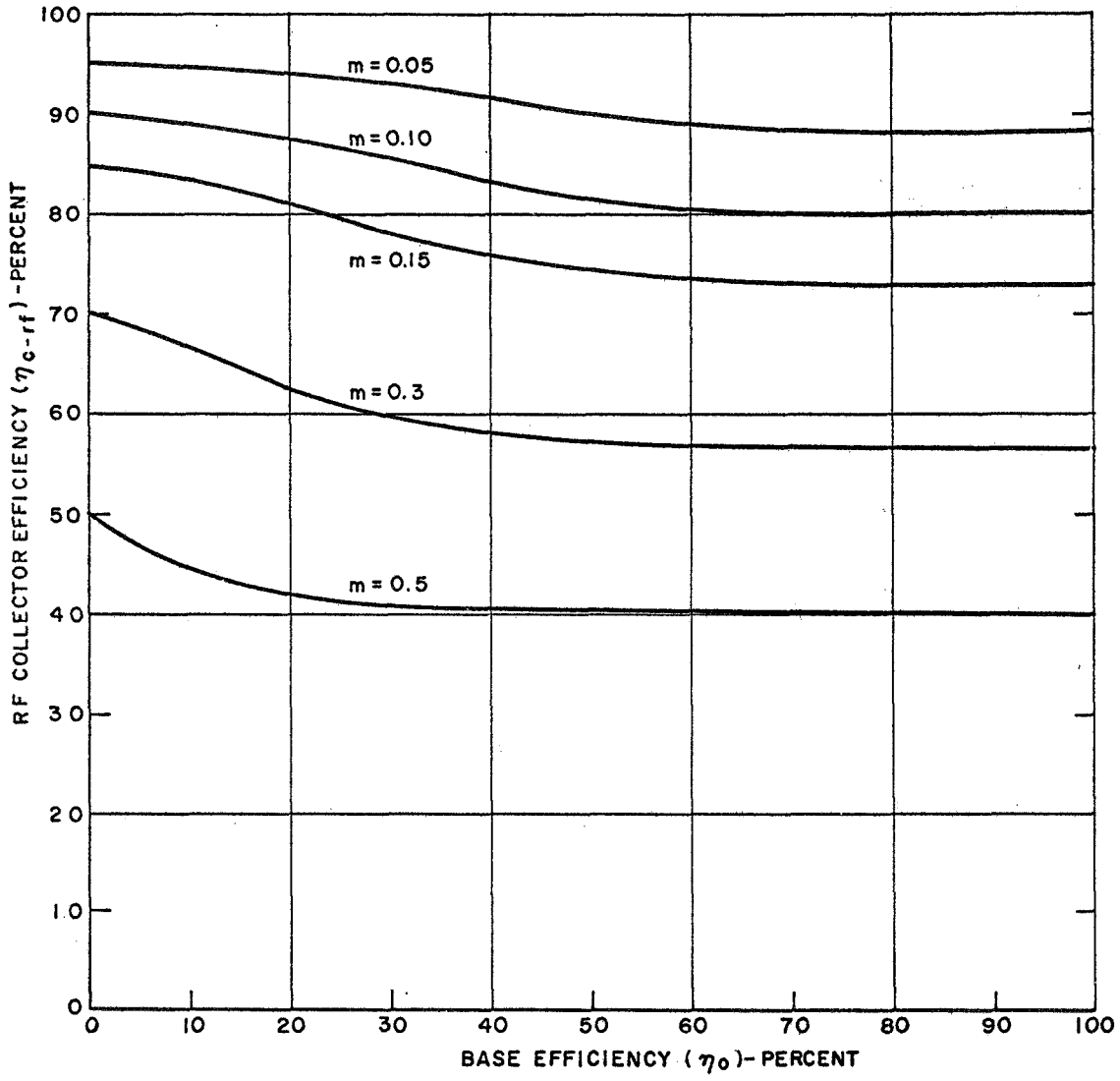

Figure 11 - RF Collector Efficiency of a Constant Margin Collector as a Function of Base Tube Efficiency with Margin as a Parameter, Assuming a Symmetric Flat Power Density Distribution

versus electron energy curve. Since the curves of Figure 11 are relatively flat for high base efficiencies, the asymtotic value $\bar{\eta}_c$ is a good estimate of the rf collector efficiency η_{c-rf}. This approximation is particularly good if the base tube efficiency is 40 percent or higher. Figure 11 also shows that the asymtotic value of η_{c-rf}, $\bar{\eta}_c$, is always a pessimistic measure of collector efficiency.

Substitution of Equation (19) into Equation (12) yields the net tube efficiency as a function of base efficiency and margin. For $m < 1 - \alpha$ the result is given by:

$$\eta = \frac{\eta_o}{\eta_o + m} \qquad m < 1 - \alpha \qquad (20)$$

The condition $m < 1 - \alpha$ implies that every electron causes mV_o electron volts of heating in the collector and therefore Equation (20) could be written directly from considerations of energy flow. Under these circumstances in a constant-margin collector the improvement in tube efficiency from η_o to η is independent of the spent beam power distribution spectrum.

When $m > 1 - \alpha$, not all electrons possess mV_o of energy, and therefore cannot heat the collector as much as the more energetic electrons. For the latter condition, the second part of Equation (19) must be substituted into Equation (12) to obtain the net tube efficiency. The result is given in Figure 12 where net tube efficiency is shown as a function of η_o and m. It can be seen from Figure 12 that for sizable improvement in tube efficiency, the margin of a collector should be as small as possible.

Tent Collector

In certain applications for depressed collectors it may be undesirable to construct power supplies having voltage terminals more negative than cathode potential and having the ability to absorb high voltage dc power and converting it to useful electrical power. In a constant-margin collector all the supplies between 0 and V_o deliver power to the tube while all the supplies between V_o and $2V_o$ must in some way be made to accept power. This situation may be avoided by specifying that the most negative collector electrodes be at cathode potential. Unfortunately, this is accompanied by a loss of collector efficiency. The efficiency characteristic of this type of collector, shown in Figure 13, drops between V_o and $2V_o$, and this suggests the name "tent collector". For electron energies below $(1+m)V_o$, the behavior of this collector is identical to that of a constant-margin collector. All electrons having energies above $(1+m)V_o$ are collected on the V_o electrode and,

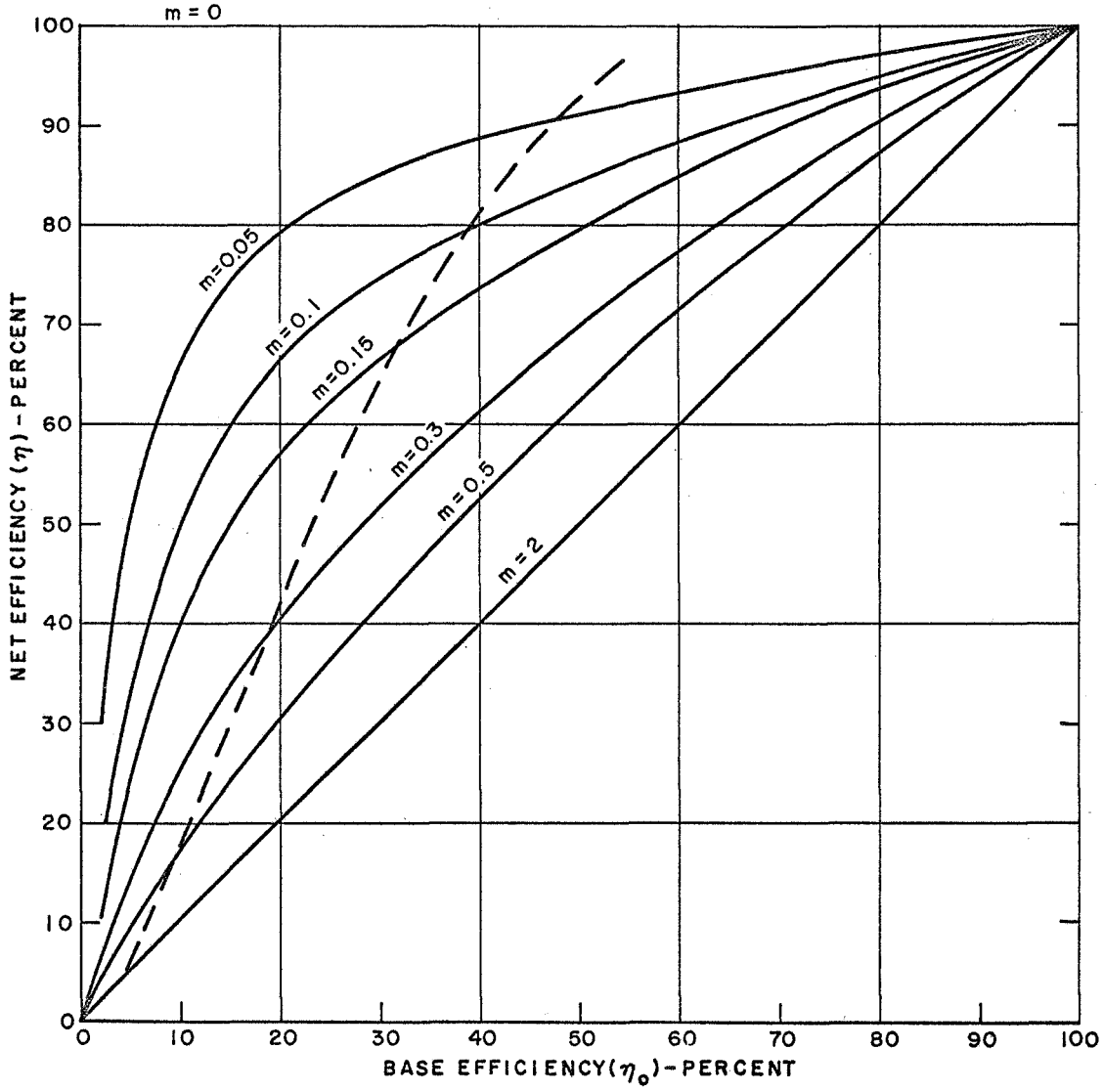

Figure 12 - Net Tube Efficiency with Collector Depression as a Function of Base Tube Efficiency, with Margin as a Parameter, Assuming Symmetric Flat Power Density Distribution

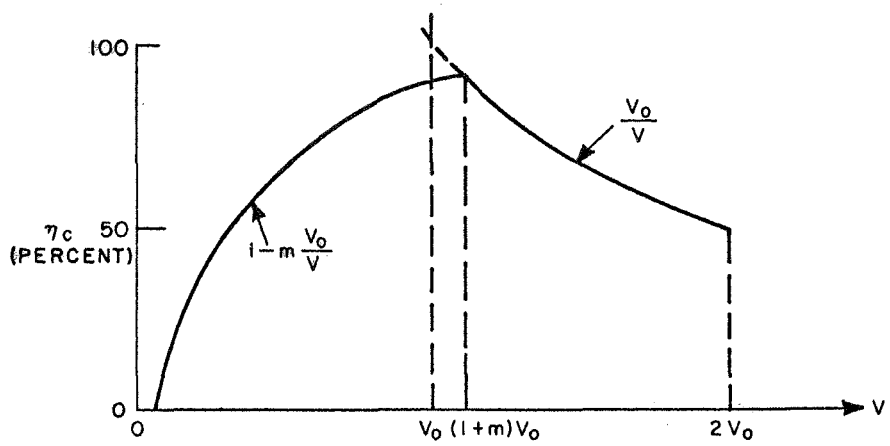

Figure 13 - Tent-Collector Efficiency as a Function of Beam Energy

therefore, the collection efficiency for these electrons is merely the ratio V_o/V. Special precautions must be taken to prevent secondary electron emission at the V_o electrode if this is the final electrode in the collector.

The tent collector can be analyzed by the method previously outlined. If a flat, symmetric power density distribution is assumed, the expression for the rf collector efficiency is

$$\eta_{c\text{-}rf} = \begin{cases} \dfrac{m+\alpha}{2\alpha} - \dfrac{m}{2\alpha}\,\ell n\left(\dfrac{1+m}{1-\alpha}\right) + \dfrac{1}{2\alpha}\,\ell n\left(\dfrac{1+\alpha}{1+m}\right) & m < 1-\alpha \\[2ex] \dfrac{1}{2\alpha} - \dfrac{m}{2\alpha}\,\ell n\left(\dfrac{1+m}{m}\right) + \dfrac{1}{2\alpha}\,\ell n\left(\dfrac{1+\alpha}{1+m}\right) & m > 1-\alpha \end{cases} \tag{21}$$

provided $m < \alpha$, which is true for cases of practical interest. The rf collector efficiency as computed from Equation (21) is shown in Figure 14 as a function of the basic tube efficiency. When compared with the constant-

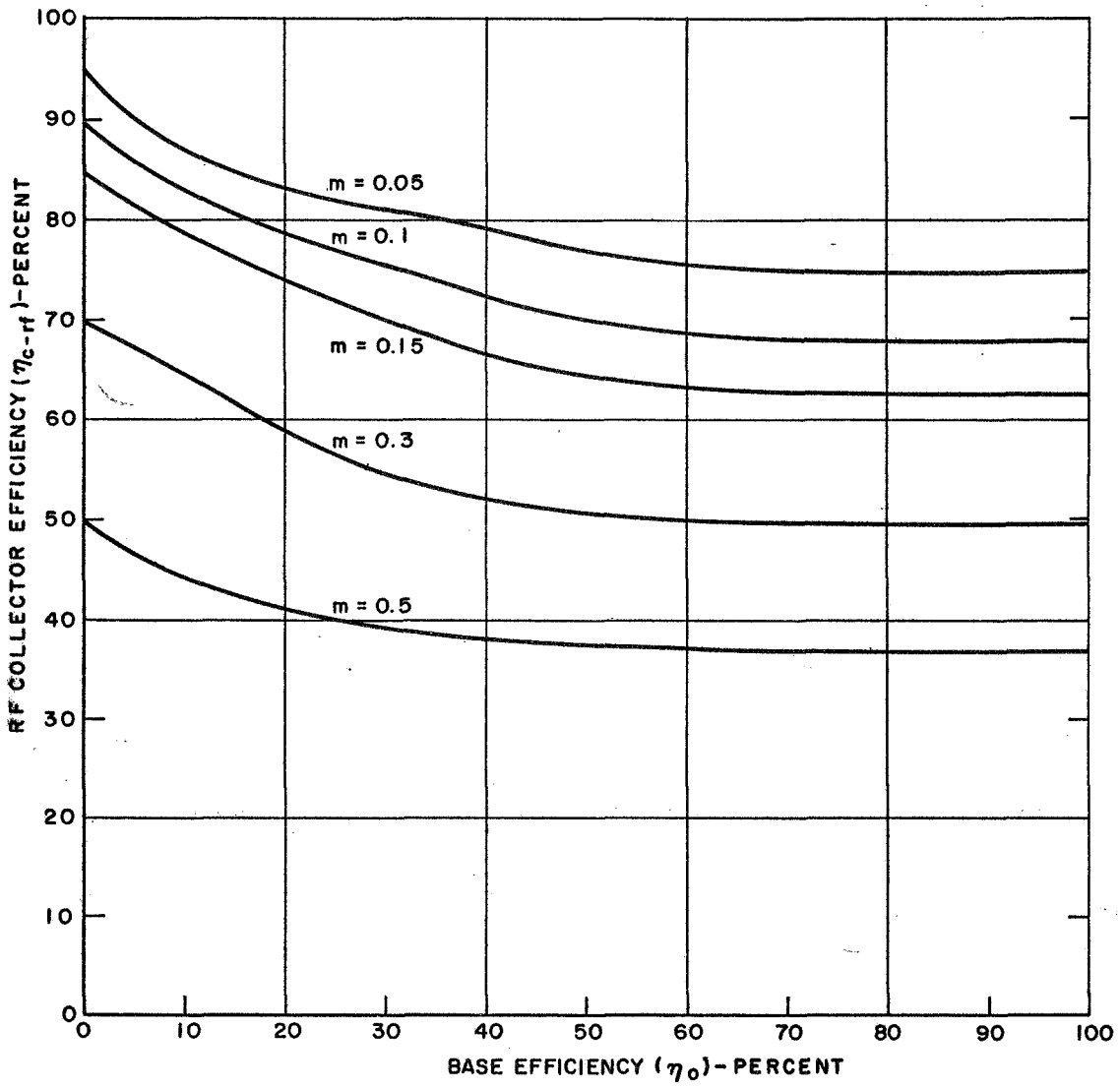

Figure 14 - RF Collector Efficiency of a Tent-Collector as a Function of Base Tube Efficiency with Margin as a Parameter, Assuming a Symmetric Flat Power Density Distribution

margin collector performance shown in Figure 11 it can be seen that the rf collector efficiency of the tent collector is significantly lower for tubes of practical interest. The dc efficiency of both collector types is the same for the same margin, namely, 1-m, but the right hand asymtote, namely $\bar{\eta}_c$, is lower for the tent collector.

The net tube efficiency with a tent collector has been calculated from Equations (21) and (12) and is shown in Figure 15. Here, too, it may be seen that the net tube performance has suffered, especially for low margin collectors. For margins greater than 0.5 the performance is equally poor for both types of collectors.

Collector Performance with Tubes Having One-Sided Power Density Distributions

When the spent beam power density distribution is flat between $(1-\alpha)V_o$ and V_o and zero above V_o, the expression for the rf collector efficiency is the same for both a constant-margin collector and a tent collector and can be written as

$$\eta_{c-rf} = \begin{cases} 1 - \dfrac{m}{1-\eta_o} & m < 1-\alpha \\[2ex] \dfrac{1-m}{\alpha} - \dfrac{m}{\alpha}\,\ell n\left(\dfrac{1}{m}\right) & m > 1-\alpha \end{cases} \tag{22}$$

In this case α and η_o are related by Equation (15). Figure 16 shows the variation of the rf collector efficiency with η_o for various collector margins. Comparison with Figure 11 reveals that η_{c-rf} slumps much more with increasing η_o if the spent beam has the one-sided power density distribution which approximates a TWT beam.

The net tube efficiency with a one-sided spent beam spectrum is found by substituting the result of Equation (22) into Equation (12) and is plotted in Figure 17. For low base efficiencies these curves are the same as those for a symmetric spectrum, as shown in Figure 12. For higher base tube efficiencies, the net tube efficiency with a one-sided spectrum lies below that of a tube with a symmetric spectrum for a collector of the same margin.

In this section several idealized examples have been analyzed in detail to demonstrate the relationships that exist for collectors operating on tubes with different base efficiencies. In the next section attention will be restricted

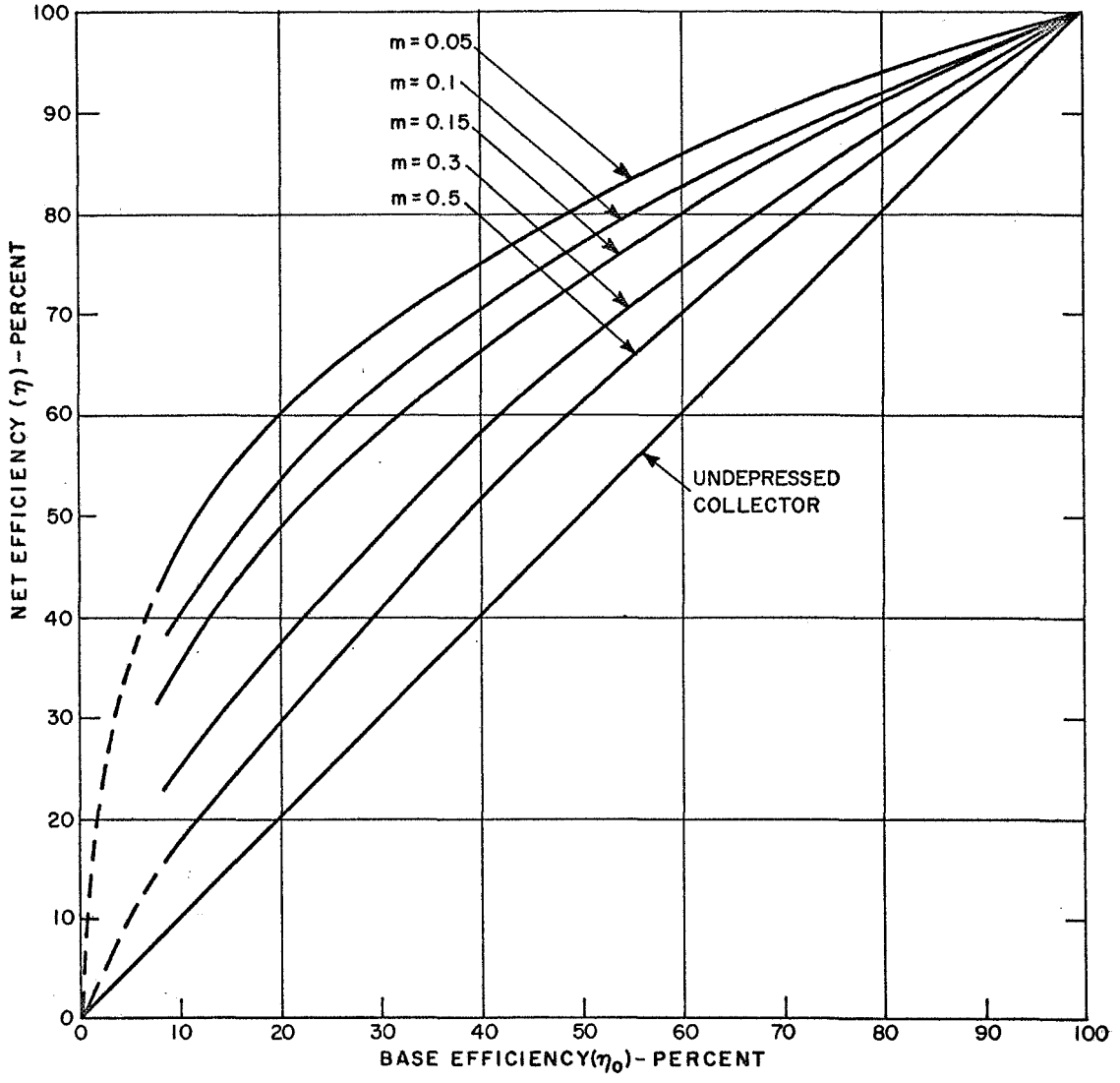

Figure 15 - Net Tube Efficiency of a Tent-Collector as a Function of Base Tube Efficiency with Margin as a Parameter, Assuming a Symmetric Flat Power Density Distribution

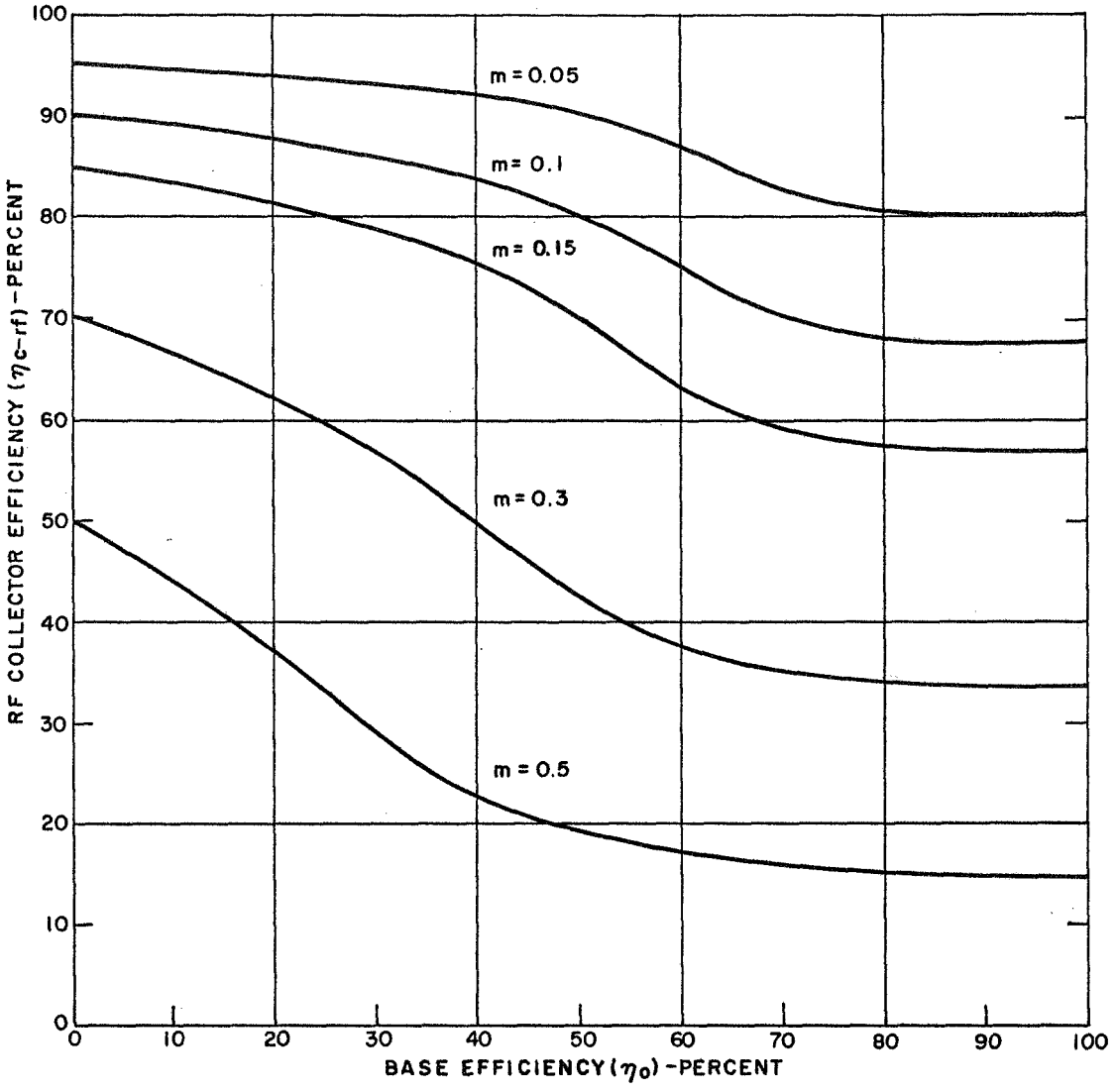

Figure 16 - RF Collector Efficiency as a Function of Base Tube Efficiency, with Margin as a Parameter, Assuming a One-Sided Power Density Distribution

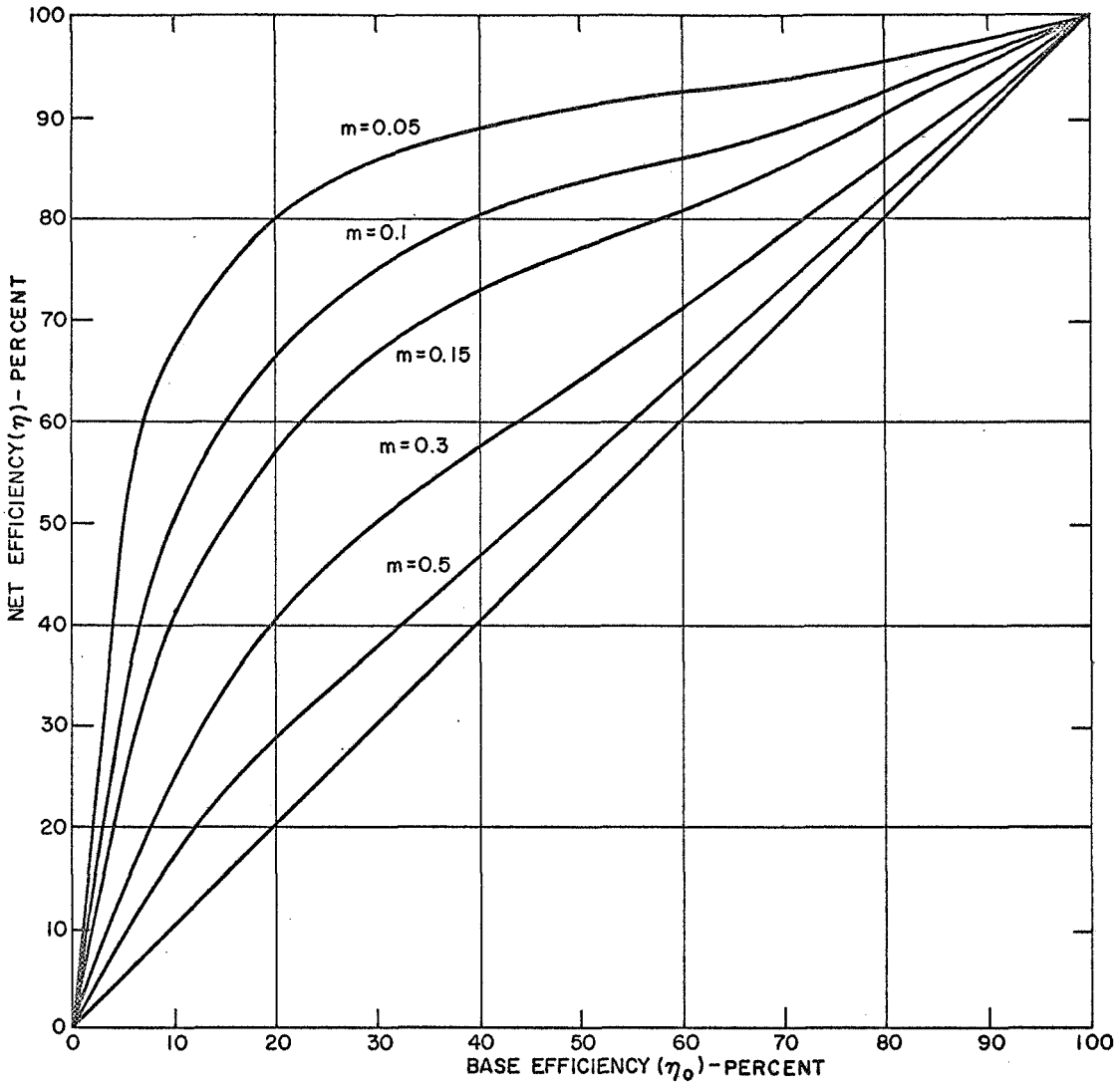

Figure 17 - Net Tube Efficiency as a Function of Base Tube Efficiency, with Margin as a Parameter, Assuming a One-Sided Power Density Distribution

to cases in which the average collection efficiency $\bar{\eta}_c$ can be used as an approximate measure of rf collector efficiency η_{c-rf}. This allows the collector to be treated as a distinct unit, independent of the tube to which it is attached.

EFFECT OF NUMBER OF ELECTRODES

In ideal collector operation each electron in the incoming velocity spectrum is sorted as to its velocity, retarded, and collected at zero potential. The following are three reasons why this ideal collection of electrons is not achieved in practice: (1) it would be necessary to utilize as many collecting electrodes as there are electron energy classes in the spectrum, (2) to prevent backstreaming some energy usually must be diverted to a direction parallel to the collecting electrode surface, hence this energy is unavailable for recovery, and (3) the optimum placement of a given electrode varies with the input position and transverse velocity of the electron energy class it is intended to collect; therefore, a compromise position must be employed which is not completely effective for all input conditions. Only the first of these effects, finite electrode number, can be treated in a general manner.

In the first portion of this section the effect of a finite number of electrodes will be evaluated using the average collection efficiency $\bar{\eta}_c$ to approximate the rf collector efficiency η_{c-rf}. This is an excellent approximation in most high efficiency klystrons as shown previously. It will be shown that the effect of electrode number can be considered by assigning it an energy loss margin $m_N = 1/N$. The remaining margin in a given collector is not directly assignable to a single cause; this leads to the concept of the "intrinsic" margin. The intrinsic margin is found to limit the usefulness of an increase in electrode number. In the final portion of this section more accurate calculations are given for idealized low and high efficiency klystrons and TWT's, assuming that the intrinsic margin is zero.

Equal-Potential-Increment (e.p.i.) and Tent-Collector Efficiency

It is useful to identify and investigate two distinct electrode potential arrangements out of the infinite variety of arrangements available. These are: (1) the "equal-potential-increment" (e.p.i.) arrangement, and (2) the "tent" arrangement. "Transitional" arrangements of electrodes, which bridge the gap between the above two types are discussed in the next portion of this section. In the e.p.i.-arrangement the electrode potentials are

spaced equally from $-2V_o/N$ to $-2V_o$ with an increment $\Delta V = 2V_o/N$, where N is the number of electrodes whose potential is different from the drift tube potential. In the tent-arrangement, N-1 electrodes are equally spaced in potential from $-V_o/(N-1)$ to $-V_o$, and the final electrode is placed at a potential of $-2V_o$. These electrode arrangements would be commonly used for high efficiency tubes. Low efficiency tubes are discussed at the end of this section.

The collection efficiency curves for the two types of collector electrode arrangement are shown in Figure 18 with N = 4 and N = 3 for the e.p.i. and tent-arrangements, respectively. In both arrangements electrons with energies in the increment from 0 to $0.5\,V_o$ are not retarded, hence their collection efficiency is zero. For electrons with energies slightly greater than the first electrode potential the collection efficiency ideally jumps to 100 percent. For electron energies between $0.5\,V_o$ and V_o, the electrons give up a fraction $V_o/2V$ of their energy, as indicated by the left-hand hyperbolic segments in Figure 18, dropping to 50 percent at V_o. Above V_o the collection efficiency again jumps to 100 percent and falls hyperbolically for higher voltages, in this case as V_o/V. In the tent-arrangement this drop-off in efficiency continues to $2\,V_o$ where the collection efficiency is 50 percent. In the e.p.i.-arrangement an additional sawtooth segment is generated at $1.5\,V_o$ at which point the collection efficiency again jumps to 100 percent. The efficiency in the uppermost increment in the e.p.i.-arrangement is given by $1.5\,V_o/V$, terminating at 75 percent at $2\,V_o$.

It is clear from Figure 18 that the collection efficiency of the e.p.i.-arrangement will generally be higher than the efficiency of the tent-arrangement. However, the tent-arrangement has the advantage that all electrode power supplies are being discharged, provided their negative terminals are connected to the cathode. In the e.p.i.-arrangement, power supplies for the electrodes between $-V_o$ and $-2\,V_o$ are being charged and provision must be made for feeding this energy back into the power system to reduce overall power requirements. In either case, ideally no current flows to the electrode at a potential of $-2\,V_o$.

The area under the two curves of Figure 18 may be calculated as a function of the number of electrodes. For the e.p.i.-arrangement a simple integration gives the expression

$$\bar{\eta}_c = \frac{1}{N}\left[\ell n \frac{2}{1} + 2\,\ell n \frac{3}{2} + \ldots + (N-1)\,\ell n \frac{N}{N-1}\right] \tag{23}$$

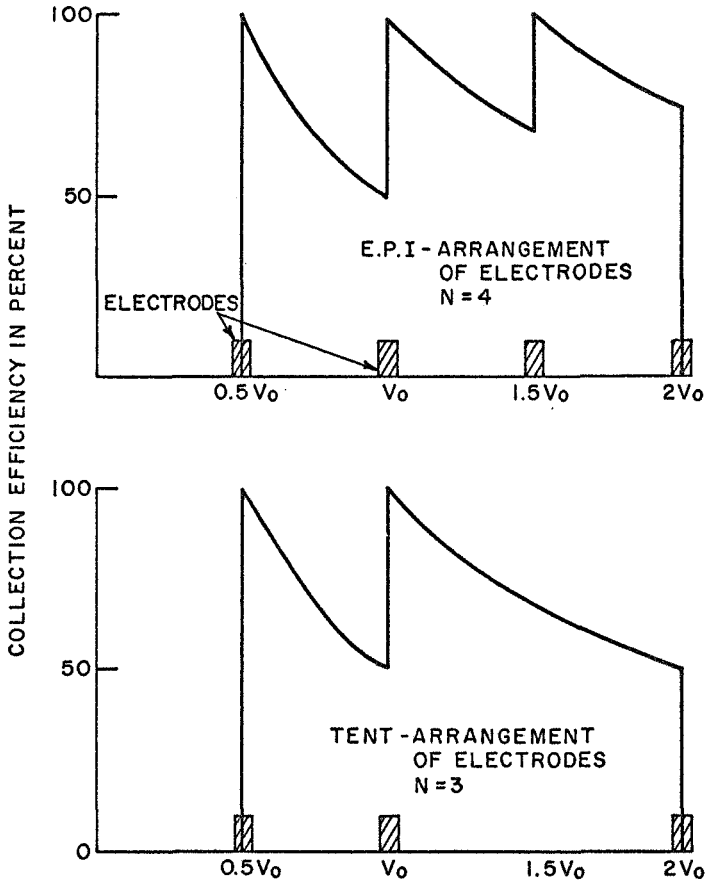

Figure 18 - Comparison of Collection Efficiency for N = 4 Equal-Potential-Increment Arrangment and N = 3 Tent-Arrangement of Electrodes

With a tent-arrangement of N electrodes, the upper half of the spectrum is collected with $\ell n(2) = 69.3$ percent efficiency, and this figure must be averaged with the efficiency of the lower half, which is given by Equation (23), except that only N-1 electrodes are used in this portion of the energy spectrum. Thus, the efficiency of an N-electrode tent-arrangement collector is given by the expression

$$\bar{\eta}_c = \frac{1}{2}\left\{\ell n\, 2 + \frac{1}{N-1}\left[\ell n \frac{2}{1} + 2\, \ell n \frac{3}{2} + \ldots + (N-2)\, \ell n \frac{N-1}{N-2}\right]\right\} \tag{24}$$

The collector efficiencies of the e.p.i.- and tent-arrangements given by Equations (23) and (24) are plotted in Figure 19. This figure shows that the e.p.i.-arrangement is better than the tent arrangement if N is greater than five. Unless the number of electrodes exceeds ten, however, this gain in efficiency is not large, and may be offset by the disadvantage of the requirement of more complex power conditioning circuity.

It is interesting to note that the expression (23) for average collection efficiency can be replaced by an approximate, but simpler expression based on the use of a "block" treatment of the spent beam rather than an accurate integration. In the "block" treatment, each electrode potential of an e.p.i.-arrangement establishes the boundaries of blocks of energy which are then assumed to reside only at the single mid-electrode potentials. Assuming an e.p.i.-arrangement and a flat energy spectrum from 0 to $2\,V_o$, each block contains a fraction $1/N$ of the total beam energy. The first block loses all of its energy as it strikes the portion of the collector at drift tube potential, but subsequent blocks lose only a fraction $1/(2n-1)$ of their energy where $n = 2$ to N. The general expression for energy lost can be summed and subtracted from unity to give an approximate expression for average collection efficiency

$$\bar{\eta}_c = 1 - \frac{1}{N} \sum_{n=1}^{N} \frac{1}{2n-1} = \frac{1}{N} \sum_{n=1}^{N} \frac{2\,(n-1)}{2\,n-1} \tag{25}$$

This expression for $\bar{\eta}_c$ is conceptually easier to visualize than Equation (23) and yet is accurate to within a few percent for all N, as shown by the dotted line in Figure 19.

The "block" model is particularly useful if the spent beam width parameter α is less than unity. A discussion of both symmetric and one-sided spectra for this case is included in the final portion of this section.

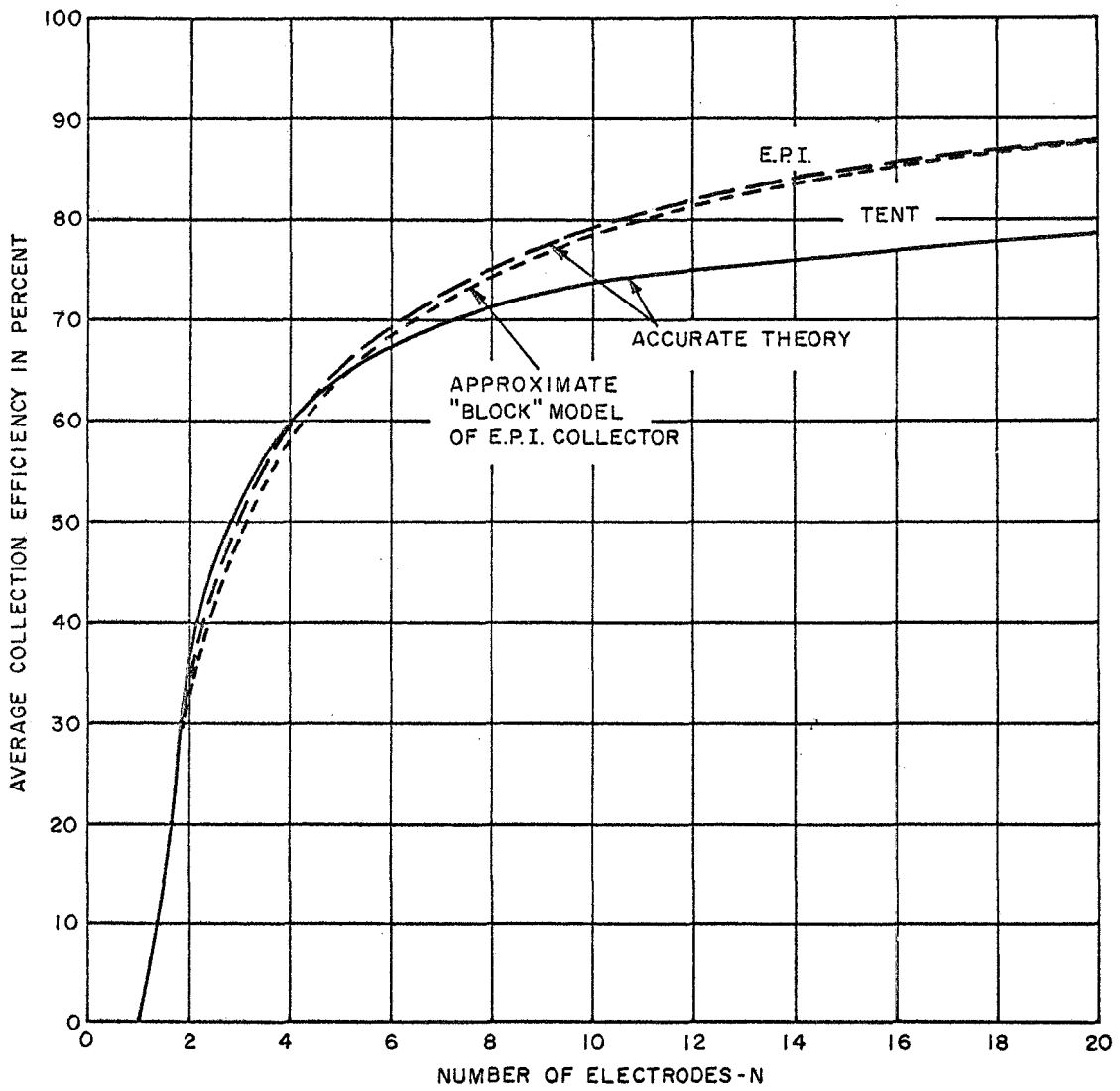

Figure 19 - Average Collector Efficiency of e.p.i.-Arrangement and Tent-Arrangement as a Function of the Number of Electrodes

Transitional-Collector Efficiency

The e.p.i.- and tent-arrangements of collector electrodes constitute two limiting cases of special interest. In a practical case it may prove desirable to space N-1 electrodes equally in potential up to a potential of fV_o, where f is a factor between unity and $2(1-1/N)$. Above fV_o a partial tent is used to capture electrons in the potential region between fV_o and $2V_o$. These electrode arrangements are termed "transitional". A transitional-arrangement generally provides a slightly higher efficiency than either the tent-arrangement, where $f = 1$, or the e.p.i.-arrangement, where $f = 2(1-1/N)$. The Nth electrode potential is always assumed to be $2\,V_o$.

The variation of average collection efficiency with the transitional factor f is readily derived by a procedure similar to that used in obtaining Equation (23) if the spent beam power density spectrum is flat between 0 and $2\,V_o$. The corresponding expression for average collection efficiency of a transitional-arrangement is

$$\bar{\eta}_c = \frac{f}{2(N-1)} \left[\ell n \frac{2}{1} + 2\ell n \frac{3}{2} + \ldots + (N-2)\,\ell n \frac{N-1}{N-2} + (N-1)\,\ell n \frac{2}{f} \right] \qquad (26)$$

In Figure 20 the average collection efficiency given by Equation (26) is plotted as a function of the transitional factor f for various numbers of electrodes. For $N = 5$ the tent-arrangement is almost as good as the e.p.i.-arrangement, and a transitional-arrangement with $f = 1.3$ increases the efficiency less than three percentage points over the tent-arrangement. As N increases to 20, however, the transitional-arrangement with $f = 1.75$ picks up ten points of efficiency over the tent-arrangement.

Thus Figure 20 suggests that for fewer than five electrodes, the tent-arrangement be used, but that with ten or more electrodes a transitional- or e.p.i.-arrangement of electrodes seriously be considered, even though the power conditioning problem is compounded.

e.p.i.-Collector as a Constant-Margin Collector

If the number of electrodes is increased indefinitely, both Equations (23) and (24) predict a collector efficiency of 100 percent. This will not be attained, however, due to reasons indicated at the beginning of this section. It is useful at this point to develop the close relationship between the "constant-margin" collector concept and the e.p.i.-arrangement of electrodes.

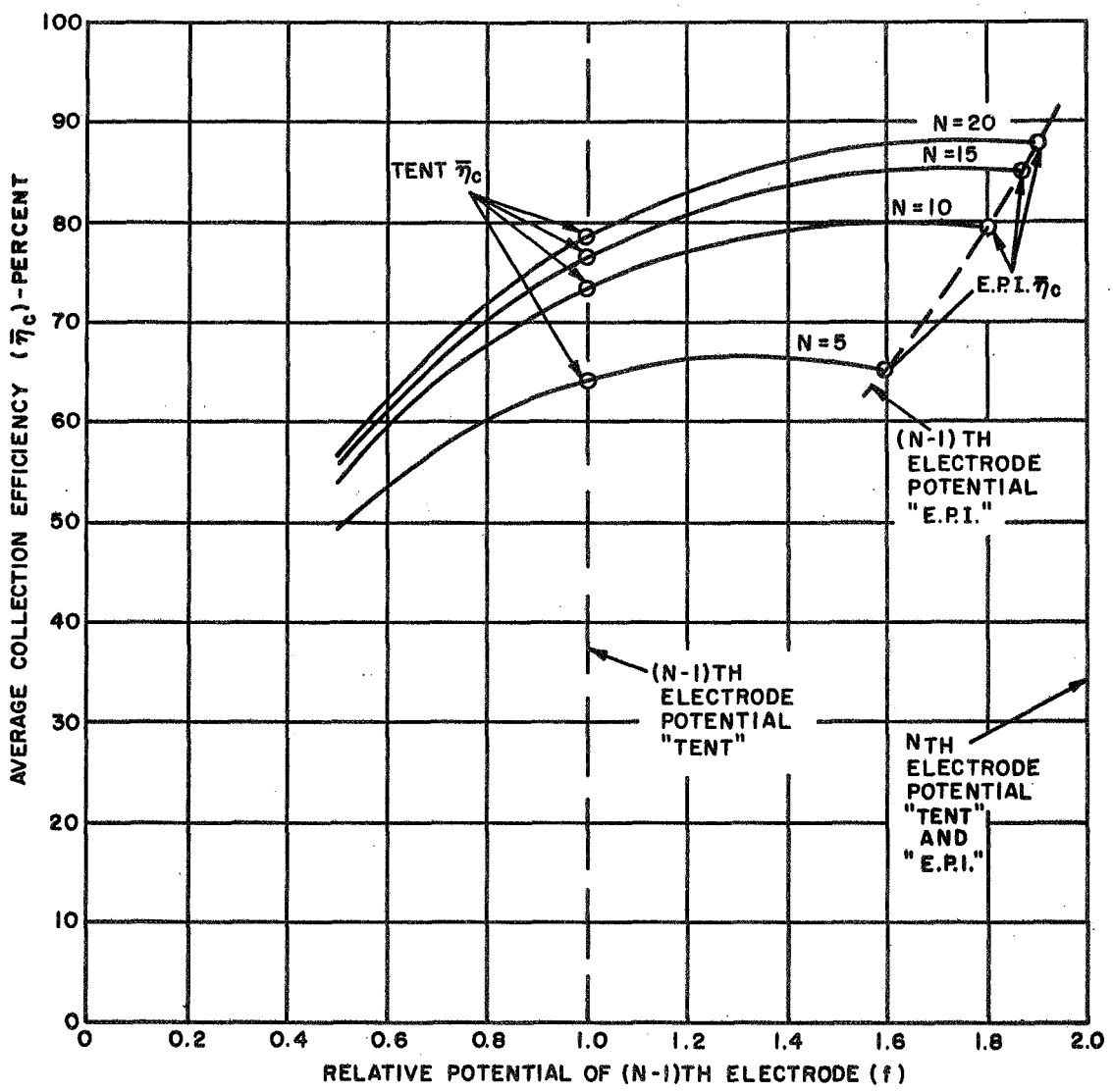

Figure 20 - Average Collector Efficiency of a Transitional-Collector as a Function (N - 1)th Electrode Potential with Number of Electrodes as a Parameter

Consider an e.p.i.-arrangement with ten electrodes equally spaced from 0 to $2V_o$. A plot is given in Figure 21 of the ideal collection efficiency η_c as a function of V. The sawtooth curve has straight vertical portions spaced $0.2V_o$. The lower points of the sawteeth are given by the series 0, 1/2, 2/3, 3/4, ... (N-1)/N. The equation of a curve passing through these points is given by the expression $\eta_1 = 1 - 2V_o/NV$. The equation of a curve passing through the midpoints of the vertical segments of the sawteeth is therefore given by the expression $\eta_2 = 1 - V_o/NV$. This equation is quite similar to Equation (17) developed for a constant-margin collector. Thus, the collection efficiency of an ideal e.p.i.-arrangement is closely related to that of a constant-margin collector, provided the margin m is identified with the reciprocal of the number of electrodes, i.e.

$$m_N = 1/N \qquad (N \geq 3) \tag{27}$$

It should be noted that a slight error enters for $N < 3$ because for large step size the areas under the two curves of Figure 22 are somewhat unequal.

Intrinsic Margin

Equation (27) shows that as the electrode number increases without limit, the electrode margin m_N goes to zero. According to Equation (20) this would lead to an average collection efficiency of 100 percent. The main reason this does not happen is that factors other than the electrode number contribute to the margin, as indicated previously. In general, margin can be written as the sum of two terms,

$$m = m_i + m_N = m_i + 1/N$$

where the term m_i has been included to allow for the "intrinsic" margin, i.e., the energy loss margin due to effects other than electrode number.

A useful expression can be derived for $\bar{\eta}_c$ in the case of a constant margin collector by integrating Equation (17) from m to $2V_o$. This gives an approximate but reasonably accurate estimate of collector efficiency in cases where the base tube efficiency is 40 percent or greater. The integration yields the result

$$\bar{\eta}_c = 1 - \frac{m}{2}\left(1 + \ln \frac{2}{m}\right) \tag{28}$$

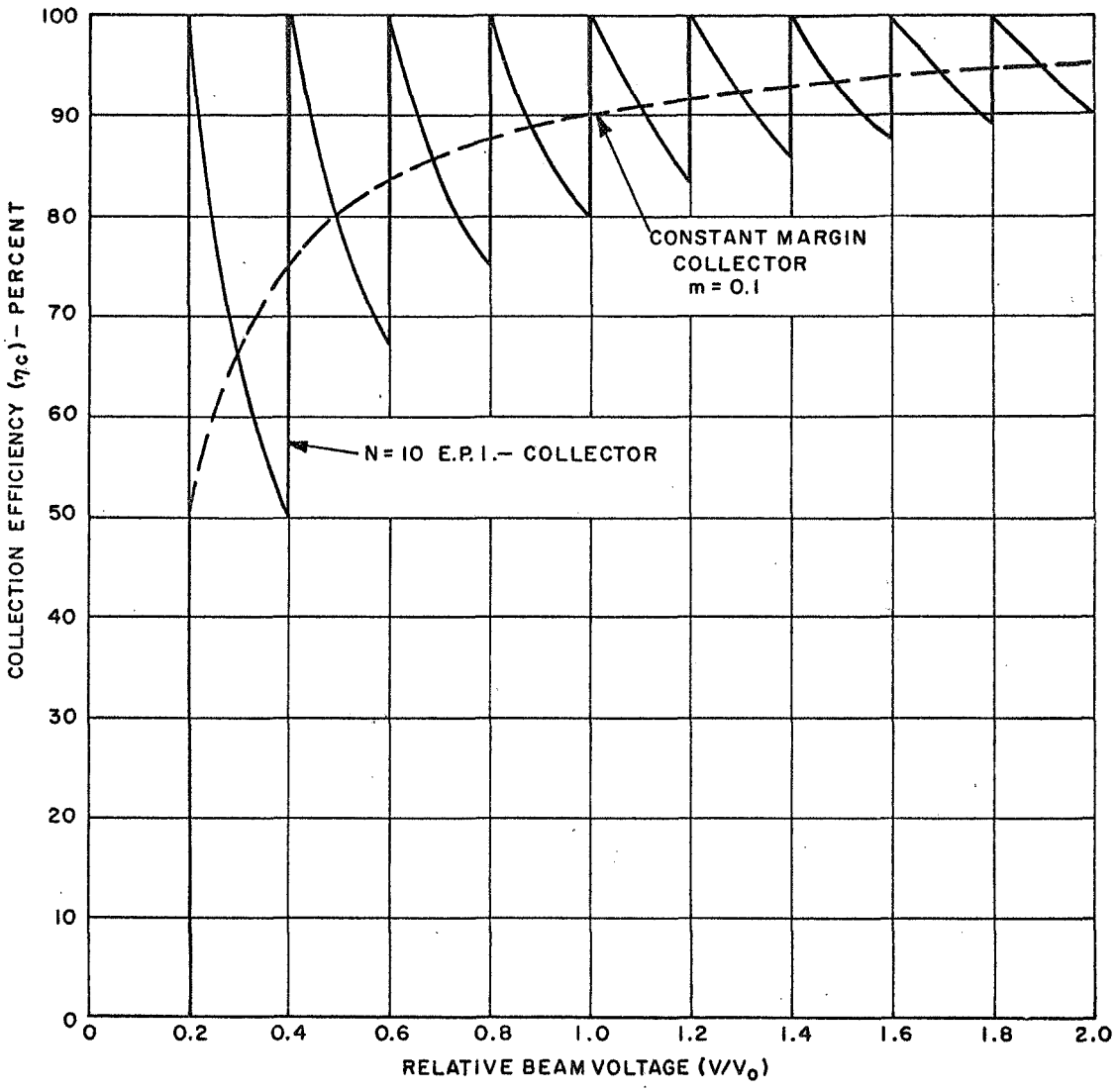

Figure 21 - Comparison of Collection Efficiency for N = 10 e.p.i.-Collector and Constant-Margin (m = 0.1) Collector as a Function of Beam Energy

This result can also be obtained by letting $\alpha = 1$ in Equation (19). Writing m as $m_i + 1/N$ gives the expression

$$\bar{\eta}_c = 1 - \frac{m_i + 1/N}{2} \left(1 + \ell n \frac{2}{m_i + 1/N}\right) \tag{29}$$

This expression for average collection efficiency is plotted in Figure 22 versus N with the intrinsic margin m_i as a parameter. Equation (29) becomes inaccurate as N approaches 1, but for $N \geq 3$ the error is less than three percentage points. It is clear from Figure 22 that the intrinsic margin limits the efficiency that can be achieved even using an infinite number of electrodes. The dashed line in Figure 22 shows the locus of points for which the average collection efficiency drops ten percentage points below the efficiency $\bar{\eta}_{c-\infty}$ obtained with an infinite number of electrodes. The lower the intrinsic margin, the higher the number of electrodes that can effectively be used. The only way to determine the intrinsic margin for a given tube/collector system is to make a detailed study of trajectories. A description of this study performed for the Type 4.3 (TEF) collector selected for final evaluation is contained in the following section.

Design Curves for Ideal Collectors

In the initial portion of this section attention was restricted to tubes of moderate-to-high efficiency (η_o = 40 to 60 percent) with a symmetric spent beam distribution (similar to klystrons) because this simplified the presentation of the effect of electrode number and the concept of intrinsic margin. In this portion of this section this restriction will be relaxed, and the effect of electrode number will be evaluated on the performance of tubes of any efficiency, whether low or high. To keep the treatment within reasonable bounds, the intrinsic margin is assumed to be zero.

The most important conclusion of this analysis is that tubes with one-sided spent beam spectra, like TWT's, differ significantly from tubes with symmetric spectra, like klystrons, in their response to the use of depressed collectors. Specifically, for a given complexity of collector structure (e.g. same number of electrodes) this idealized analysis shows that a low efficiency TWT will perform as well as, or slightly better than, a high efficiency klystron. This is a direct consequence of the identification of a one-sided, flat spent beam power distribution with TWT's and a symmetrical, flat spent beam power spectrum with klystrons. This identification, while not strictly accurate, is considered useful as an indictor of a valid trend.

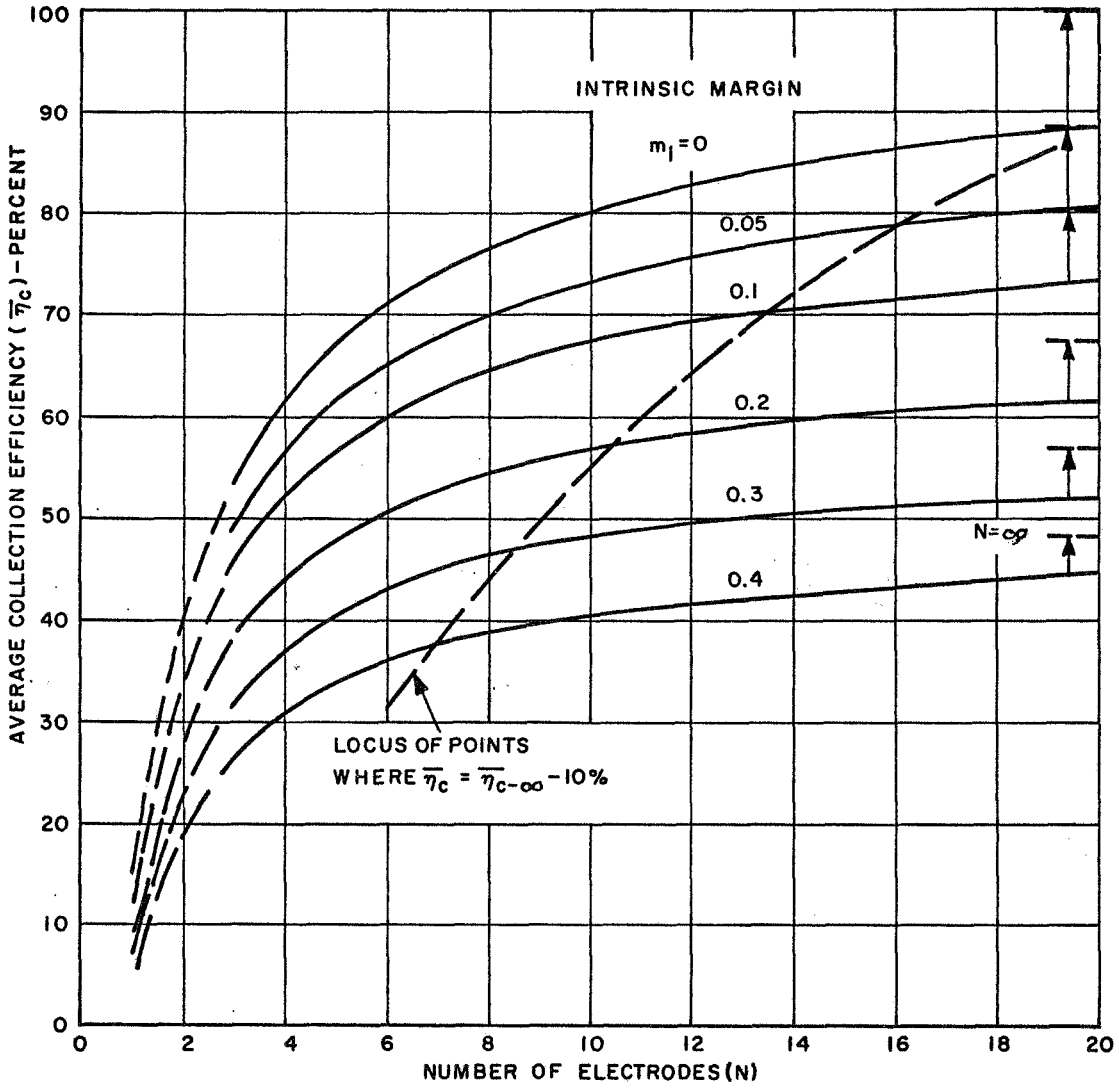

Figure 22 - Average Collection Efficiency of an e.p.i.-Collector as a Function of Electrode Number with Intrinsic Margin as a Parameter

In the calculation of rf collection efficiency for one-sided and symmetrical spent beam power distributions the "block" model (justified in Figure 19) will be utilized. For each spectrum the relationship between α and η_o is determined from Equations (14) and (15), or Figure 10, and N electrodes are spaced uniformly within the energy span of the spent beam distribution. For the one-sided spectrum extending from $(1-\alpha)V_o$ to V_o, the block model gives the following expression for average collection efficiency:

$$\bar{\eta}_c = 1 - \frac{\alpha}{N} \sum_{n=1}^{N} \frac{1}{2N(1-\alpha) + (2n-1)\alpha} \tag{30}$$

For the symmetrical spectrum, with electrodes evenly spaced from $(1-\alpha)V_o$ to $(1+\alpha)V_o$, the collection efficiency is given by the expression:

$$\bar{\eta}_c = 1 - \frac{\alpha}{N} \sum_{n=1}^{N} \frac{1}{N(1-\alpha) + (2n-1)\alpha} \tag{31}$$

Equations (30) and (31) have been used to plot Figures 23 - 30. In Figures 23 - 26, the average collection efficiency $\bar{\eta}_c$ and the tube efficiency with depression η have been plotted as a function of tube efficiency without depression, η_o, with electrode number N as a parameter. Figures 23 and 24 apply when the spent beam power spectrum is flat and symmetrical, as is approximately the case in klystrons. When the spent beam power spectrum is flat and one-sided, as is approximately the case in TWT's, Figures 25 and 26 apply.

The striking feature of these curves is the marked improvement of the efficiency of one-sided spectra tubes with collector depression compared to the more sluggish response of tubes with symmetric spectra to collector depression. For example, using η_o = 40 percent as a starting point, Figure 25 shows that an idealized one-sided spectra tube with an N = 3 collector would perform with a collector efficiency η_{c-rf} of 81 percent. To get the same performance in a symmetric-spectra tube, eight electrodes would be required, according to Figure 23. This ratio is approximately three-to-one in electrode number is probably a valid indication why more collector electrodes must be used in a klystron to achieve the same efficiency improvement possible with a TWT. The identification between tube type and

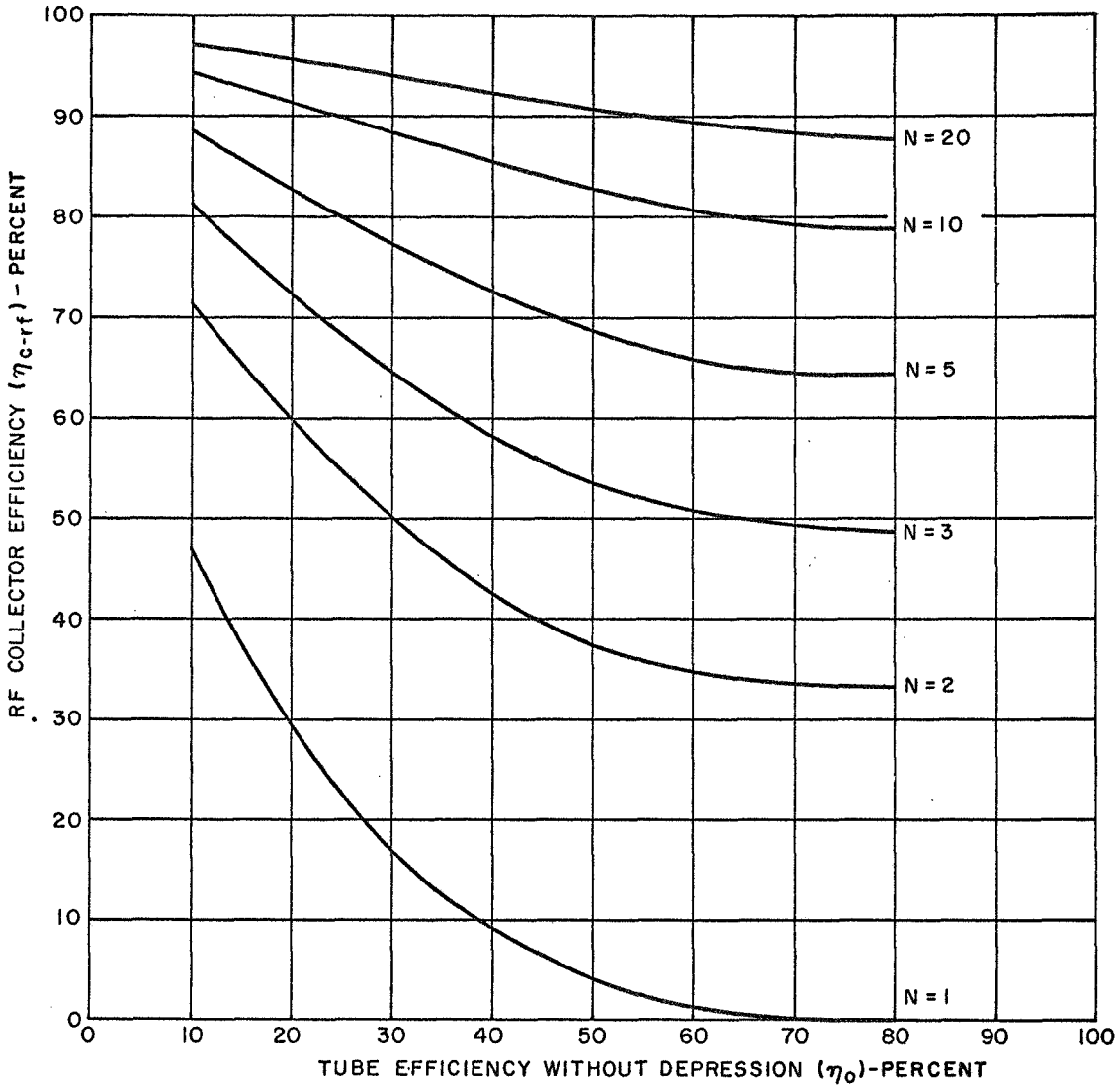

Figure 23 - RF Collector Efficiency as a Function of Base Tube Efficiency, with Number of Electrodes as a Parameter, for Tubes with a Symmetric Flat Spent Beam Spectrum (Klystrons)

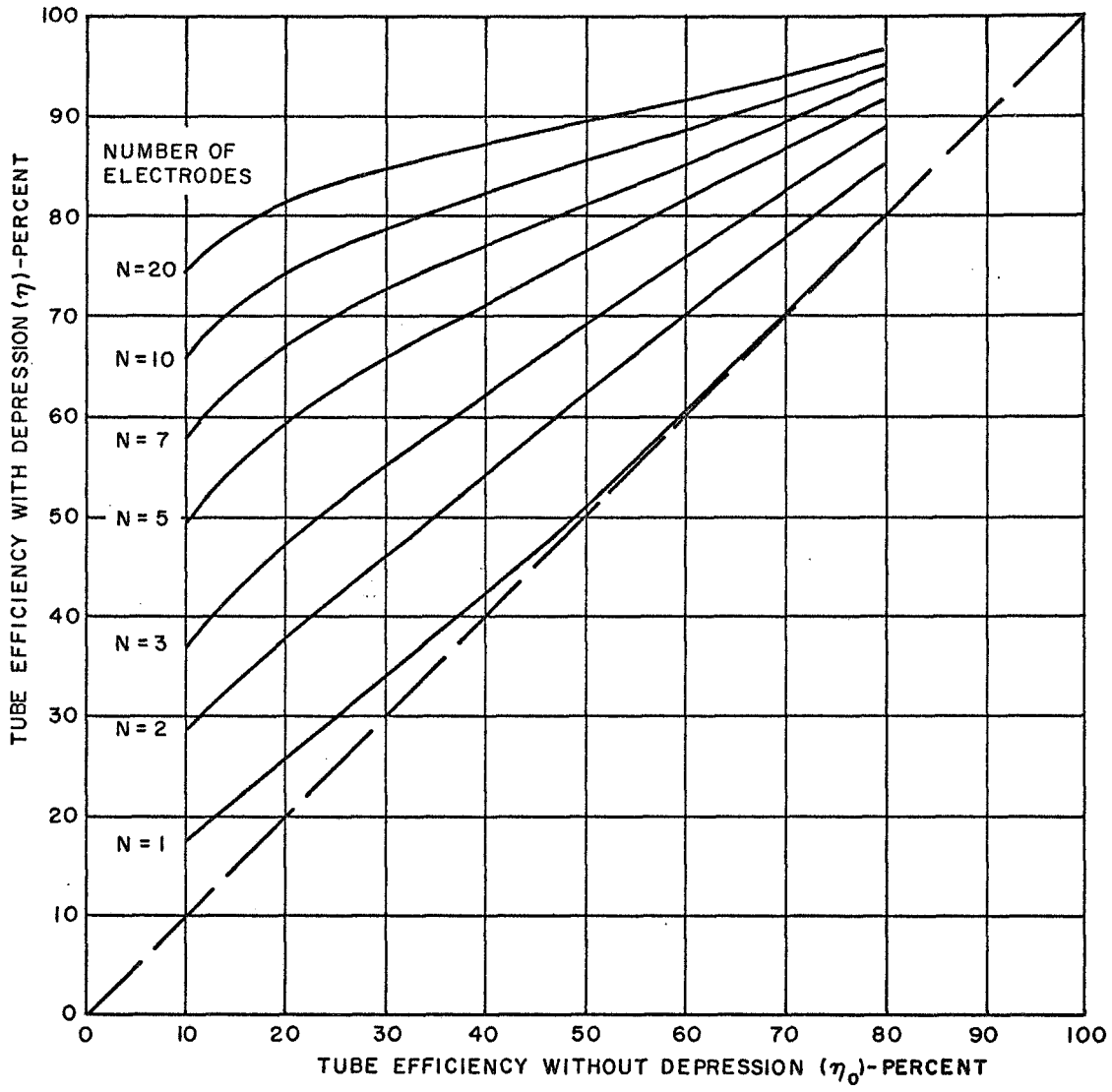

Figure 24 - Net Tube Efficiency as a Function of Base Tube Efficiency, with Number of Electrodes as a Parameter, for Tubes with a Symmetric Flat Spent Beam Spectrum (Klystrons)

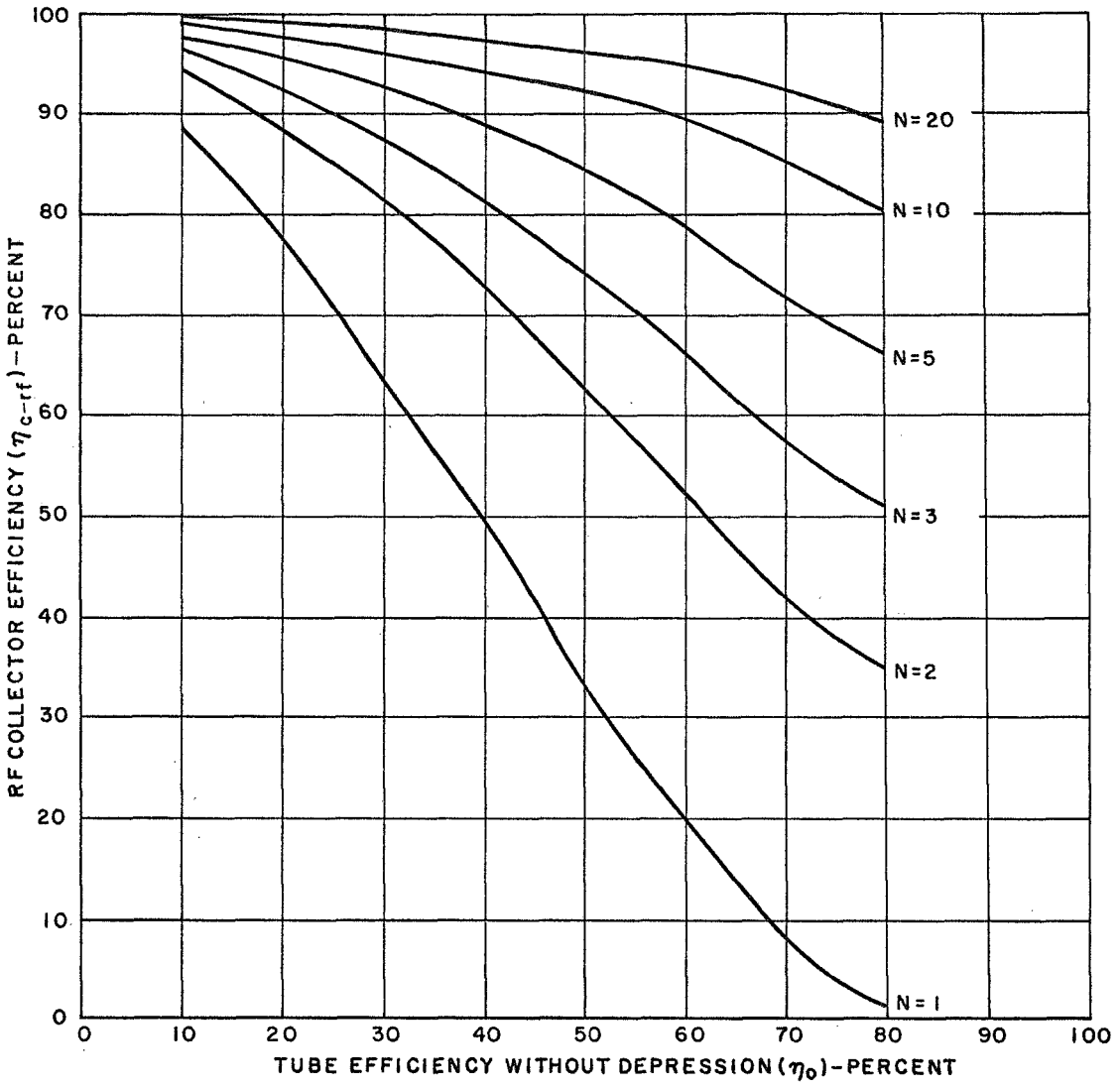

Figure 25 - RF Collector Efficiency as a Function of Base Tube Efficiency, with Number of Electrodes as a Parameter for Tubes with a One-Sided Flat Spent Beam Spectrum (TWT's)

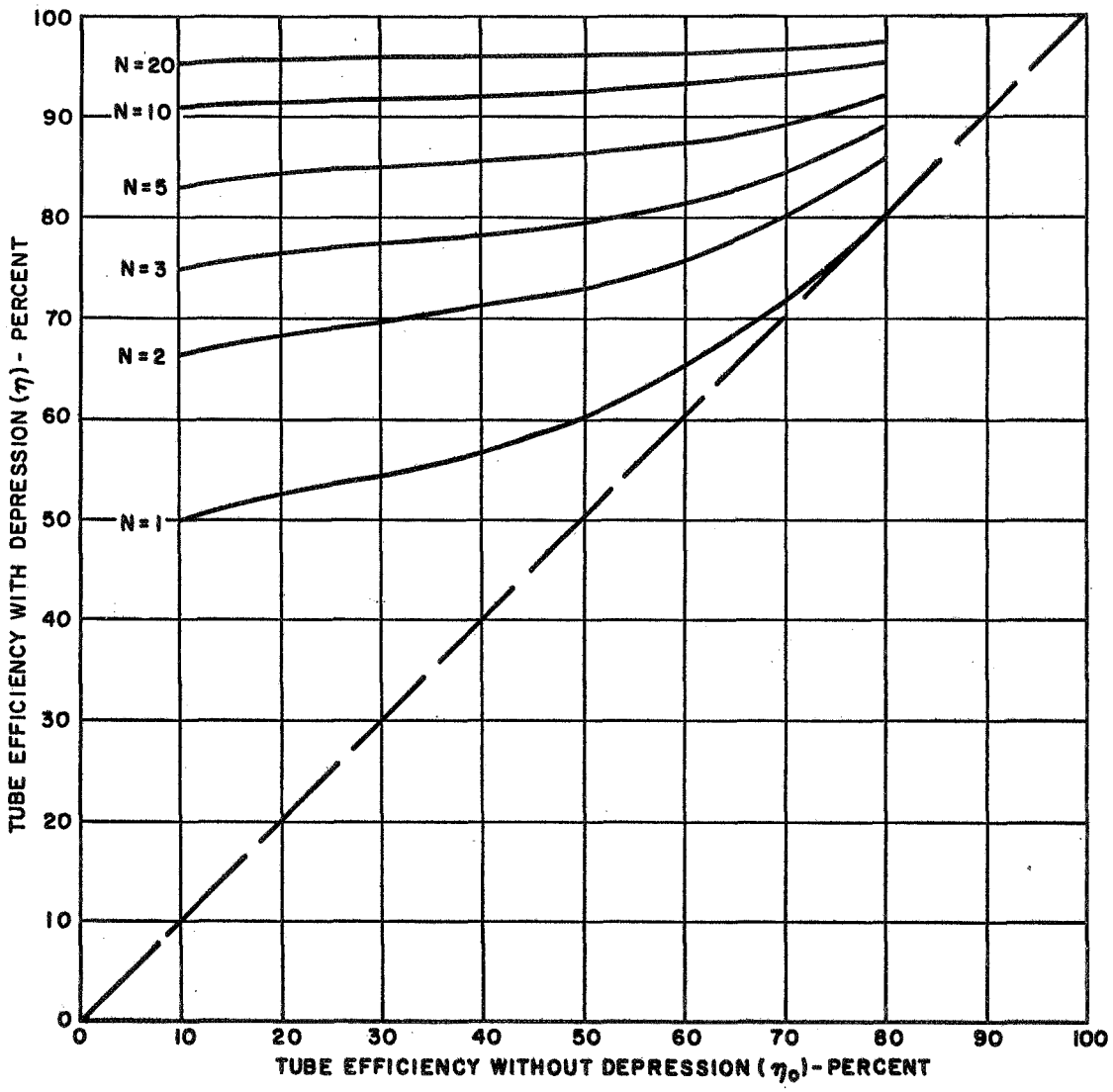

Figure 26 - Net Tube Efficiency as a Function of Base Tube Efficiency, with Number of Electrodes as a Parameter, for Tubes with a One-Sided Flat Spent Beam Spectrum (TWT's)

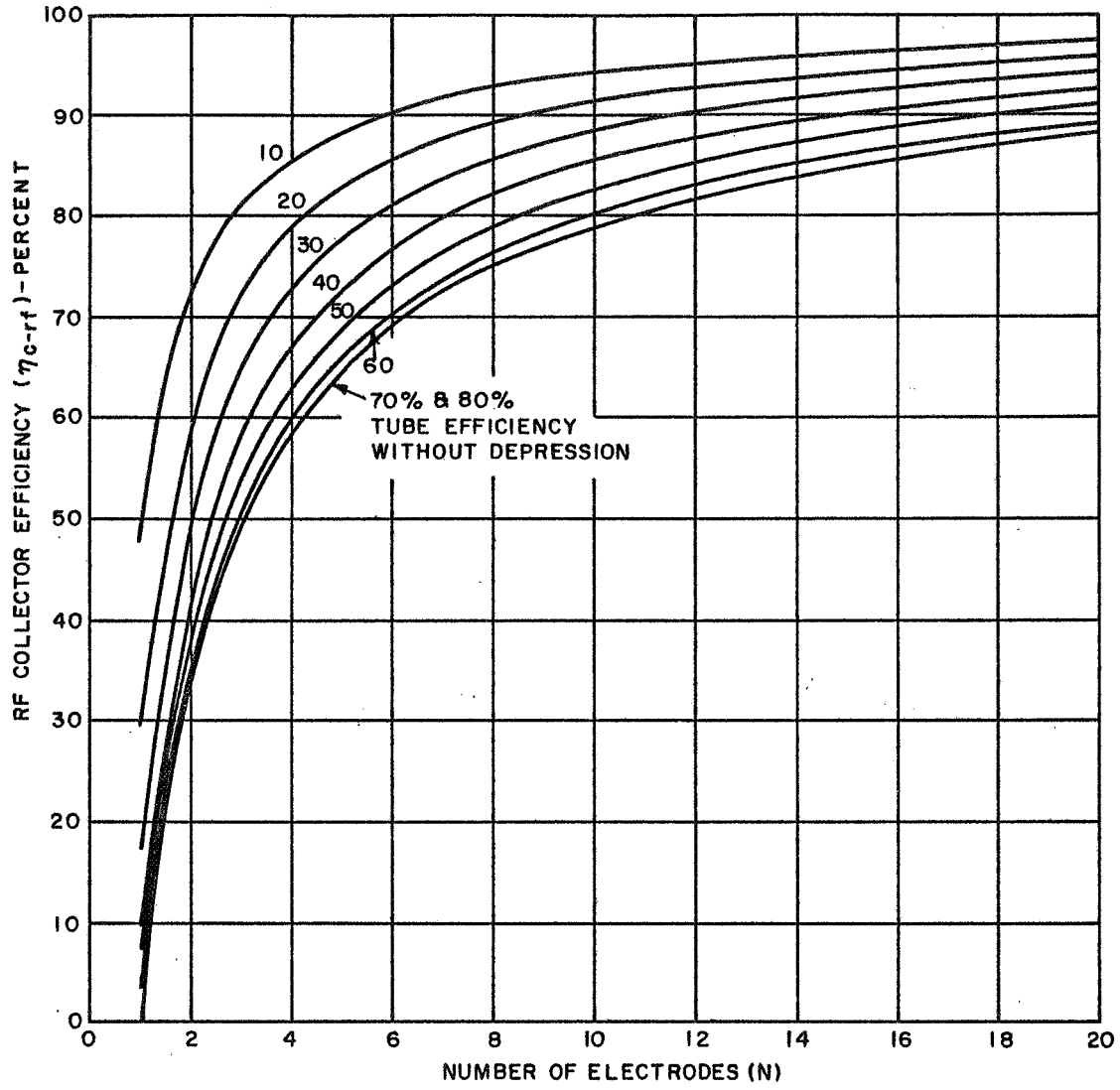

Figure 27 - RF Collector Efficiency as a Function of Number of Electrodes, with Base Tube Efficiency as a Parameter, for Tubes with a Symmetric Flat Spent Beam Spectrum (Klystrons)

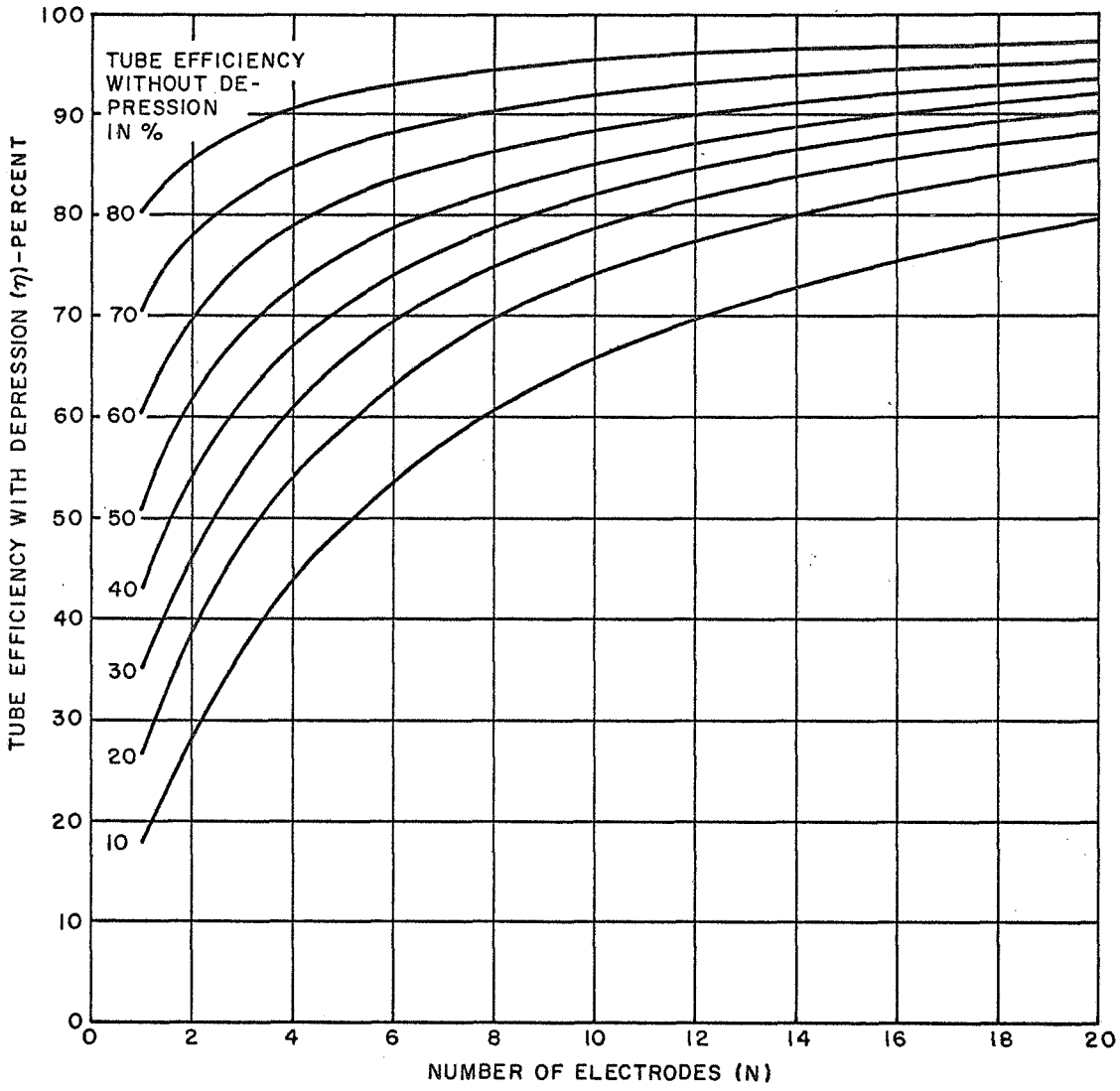

Figure 28 - Net Tube Efficiency as a Function of Number of Electrodes, with Base Tube Efficiency as a Parameter, for Tubes with a Symmetric Flat Spent Beam Spectrum (Klystrons)

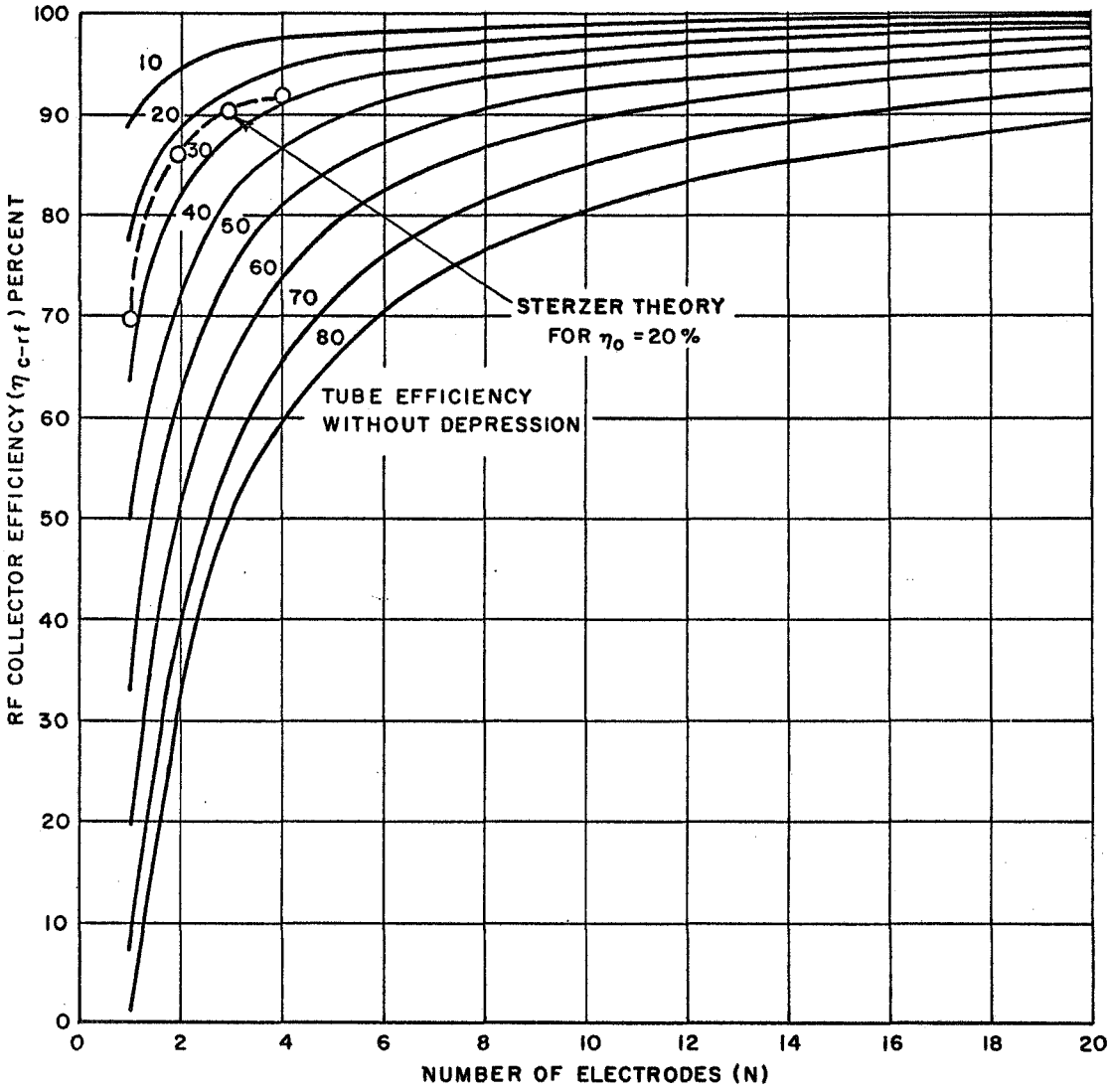

Figure 29 - RF Collector Efficiency as a Function of Number of Electrodes, with Base Tube Efficiency as a Parameter, for Tubes with a One-Sided Flat Spent Beam Spectrum (TWT's)

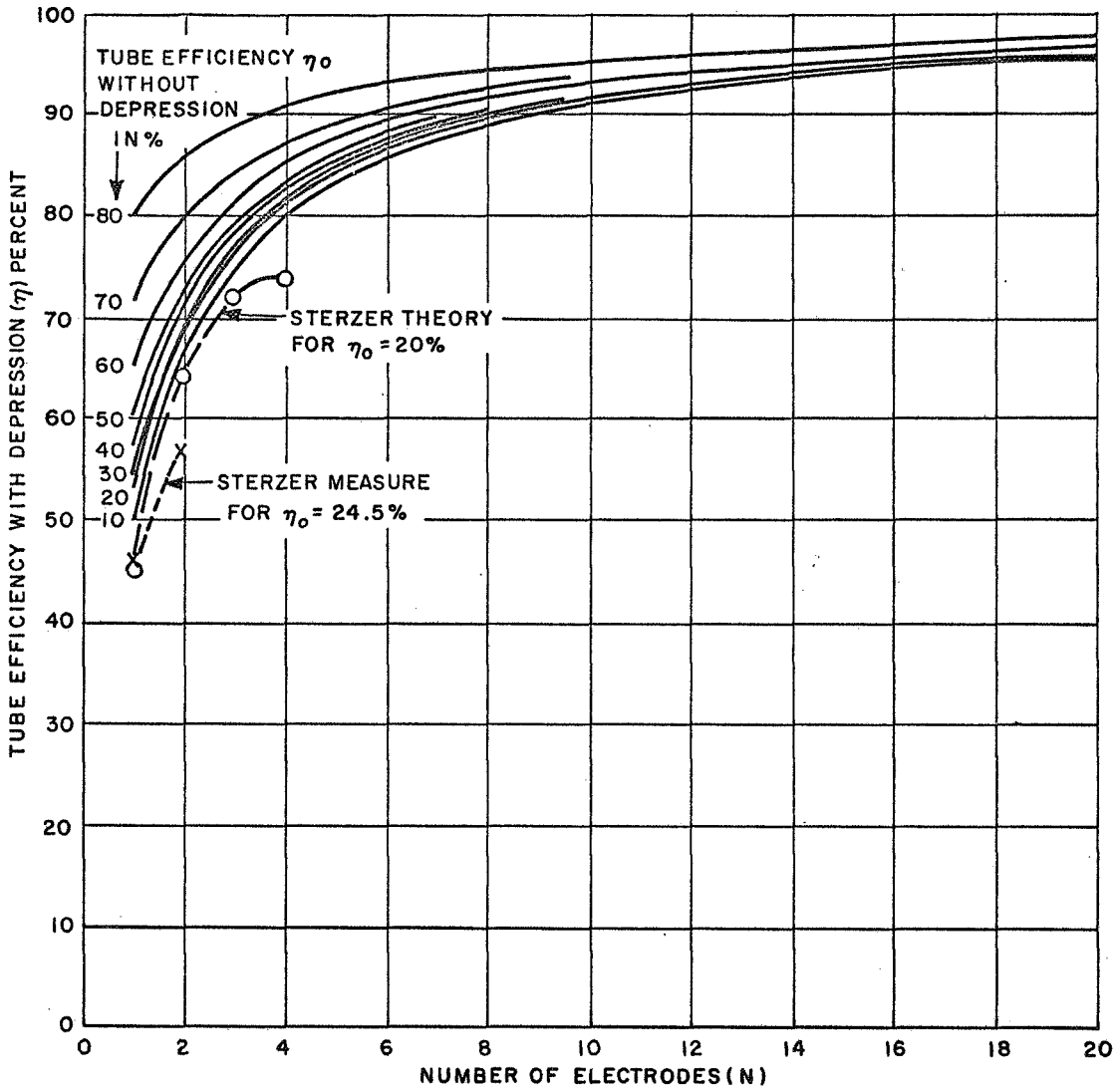

Figure 30 - Net Tube Efficiency as a Function of Number of Electrodes, with Base Tube Efficiency as a Parameter, for Tubes with a One-Sided Flat Spent Beam Spectrum (TWT's)

spectrum type is only approximate, as shown in Appendix A, hence, the results of this discussion should be taken only to indicate trends and not as precise evaluations.

Figures 23 - 26 closely resemble Figures 11, 12, 16 and 17 which depict the behavior of constant margin collectors, with the identification that $m_N = 1/N$. There is one important difference which appears in the consideration of low efficiency TWT's. In Figure 26, the curves of tube efficiency with depression do not crowd toward the origin as they do in Figure 17. The reason is that the identification $m_N = 1/N$ only applies if the spent beam spectrum is wide, i.e. $\alpha \approx 1$. For low efficiency tubes, the spent beam spectrum is much narrower than the range from 0 to V_o. In the present analysis the lowest potential electrode is placed at $(1-\alpha)V_o$, and not at $2V_o/N$ as in the constant-margin collector. Hence, in this analysis fewer electrodes are required to span the populated portion of the spent beam power spectrum of a low efficiency tube than are required in the constant-margin collector.

It is useful to replot the curves in Figures 23 - 26 in the form shown in Figures 27-30, in which case electrode number N has been taken as the independent variable along the abscissa and undepressed tube efficiency η_o has been used as a parameter. Figures 27 and 28 apply to symmetric klystron-like spectra and Figures 29 and 30 apply to one-sided TWT-like spectra, respectively. In this form the latter two figures enable direct comparison of the one-sided spent beam results with Sterzer's calculations for a TWT with an undepressed efficiency of 20 percent. Sterzer presumably used an actual calculated TWT spent beam spectrum to obtain his results. Sterzer's theoretical results are shown in both Figures 29 and 30, where they are seen to be in close agreement with the results of the approximate analysis presented here. Sterzer's measurements, shown in Figure 30, fall somewhat below the theoretical curves, but this is not surprising since the intrinsic margin has been assumed to be zero for these calculations.

A significant conclusion can be drawn by comparing Figure 30, for a one-sided spectrum tube (TWT) with Figure 28, a symmetrical spectrum tube (klystron). From Figure 30 it appears that a low efficiency TWT (e.g. $\eta_o = 20$ percent) followed by a modest collector (e.g. N = 4) will yield a tube efficiency with depression of over 80 percent. For a klystron with a four-electrode collector to yield the same overall efficiency, according to Figure 28, the base efficiency η_o of the klystron would have to be over 60 percent. Thus, TWT efficiency appears to be much more responsive to improvement by collector depression than does klystron efficiency. The idealized spent

beam models used to arrive at this conclusion probably over-emphasize the quantitative difference between the tubes. But undoubtedly the qualitative trend has basic validity.

In the following section the final design of a Type 4.3 (TEF) collector will be evaluated both as an e.p.i.-collector and as a tent-collector.

FINAL COLLECTOR DESIGN AND EVALUATION

The preliminary and intermediate evaluation of collector efficiency presented previously led to the choice of a Type 4.3 (TEF) collector for final evaluation. The analyses given earlier provide the theoretical basis for evaluating the performance of this collector by using the area under the η_c versus V_o collector characteristic as a useful measure of the rf collector efficiency. In this section a brief description of the electron dynamics in the Type 4.3 (TEF) collector will be given, followed by an evaluation of the collector performance under typical operating conditions in a high efficiency klystron application at 12 GHz.

Description of the Type 4.3 (TEF) Collector

The tilted electric field collector consists of a set of plane parallel electrodes inclined at an angle with respect to the beam axis as shown in Figure 31. In addition, a magnetic field parallel to the original beam axis is present throughout the collector volume. The strength of this field is generally well below that of the main focusing field. If the coordinate system is chosen as in Figure 31, the electrodes are perpendicular to the y-z plane. The x axis points into the y-z plane such that the cross product of the unit vectors $i_x \times i_y$ is equal to i_z.

As the beam enters the TEF collector it is immediately subjected to a drift velocity in the -x direction.

$$v_x = \frac{E_y}{B_z} \tag{32}$$

As the beam drifts off axis, it is also decelerated by the action of the axial electric field. Eventually the electrons will come to a stop and reverse their motion in the z direction, all the time being subject to the -x drift velocity. In an optimum collector the electrode apertures are located such that the electrons strike the far side of these plates shortly after their

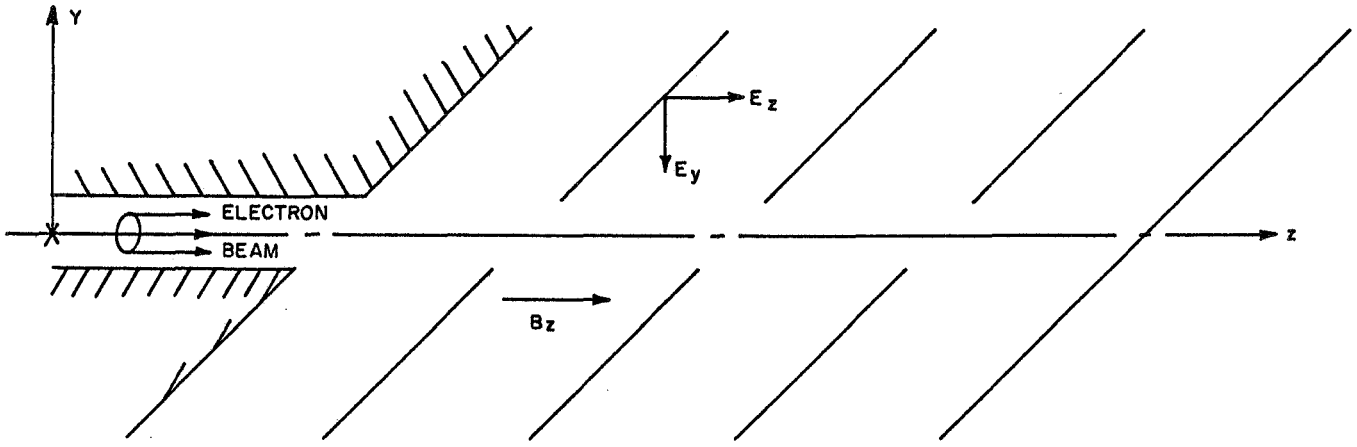

Figure 31 - Basic Type 4.3 (TEF) Tilted Electric Field Collector

motion in the z direction has been reversed. Secondary electron emission on the far side of any electrode is completely suppressed by the electric field. If any electron strikes the near side of an electrode, the secondary electron that may be emitted will still be subject to the E_y/B_z drift velocity and will therefore keep moving away from the original beam axis until it strikes the far side of the preceding electrode. Thus, the TEF collector completely eliminates the problems associated with electron backstreaming.

Electron Beam Model

For the purposes of analog computation the beam area is divided into five equal parts as shown in Figure 32. If r_b is the beam radius, electrons are injected at x and y equal to zero and $\pm \sqrt{.6}\ r_b$ as shown. Electrons located at various angular positions of the beam must be analyzed because the collector is asymmetric. At each of the five starting positions ten electrons having different energies are injected so that a total of 50 trajectories are available for the evaluation of any given collector structure. The angular velocity v_θ of the off axis electrons is determined from the law of momentum conservation as developed by Branch et al[19]

$$v_\theta = r \frac{eB}{2m} \left[1 \pm \sqrt{1 - \left(\frac{B_b}{B}\right)^2} \right] \tag{33}$$

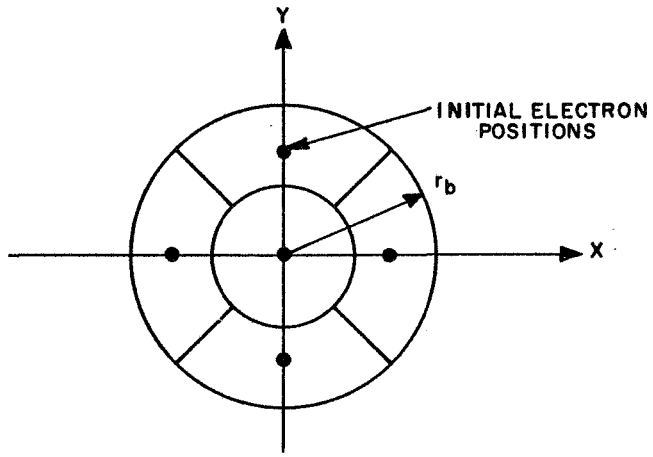

Figure 32 - Five-Beam Model of Solid Beam Cross-Section as Used in Analog Computations

where r is the radius, B is the actual magnetic field, and B_b is the Brillouin field for the beam under consideration. If the sense of the magnetic field at the cathode and the collector injection plane is the same then the minus sign in Equation (33) is applicable. The cathode magnetic field immersion K for any given B/B_b ratio is given by

$$K = \mp \sqrt{1 - \left(\frac{B_b}{B}\right)^2} \tag{34}$$

where the plus sign is applicable if there is no field reversal between the cathode and the point in the beam under study.

Final Collector without Space Charge

The initial conditions used for the analog computer analysis include the effects of cathode immersion. The beam used for this collector study has a microperveance of 0.5, a B/B_b of 2, a filling factor b/a of 0.6 in a drift tube of 0.055 inch in diameter. The Brillouin field for the beam is 0.155 Tesla while the main field is 0.31 Tesla. The basic tube efficiency is assumed to be 50 percent so that the average energy of the spent beam electrons is $V_o/2$ electron volts and their average velocity is $1/\sqrt{2}$ times the dc beam velocity. This average velocity is used in the approximate

calculation of space charge effects. The ratio L/b of collector length to beam diameter was chosen to be 160 if a constant margin collector is being designed or L/b = 80 if a tent collector is under consideration.

The trajectories of Figure 33 show the beam described above without the effect of space charge. The trajectories are started in the main field of $2 B_b$ and traverse a linear transition region at the approximate pole piece location to a magnetic field strength equal to $B_b/2$ in the collector. An electrode line is chosen on the basis of the intersections of the $\pm x$ trajectories of equal energy in Figure 33 near their point of minimum kinetic energy. The initial and final kinetic energy of all 50 electrons as they cross the electrode line are recorded in Table V for the collector evaluation.

- - - - - - -

TABLE V - KINETIC ENERGIES FOR TRAJECTORIES WITHOUT SPACE CHARGE

Initial KE	Final KE					η_c
	+x	-x	+y	-y	o	
1.0	.0770	.0745	.0410	.0016	.0003	96.1%
.9	.0800	.0836	.0503	.0080	.0032	95.0
.8	.0686	.0833	.0499	.0093	.0173	94.3
.7	.0174	.0348	.0364	.0093	.0119	96.9
.6	.0268	.0322	.0244	.0114	.0110	96.5
.5	.0341	.0324	.0226	.0118	.0114	95.5
.4	.0420	.0343	.0201	.0090	.0102	94.2
.3	.0586	.0534	.0200	.0018	.0129	90.2
.2	.0630	.0685	.0456	.0135	.0136	79.6
.1	.0136	.0166	.0118	.0160	.0101	86.4

- - - - - - -

The collector efficiency characteristic η_c is derived from the average recovered power in each energy class and is plotted in Figure 34 as a function of initial energy. It is unnecessary to analyze electrons having energies greater than V_o because the collector efficiency is essentially flat for these energies. Several trajectories were calculated to confirm this fact. For energies greater than V_o either a constant margin or a tent collector characteristic is applicable depending on the choice of power supplies. The rf collector efficiency is essentially the average value of the curves of

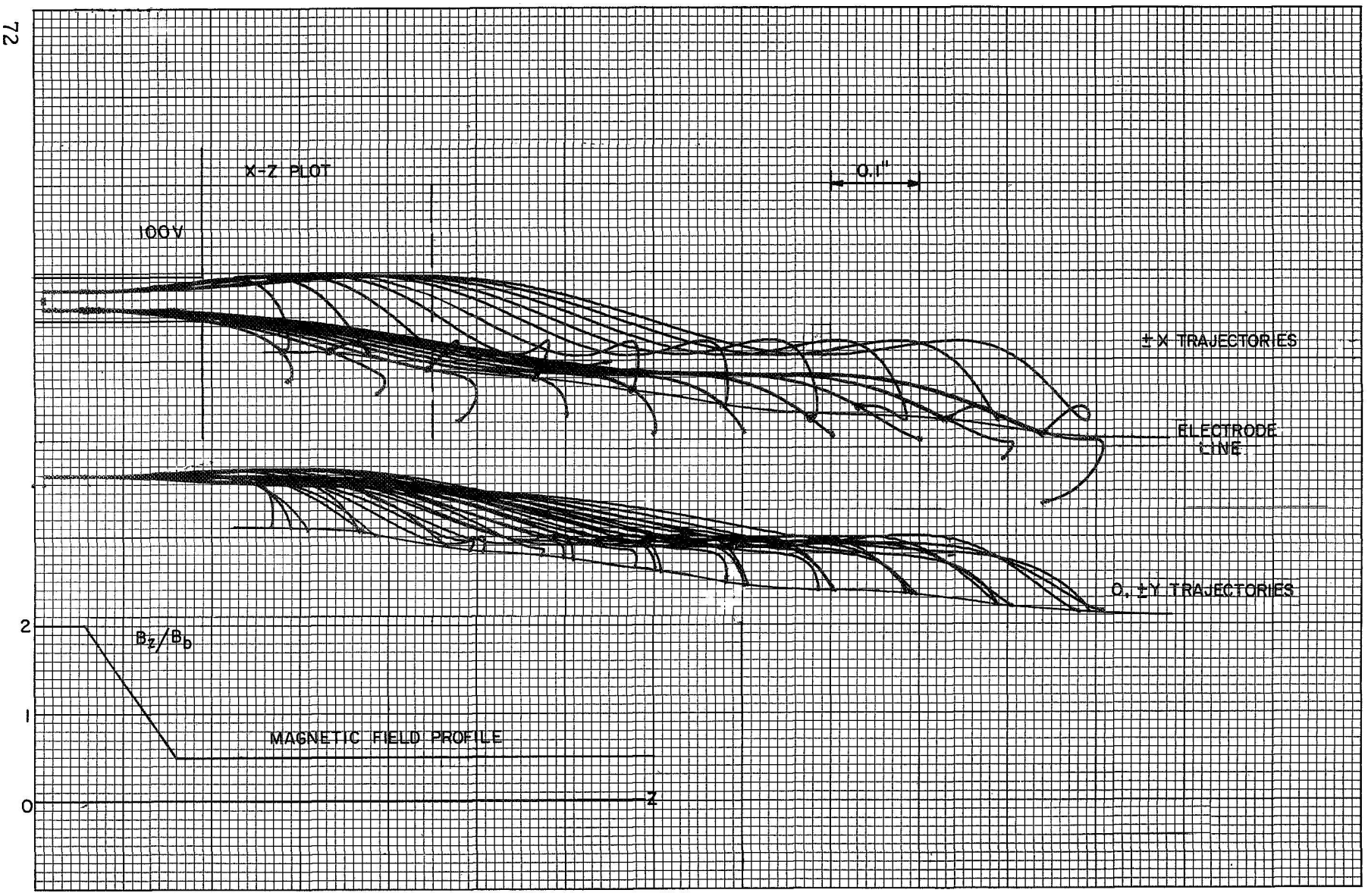

Figure 33 - Electron Trajectories in Final Type 4.3 (TEF) Collector in x-z Plane with 0, $\pm x_o$, $\pm y_o$ Initial Positions, Neglecting Space Charge

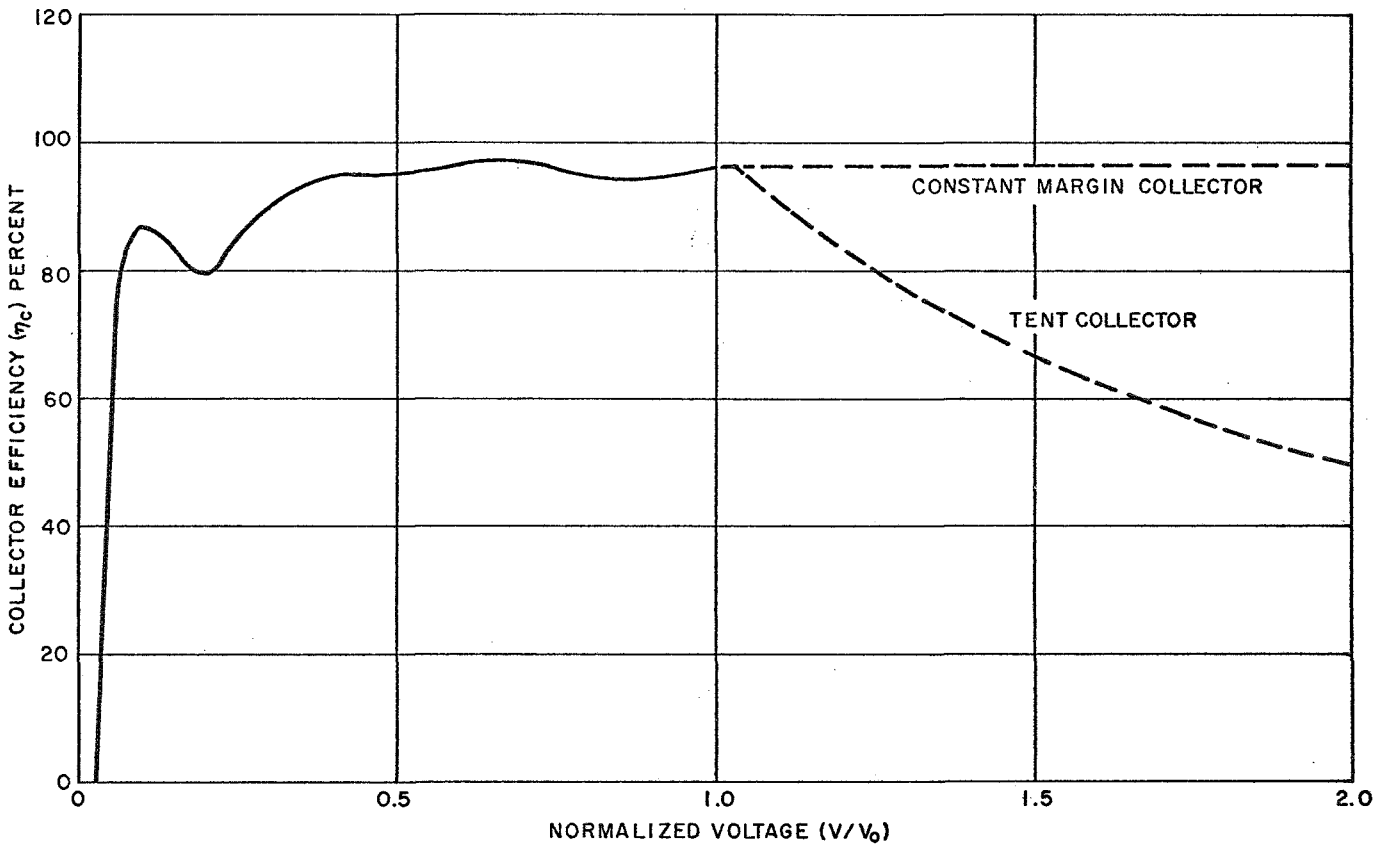

Figure 34 - Computed DC Collection Efficiency of Final Type 4.3 (TEF) Collector as a Function of DC Energy, Neglecting Space Charge

Figure 34 if the basic tube efficiency is greater than 50 percent. Mechanical integration of the curves of Figure 34 yields rf collector efficiencies of 92.6 and 79.0 percent for the constant margin and the tent collector, respectively. These efficiencies can be obtained if the collectors have an infinite number of electrodes. This is a result of stopping all electrons at the electrode line where they are assumed as being collected. The effect of a finite number of electrodes can easily be taken into account by truncating the recovered power for each electron to those allowable by the electrode voltages. Thus, a full energy electron may yield a recovered energy of 0.96 if there were a 0.96 electrode. If the next lower electrode happens to be at 0.9 then the recovered energy for this electron can only be 0.9. A finite number of electrodes clearly reduces the collector efficiency below that obtainable with an infinite number. This effect will be quantitatively included in the collector analysis with space charge.

Final Collector with Space Charge

The trajectories with space charge for a 0.5 microperveance beam are given in Figure 35. Considerably greater beam bulging, especially for the $\pm y$ trajectories, can be seen in comparison with Figure 33. The introduction of space charge also necessitated a change in the electrode line location to avoid a great number of inefficient near side strikes. The initial spreading of the beam also requires a tapering of the drift tube to avoid direct interception.

The initial and final kinetic energies of all fifty electrons are given in Table VI. The collection efficiency for an infinite number of electrodes is again computed from the average behavior of five electrons at each energy level and is shown in Figure 36 as a function of energy. The dip in the curve for $N = \infty$ at 0.2 energy is due to scalloping action associated with the magnetic field contour and the entrance conditions. Again the $N = \infty$ curve is seen to be very flat, above 0.5 energy, making it unnecessary to analyze electrons having initial energies greater than V_o.

The collector characteristic for a finite number of electrodes is calculated by quantizing the recovered energies to the next lower allowable level. The number N is the number of electrodes at potentials between zero and V_o. A tent collector will have N electrodes while a constant margin collector must have 2N electrodes. Note that when the intrinsic margin exceeds the 1/N margin due to electrode number, the collector efficiency η_c becomes smooth and does not exhibit the characteristic sawtooth nature of an ideal collector. In Figure 36 this transition occurs between five and ten electrodes.

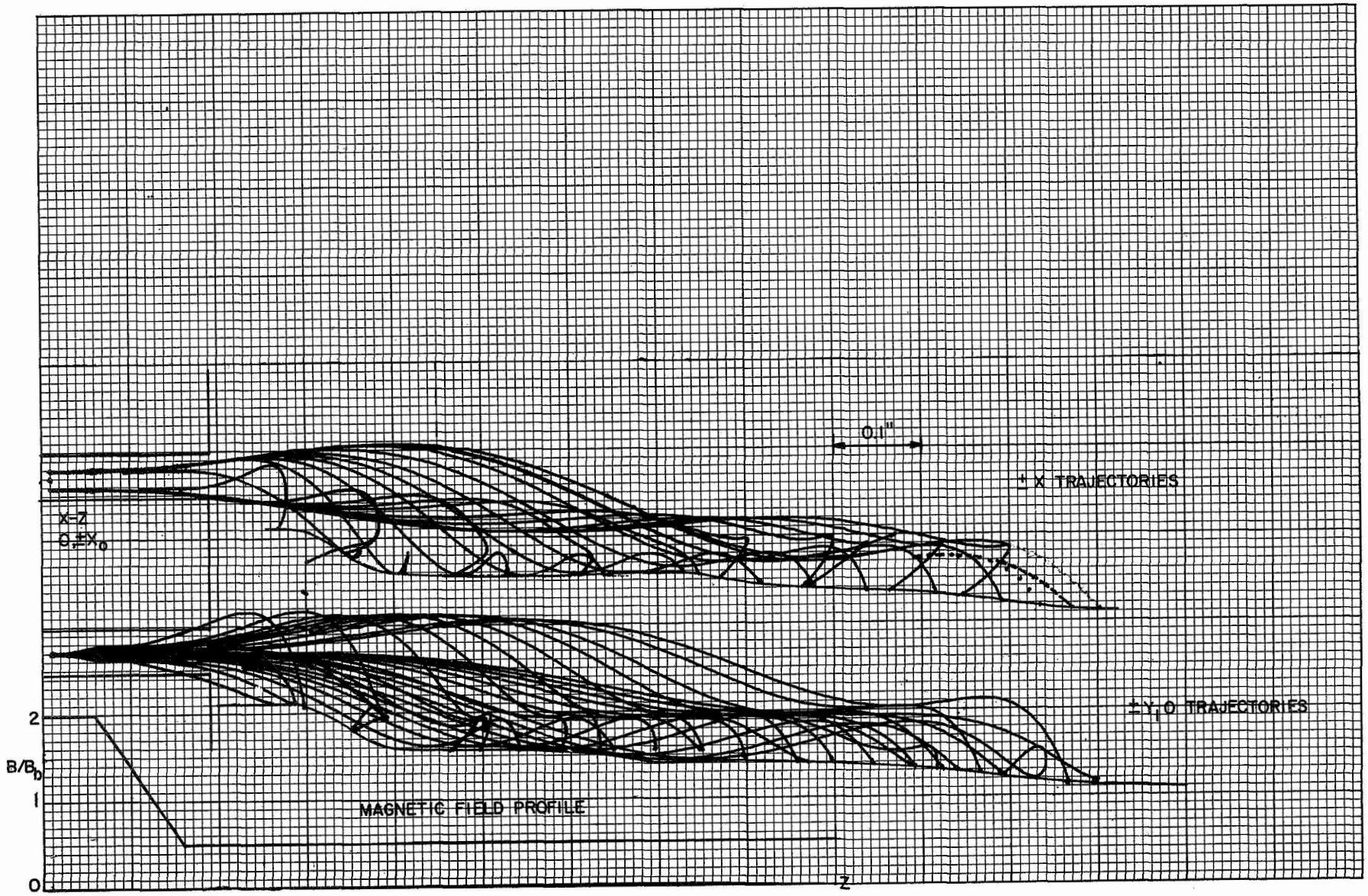

Figure 35 - Computed Electron Trajectories in Final Type 4.3 (TEF) Collector in x-z Plane with 0, $\pm x_o$, $\pm y_o$ Initial Positions, Including Space Charge

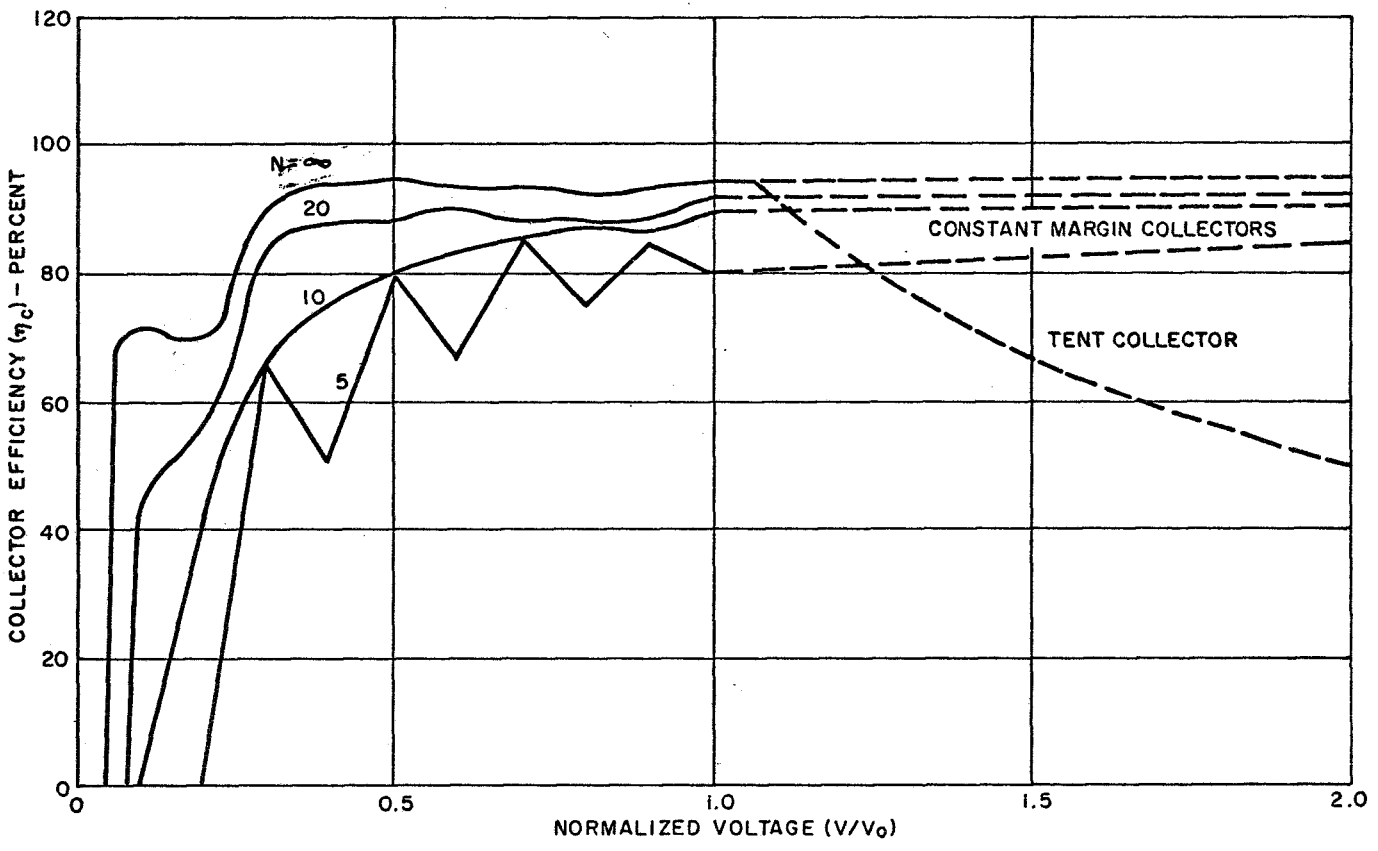

Figure 36 - Computed DC Collection Efficiency of Final Type 4.3 (TEF) Collector as a Function of DC Energy, Including Space Charge, for 5, 10, 20 and an Infinite Number of Electrodes

TABLE VI - KINETIC ENERGIES FOR TRAJECTORIES WITH SPACE CHARGE

Initial KE	Final KE					η_c for N electrodes between 0 and V_o			
	+x	-x	+y	-y	o	N=∞	20	10	5
1.0	.0706	.0786	.0953	.0456	.0120	94.0	92.0	90.0	80.0
.9	.0612	.0862	.1020	.0610	.0094	92.9	88.9	86.7	84.4
.8	.0591	.0962	.0542	.0852	.0172	92.2	88.8	87.5	75.0
.7	.0713	.0516	.0163	.0642	.0126	93.8	88.6	85.7	85.7
.6	.0686	.0438	.0306	.0381	.0116	93.6	90.0	83.3	66.7
.5	.0536	.0060	.0460	.0238	.0120	94.3	88.0	80.0	80.0
.4	.0332	.0172	.0300	.0213	.0206	93.9	87.5	75.0	50.0
.3	.0267	.0347	.0192	.0316	.0418	89.7	83.3	66.7	66.7
.2	.0290	.0248	.1546	.0502	.0473	69.4	55.0	40.0	0
.1	.0164	.0150	.0574	.0432	.0098	71.6	40.0	0	0

- - - - - - -

TABLE VII - RF COLLECTOR EFFICIENCY OF FINAL CONSTANT-MARGIN AND TENT COLLECTORS

No. of Electrodes Between 0 and V_o	RF Collector Efficiency			
	Constant Margin Collector		Tent Collector	
	η_{c-rf}	Total No. of Electrodes	η_{c-rf}	Total No. of Electrodes
∞	89.3	∞	76.6	∞
20	83.5	40	72.1	20
10	78.0	20	67.4	10
5	68.8	10	61.2	5

- - - - - - -

For tubes having a base efficiency greater than 50 percent the average value of the curves in Figure 36 is an excellent measure of the rf collector efficiency as shown previously. Mechanical integration of the curves of Figure 36 yields the rf efficiencies listed in Table VII for different numbers of electrodes between zero and V_o. A constant-margin type collector with 40 electrodes (n= 20) is seen to have an efficiency greater than 80 percent. This collector will fit directly on the proposed 12-GHz tube without a refocusing section. The rf collector efficiencies for various "tent" type collectors is also given in Table VII to facilitate the choice of power supplies.

If the total number of electrodes is limited to ten then there is little advantage in constructing a constant-margin collector. Only if the total number is greater than 10 does the advantage become significant.

Mechanical Collector Design

As indicated in Figure 35, a "tent" type collector for a 12-GHz tube will have an L/b ratio of 80 or an actual length of approximately one inch. While this may appear small it is not unreasonable relative to power flow.

Presuming the dc beam power is 8 kW, the base tube efficiency is 50 percent, and there are 10 electrodes in the collector as shown in Figure 37, the power entering the collector will clearly be 4 kW of which 67.4 percent or 2.7 kW is recovered electrically. The remaining 1.3 kW will be dissipated as heat in the collector. Approximately half of this, 650 watts, will be dissipated in the large, heat pipe cooled end cap as shown, assuming that a flat, symmetrical spent beam power density distribution is applicable. The remaining 650 watts will be evenly distributed among the remaining electrodes which must dissipate approximately 65 watts each. This amount of power can easily be radiated from the electrodes. A constant margin collector with twenty electrodes would be twice as long and each electrode would have to dissipate only 44 watts on the average. While this analysis of power flow is somewhat approximate, it does show that not more than 100 watts will have to be dissipated by any individual electrode.

A special problem arises in the absence of an rf signal. In this case the full dc beam power enters the collector which has an efficiency of approximately 90 percent for electrons of this energy. This means that 800 watts must be dissipated as heat on one electrode. This electrode will require either special cooling or an electrical interlock to shut off the beam during the absence of an rf signal.

Applicability to Tubes with Non-Solenoidal Beam Focusing

The specific Type 4.3 (TEF) collector described in this section was developed to fit a tube having a solenoidal focusing field of twice the Brillouin value. This field could also be produced, without affecting the collector design, by a single permanent magnet with no reversals. The collector could have been designed for beams with pure Brillouin focusing, with the major design difference being in the location of the electrode line. As discussed below, a collector designed for a pure Brillouin beam is also applicable to beams having PPM or PM focusing with a single reversal.

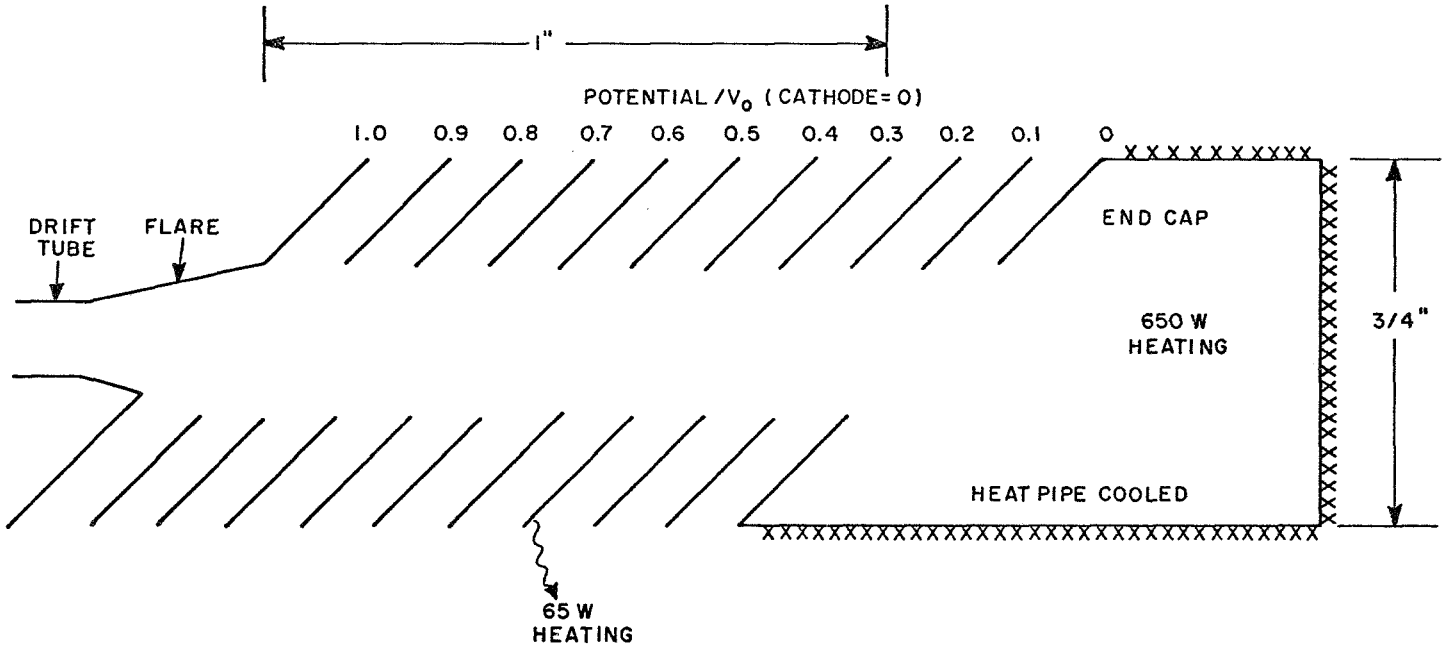

Figure 37 - Layout of Final 12-GHz Type 4.3 (TEF) Box-Tent Collector Using Ten Electrodes

According to Branch et al[19] the sign before the square root in Equation (33) changes whenever a reversal of the axial magnetic field occurs. In the normal case of immersed beams the negative sign is applicable and the angular velocity of the electrons is quite low. If the field should be reversed in a heavily immersed beam, this angular velocity will become very large, leading to difficult focusing problems. In addition, a much larger fraction of the beam energy will be contained in rotational motion as long as the reversal persists. The kinetic energy in rotational motion is generally unavailable for useful rf energy extraction in "O" type devices. Both these arguments indicate the desirability of shielding the cathode from magnetic field such that $B = B_b$ in Equation (33) and therefore the peak angular velocity of any electron will be the same both before and after a field reversal. If the cathode is shielded, the angular velocities in the beam will be the same as those associated with a Brillouin beam and the collector design will be essentially the same.

DISCUSSION OF RESULTS

The most important result of the work performed on this contract is that the presence of a magnetic field can increase the efficiency of a depressed collector beyond that achieved by electrostatic collection alone. This result, however, must be tempered by the fact that the treatment of space charge in the magnetic collector is more approximate than it is in the electrostatic collector. Nevertheless, there are indications that a magnetic field in the collector region can serve the useful function of preventing harmful space charge effects on the spent beam in a depressed collector just as it prevents harmful spreading due to space charge in the drift tube.

There are a number of ways a magnetic field can be introduced into a depressed collector. The preliminary investigations made early in this contract suggest that if a tilted electric field is used, an axial (Type 4.3) or a tilted (Type 4.41) magnetic field would lead to excellent energy removal. A transverse electric field, a tilted (Type 5.47) or transverse (Type 5.51) magnetic field also leads to excellent energy removal. The Type 4.3 (TEF) collector was chosen for detailed study on this contract because the magnetic field shielding problem is minimized, but this should not exclude other magnetic collectors from future consideration and evaluation.

The Type 4.3 (TEF) collector coincides with the TEF or soft-landing collector studied to some extent by Okoshi, et al[16] in 1968. The performance of an experimental two-stage TEF collector reported by Okoshi, et al, was below theoretical expectations. No reason was given for this discrepancy, but it would appear that the neglect of space charge in their design was a serious drawback.

General theoretical work performed on this contract suggests that the response to efficiency improvement by depressed collectors is greater in TWT's than in klystrons. This is a direct consequence of the reduced velocity spread in the spent beam of a TWT compared to a klystron. The factors of improvement shown in this report are probably overly optimistic for TWT efficiency improvement because of the idealized one-sided spent beam spectrum assumed in the analysis. However, it seems reasonable to conclude that in general efficiency improvement by collector depression will be easier to attain in TWT's than in klystrons.

The effect of the number of electrodes in a depressed collector depends on the intrinsic properties of the collector. Even with an infinite number of electrodes, collection efficiency will not reach 100 percent in any depressed

collector. However, a well designed collector (such as the final TEF design) with an intrinsic margin of approximately 0.05, can advantageously utilize 20 electrodes, whereas a less well-designed collector with an intrinsic margin greater than 0.4 can derive little benefit from an increased number of electrodes. This may be verified by the curves of Figure 22 which shows an 11 point gain of efficiency with a 0.05 intrinsic margin collector while a 0.4 margin collector shows only a 7-point gain.

A number of parameter optimizations that could benefit from a second iteration still remain in the final design. For instance, very early in the program and before space charge was introduced, the angle of the electric field was chosen to be 45 degrees. It is possible that a more optimum choice of this angle can be made now that the complete design procedure has been established. Other parameters such as the tradeoff between magnetic field strength in the collector and collector length may benefit from iterated optimizations.

In order to achieve the most meaningful results in future work, it is essential that more realistic criteria be established for the spent beam spectra of klystrons and TWT's. An alternative to this approach is to concentrate on the optimization of constant margin collectors, in which case the collection efficiency is virtually independent of velocity distribution.

RECOMMENDATIONS FOR FUTURE WORK

In the course of this study several promising collector ideas have been presented. Type 4.3 (TEF) collector, has been selected as the best practical collector for future development. Most of the other collectors were considered unsuitable since they required sophisticated magnetic shielding arrangements. The future development of new magnetic materials may make these collectors worthy of further study. The TEF collector has been optimized to the extent of showing that there is an advantage to be gained over pure electrostatic collection, especially at higher frequencies, because the magnetic field in the collector tends to prevent excessive space charge defocusing. Further development and verification experiments are required, however, to achieve a working version of a Type 4.3 (TEF) collector for a 12-GHz tube.

An outline showing the orderly development of the concepts leading to the final collector applicable to a 12-GHz tube is shown in Figure 38. Much of the work under "New Collector Concepts" has been accomplished and has resulted in the selection of the Type 4.3 (TEF) collector. As new technology develops, it may be advantageous to reconsider those collectors which require intricate magnetic field shaping. The next logical step is the verification of the concept on an actual tube, preferably one on which other depressed collectors have been tested. This would result in a direct comparison among several collector types. The verification test would of course be preceeded by an optimization study which would match the electrode arrangement to the spent beam velocity distribution for the highest collection efficiency. The collector verified at low frequency should be made large enough so that it can be scaled directly in size to fit a 12-GHz tube without thermal difficulties. In other words, the collector length-to-beam radius ratio L/b should be the same for the low frequency test as it will eventually be for the final tube. If this is done, the space charge problem will be exactly the same in either case provided the beam perveance is also the same. A properly conducted low frequency test can therefore point out any space charge problem that may be encountered in the final collector. It will also show whether or not the two-electron model of space charge analysis is sufficiently accurate for the analysis of asymmetric collectors. If necessary, a program for improving the space charge analysis can be undertaken at this time.

After a successful low frequency verification test, work can begin on the 12-GHz collector. A short optimization study bringing together all the facts gathered so far should precede the fabrication of the first collector-tube

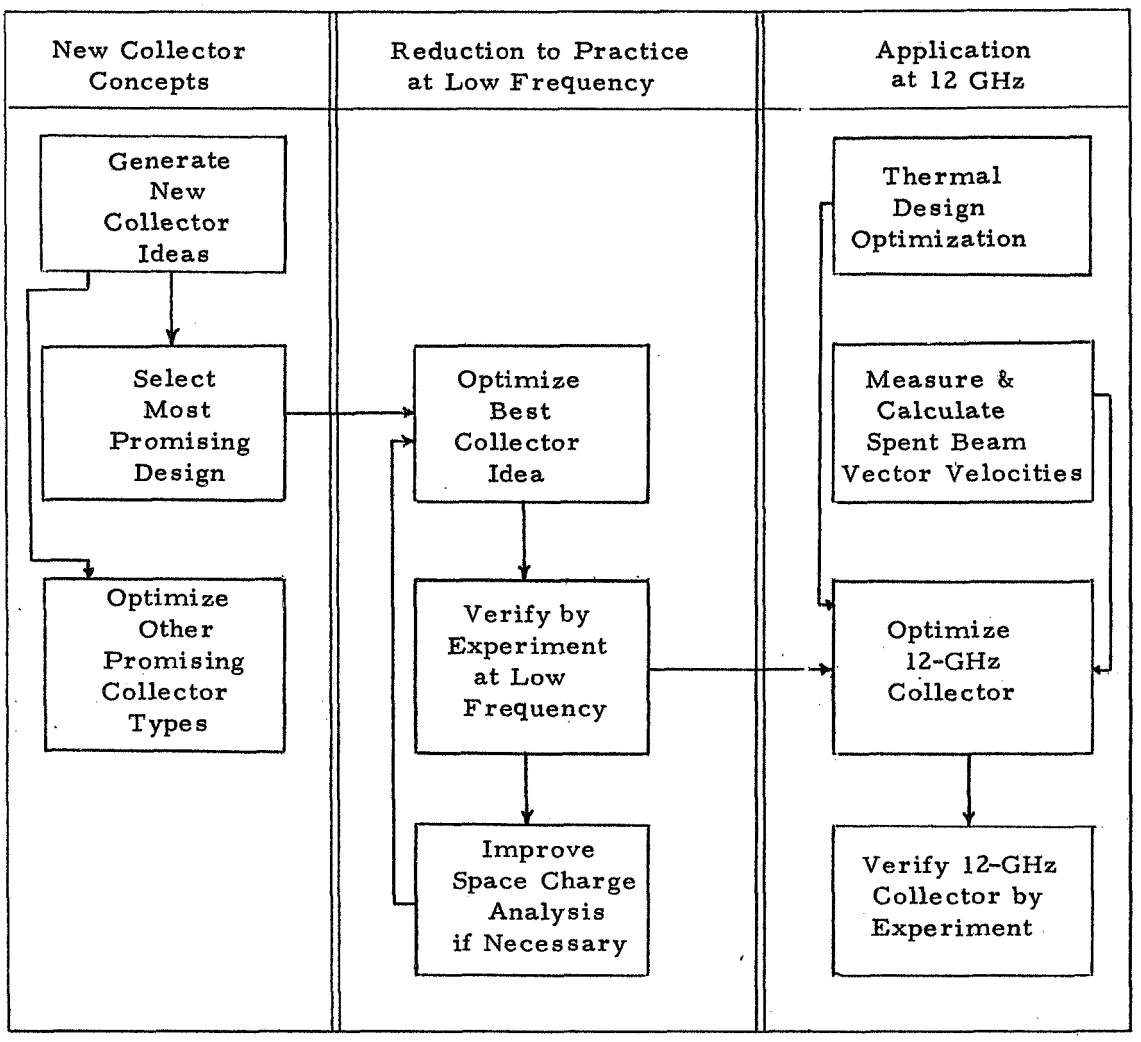

Figure 38 - Recommendations for Future Collector Development

assembly. Thermal designs may be verified at this time. The actual spent beam velocity distributions should be known preferably both by calculation and experiment so that the collector can be truly optimized. A final verification test, possibly including life tests, would then be performed.

CONCLUSIONS

To meet the objectives of this contract, a versatile analog computer program was developed for analyzing many types of depressed collectors. The effects of magnetic fields and an approximate simulation of space charge were included in this program. Of the sixty-four depressed collection methods that were studied, the most promising appeared to be the Okoshi TEF collector because of its high efficiency and simplicity of construction. A very detailed analysis of this collector resulted in a design directly applicable to a 12-GHz tube producing four kilowatts of continuous high frequency power.

A comparison of the TEF collector and the General Electric reflex collector led to the conclusion that the use of both electric and magnetic fields in the collection process can result in performance superior to that achievable with pure electrostatic fields.

Another conclusion is that the vector velocity distribution and the size of the spent beam can greatly influence the optimum efficiency obtainable with a depressed collector. The study shows that a spent beam having a narrow velocity distribution can be collected much more efficiently than a beam having a wide distribution. In order to design an optimum depressed collector for any tube, its spent beam velocity distribution must be known quite accurately.

Appendix A
SPENT BEAM ENERGY DISTRIBUTIONS IN TWT's AND KLYSTRONS

The spent beam energy spectrum of klystrons differs significantly from that of TWT's. The most accurate determination of the spectrum in a TWT has been made by Cutler[4] by using a Faraday-cage stopping-potential device. Measured data scaled from Figure 15 of Cutler's paper are plotted in the upper portion of Figure 39 as a function of energy relative to dc beam energy. The central plot in Figure 39 gives the current distribution $\Delta I/\Delta V$, and the lower plots shows the relative energy distribution $V\ \Delta I/\Delta V$. The energy distribution is seen to be asymmetric and sharply peaked at $0.64\ V_o$ which is roughly the lower limit of $0.66\ V_o$ given by Figure 10 for a flat one-sided energy distribution with 20 percent efficiency.

The current, the current distribution, and the energy distribution calculated for a typical high efficiency klystron are given in Figure 40. Contrasted to the TWT spent beam spectrum shown in Figure 39, the klystron spectrum ranges from approximately $0.05\ V_o$ to $1.95\ V_o$. This is in agreement with the range from $0.02\ V_o$ to $1.98\ V_o$ given in Figure 10 for a flat symmetrical energy distribution corresponding to a klystron with 58 percent efficiency.

Thus, the identification of a flat one-sided energy distribution with a TWT and a flat symmetrical energy distribution with a klystron is roughly justified.

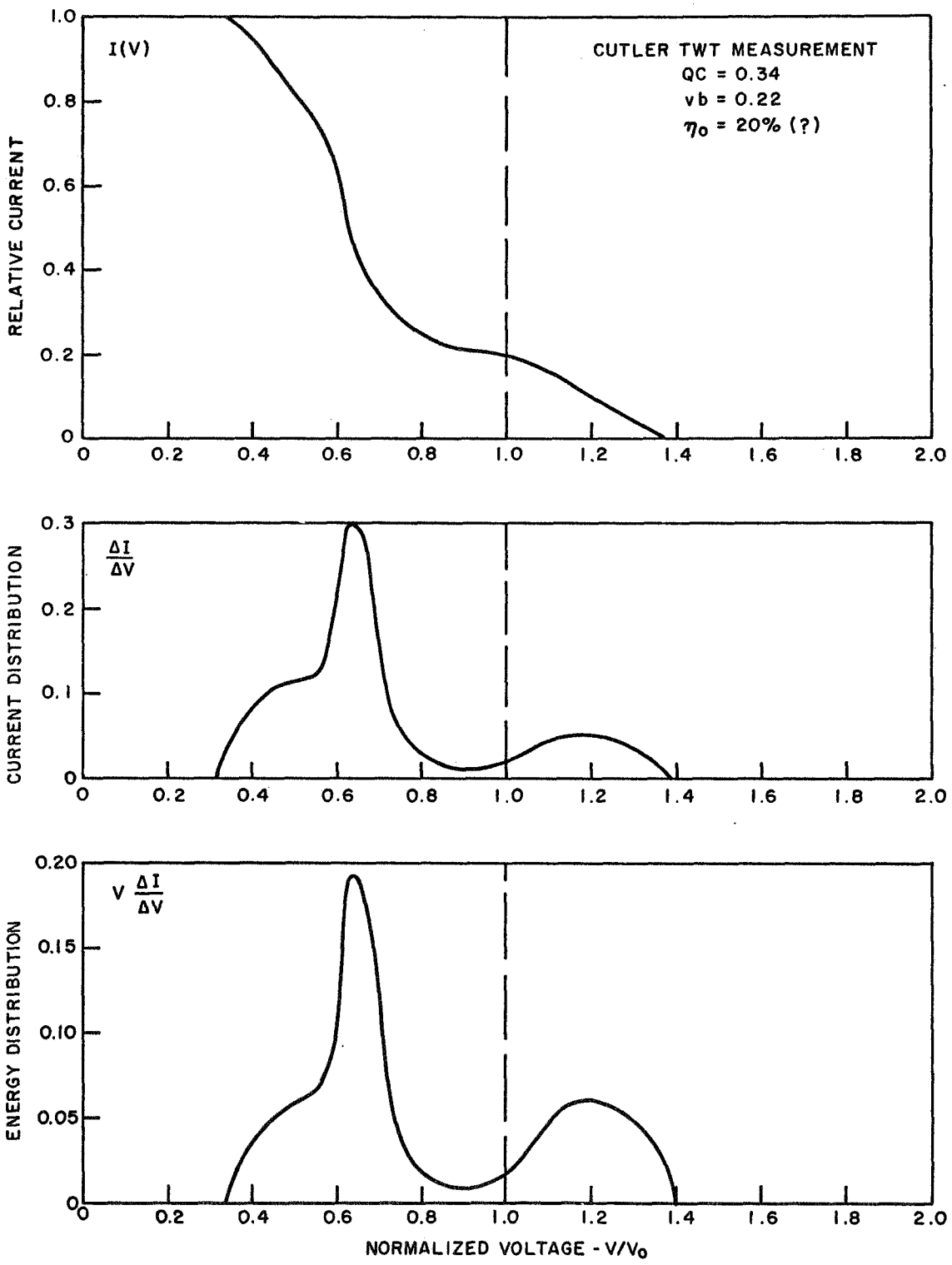

Figure 39 - Measured TWT Spent Beam Power Spectrum

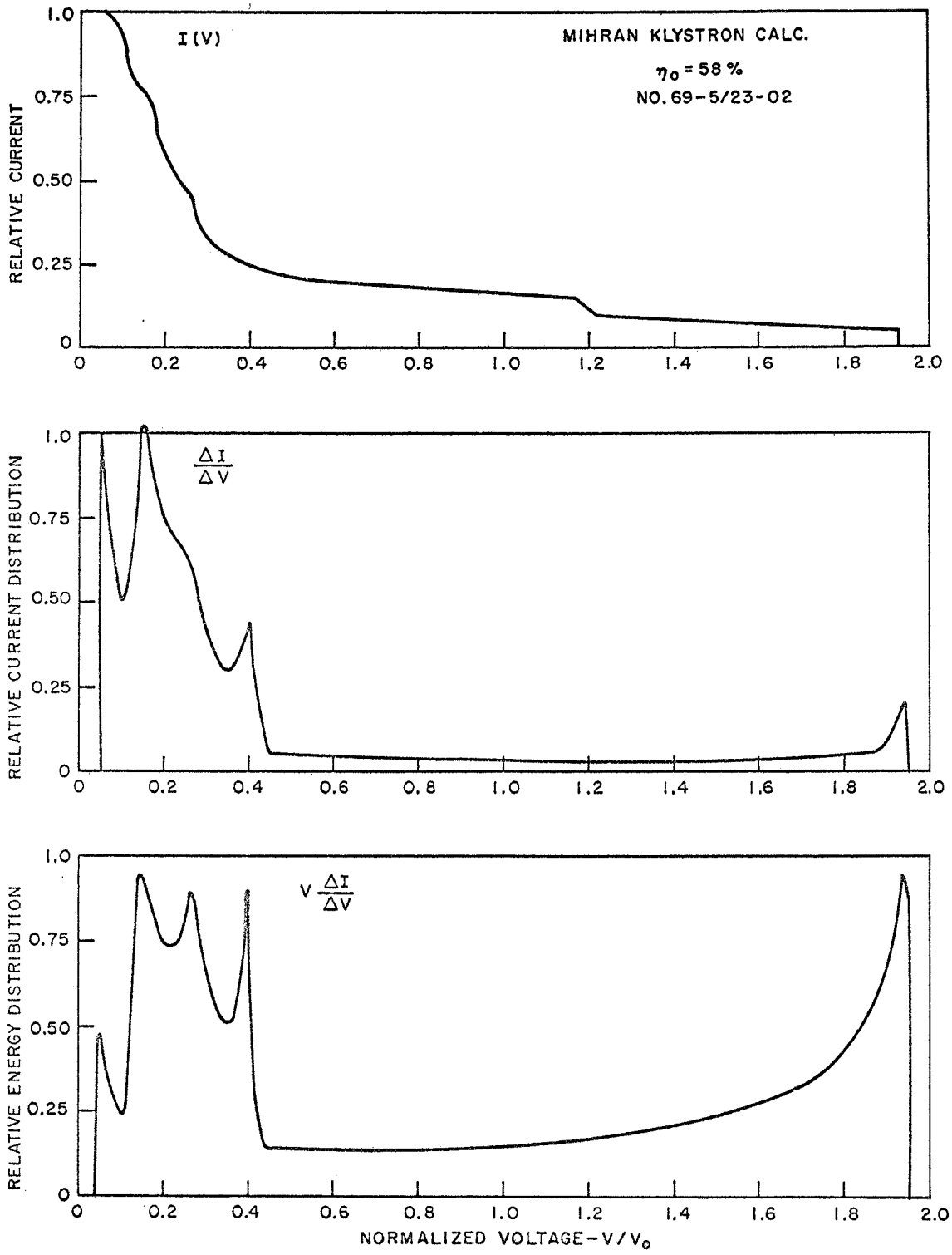

Figure 40 - Calculated Klystron Spent Beam Power Spectrum

Appendix B
LIST OF SYMBOLS

b	Electron beam radius
B	Axial magnetic field
B_x, B_y, B_z	Magnetic field components in Cartesian coordinates
B_b	Brillouin field
d	Distance between particles
e	Charge on an electron
E_x, E_y, E_z	Electric field components in Cartesian coordinates
f	Transitional factor
i	An index
I_i	Current collected on i'th electrode
I	Current contained within a given radius
I_o	Total beam current
i_x, i_y, i_z	Unit vectors
j	An index
K	Cathode magnetic immersion factor
L	Collector length
M	Number of points at which dc collector efficiency is established or tapered magnetic field amplitude
m	Electron rest mass, or collector energy margin
m_i	Intrinsic margin
m_N	Margin associated with finite electrode number
n	An index
N	Number of collector electrodes
P_o	Dc beam power
P_{rec}	Power extracted from the spent beam
$p(V)$	Power density distribution
r	Radial distance

V	Voltage
V_o	Cathode voltage
V_i	Voltage on i'th collector electrode
V_{oj}	j'th value of beam voltage
v	Velocity
v_θ	Particle velocity component in angular direction
x, y, z	Cartesian position coordinates
x_o, y_o, z_o	Position coordinates of central electron
$\dot{x}, \dot{y}, \dot{z}$	Velocity components
$\ddot{x}, \ddot{y}, \ddot{z}$	Acceleration components
z_3	Position along axis where tapered magnetic field is zero

α	Output gap voltage swing parameter
β	Analog computer time scaling factor
ϵ_o	Permittivity of free space
η	Net tube efficiency
η_o	Tube efficiency without collector depression
η_c	Dc collector efficiency
$\bar{\eta}_c$	Average dc collector efficiency
η_{c-rf}	Rf collector efficiency

REFERENCES

1. Branch, G.M. and Mihran, T.G., "Analytical Designs of a Space-Borne Magnetically-Focussed Klystron Amplifier", Final Report, Contract NAS3-11514, NASA Lewis Research Center, Cleveland, Ohio; October 25, 1968.

2. Haeff, A.V., and Nergaard, L.S., "A Wide-Band Inductive Output Amplifier", Proc. IRE, Vol. 28, pp. 126-130; March 1940.

3. Litton, C.V., "Electrode Structure for Velocity Modulation Tubes", U.S. Patent No. 2325865; August 3, 1943.

4. Cutler, C.C. and Brangaccio, D.J., "Factors Affecting Traveling-Wave Tube Power Output", IRE Trans. on Elec. Dev., Vol. PGED-3, pp. 9-23; June 1953.

5. Winkler, R.H., "A Method of Improving the Efficiency of Klystrons", Microwave Lab. Rpt. No. 235, Stanford University; May 1954.

6. Laico, J.P., McDowell, H.L., and Moster, C.R., "A Medium Power Traveling-Wave Tube for 6,000-Mc Radio Relay", BSTJ, Vol. XXXV, pp. 1285-1346; November 1956.

7. Wolkstein, H.J., "Effect of Collector Potential on the Efficiency of Traveling-Wave Tubes", RCA Rev., Vol. XIX, pp. 259-282; June 1958.

8. Sterzer, F., "Improvement of Traveling-Wave Tube Efficiency Through Collector Potential Depression", IRE Trans. on Elec. Dev., Vol. ED-5, pp. 300-305; October 1958.

9. Dunn, D.A., Luebke, W.R., and Wada, G., "A Low Potential Collector Employing an Asymmetrical Electrode in an Axially-Symmetric Magnetic Field", IRE Trans. on Elec. Dev., Vol. ED-6, pp. 294-296, July 1959.

10. Dunn, D.A., Borghi, R.P., and Wada, G., "A Crossed-Field Multi-Segment Depressed Collector for Beam-Type Tubes", IRE Trans. on Elec. Dev., Vol. ED-7, pp. 262-267; October 1960.

11. Murata, S., and Kinoshita, S., "Collector Potential Depressed Klystron", Record of Int'l Cong. on Microwave Tubes, Munich, June 7-11, 1960, Friedr. Vieweg & Sohn, Braunschweig., pp. 64-72.

12. Hansen, J.W., and Susskind, C., "Improvement of Beam-Type Performance by Collector-Potential Depression, and a Novel Design", IRE Trans. on Elec. Dev., Vol. ED-7, pp. 282-288; October 1960.

13. McCune, E., "Depressed Collector Klystron (VA-843) Development Program", Final Report Varian Associates, Contract No. DA 36-039-sc-78093; March 1961.

14. Met, V., "Depressed Collector Studies for High Power Klystrons", Final Technical Report, Contract AF 30(602)-1500, Task 45083, RADC-TR-61-204, Rome Air Development Center; March 30, 1961.

15. Chen, T.S., Wolkstein, H.J., and McMurrough, "Theory and Performance of Depressed Trochoidal Collectors for Improving Traveling-Wave-Tube Efficiency", IEEE Trans. on Elec. Dev., Vol. ED-10, pp. 243-254; July 1963.

16. Walder, J., "The Biased Gap Klystron", M.S. Thesis, Cornell University; February 1965. Also, Walder, J., and McIsaac, P.R., "Experimental Analysis of Biased Gap Klystron", IEEE Trans. on Elec. Dev., Vol. ED-13, pp. 950-955; December 1966.

17. Okoshi, T., and Chiu, E., "A 'Soft-Landing' Collector for Improving the Efficiency of Beam-Type Tubes", preprint Dept. of Electronic Engineering, Univ. of Tokoyo, Bunkyo-ku, Tokyo, Japan; undated. Also Okoshi, T., Chiu, E., and Mzusawa, J., "TEF (Tilted Electric Field) Soft-Landing Collector for Beam-Type Microwave Tubes", Trans. Inst. Electronics Comm. Engrs. Japan, Vol. 51, pp. 10-12; November 1968.

18. Sauseng, O., Basiulis, A., and Tammaru, I., "An Analytical Study Program to Develop the Theoretical Design of Traveling Wave Tubes", NASA Final Report CR-72450 under Contract NAS3-9719, October 31, 1968.

19. Branch G.M., Mihran, T.G., Neugebauer, W., and Pohl, W.J., "Space Charge Wavelengths in Electron Beams", IEEE Trans. Elec. Dev., Vol. ED-14, pp. 350-357; July 1967.

CR-72768
FINAL REPORT

	Copies
National Aeronautics & Space Administration	
Headquarters	
Washington, D.C. 20546	
Attn: SA/L. Jaffe	1
SAC/A.M.G. Andrus	10
SC/R.B. Marsten	1
NASA-Lewis Research Center	
21000 Brookpark Road	
Cleveland, Ohio 44135	
Attn: C. C. Conger (MS 54-1)	1
R. E. Alexovich (MS 54-3)	1
Dr. H. G. Kosmahl (MS 54-3)	1
Technology Utilization Officer (MS 3-19)	1
Library (MS 60-3)	2
Report Control Office (MS 5-5)	1
N. T. Musial (MS 501-3)	1
G. J. Chomos (MS 54-5)	50
Rockets & Spacecraft Procurment Section (MS 500-302)	1
Communication Systems, Inc.	
5817 Columbia Pike	
Falls Church, Virginia 22046	
Attn: J. Bisaga	1
Rand Corporation	
1700 Main Street	
Santa Monica, California 90404	
Attn: Dr. J. Holt	1
NASA-George C. Marshall Space Flight Center	
Huntsville, Alabama 35812	
Attn: RASTR-A/E. C. Hamilton	1
Library	1
NASA-Goddard Space Flight Center	
Greenbelt, Maryland 20771	
Attn: 733/R. Pickard	1
Library	1

	Copies
NASA-Ames Research Center Moffett Field, California 94035 Attn: OART/MOA/E. Van Vleck (MS 202-6)	1
Library	1
NASA-Langley Research Center Langley Station Hampton, Virginia 23365 Attn: B. Kendall (MS 173)	1
Library (MS 185)	1
NASA-Manned Spacecraft Center Houston, Texas 77001 Attn: Library	1
Jet Propulsion Laboratory 4800 Oak Grove Drive Pasadena, California 91103 Attn: L. Derr	1
Library	1
NASA Scientific & Technical Information Facility P.O. Box 33 College Park, Maryland 20740 Attn: NASA Representative	3
TRW Systems One Space Park Redondo Beach, California 90278 Attn: W. A. Finley/Space Vehicle Division	1
General Dynamics Convair Division P.O. Box 1128 San Diego, California 92112 Attn: F. J. Dore/Advanced Programs Laboratory	1
Hughes Aircraft Company Space Systems Division 1194 W. Jefferson Boulevard Culver City, California 90230 Attn: H. A. Rosen/Satellite Systems Laboratory	1

	Copies
General Electric Company Missile and Space Division Valley Forge Space Technology Center P.O. Box 8555 Philadelphia, Pennsylvania 19101	
Attn: H. Collins	1
P. Nadler	1
Federal Communications Commission 521 12th Street Washington, D.C. 20554	
Attn: M. Fine	1
U.S. Information Agency 25M St. S.W. Washington, D.C. 20547	
Attn: IBS/EF/G. Jacobs	1
General Electric Company Tube Department Microwave Tube Operation Schenectady, New York 12305	
Attn: R. Dehn	1
Litton Industries Electron Tube Division 960 Industrial Road San Carlos, California 94070	
Attn: Dr. G. Pokorney	1
J. Orr	1
W. Day	1
Dr. O. Sauseng	1
SFD Laboratories, Inc. 800 Rahway Avenue Union, New Jersey 07083	
Attn: Dr. G. Farney	1
Hughes Aircraft Company Electron Dynamics Division P.O. Box 2999 Torrance, California 90509	
Attn: Dr. J. Mendel	1
Dr. T. Tammaru	1

	Copies
Watkins Johnson Company 333 Hillview Avenue Palo Alto, California 94304 Attn: Dr. D. Watkins	1
Varian Associates 611 Hansen Way Palo Alto, California 94303 Attn: Dr. G. Caryotakis	1
Dr. J. Rentz	1
R.C.A. Industrial Tube Division Lancaster, Pennsylvania 17604 Attn: W. P. Bennett	1
Raytheon Company Research Division 28 Seyon Street Waltham, Massachusetts 02154 Attn: W. Teich	1
Dr. J. M. Osepchuk	1
Mr. Lawrence Gasch Aerospace Radar Branch U.S. NRL Washington, D.C. 20390	1
Mr. Robert Richardson Mail No. 1620 Martin-Marietta Corp. Denver Division P.O. Box 179 Denver, Colorado 80201	1
Mr. William E. Waters Sr. Engr. Staff Specialist 3939 Fabian Way MS C-70 Palo Alto, California 94303	1
Mr. George Orr Code 733 Goddard Space Flight Center Greenbelt, Maryland 20771	1

	Copies
Sperry Electronic Tube Division Gainsville, Florida 32601 Attn: H. H. Conners	1
Naval Electronic Systems Command PME 116 Washington, D.C. 20360 Attn: Lt. Commander L. Wardel	1